DIELECTRIC AND PIEZOELECTRIC PROPERTIES OF PERCOLATIVE THREE-PHASE PIEZOELECTRIC POLYMER COMPOSITES

BY UDHAY SUNDAR

A thesis submitted to the

Graduate School-New Brunswick

Rutgers, The State University of New Jersey

in partial fulfillment of the requirements

for the degree of

Master of Science

Graduate Program in Mechanical & Aerospace Engineering

Written under the direction of

Kimberly Cook-Chennault

and approved by

_____

_____

_____

New Brunswick, New Jersey

May, 2016

ABSTRACT OF THE THESIS

DIELECTRIC AND PIEZOELECTRIC PROPERTIES OF PERCOLATIVE THREE-PHASE PIEZOELECTRIC POLYMER COMPOSITES

by UDHAY SUNDAR

Thesis Director:

Kimberly Cook-Chennault

Three-phase piezoelectric bulk composites were fabricated using a mix and cast method. The composites were comprised of lead zirconate titanate (PZT), aluminum (Al) and an epoxy matrix. The volume fraction of the PZT and Al were varied from 0.1 to 0.3 and 0.0 to 0.17, respectively. The influences of three entities on piezoelectric and dielectric properties: inclusion of an electrically conductive filler (Al), poling process (contact and Corona) and Al surface treatment, were observed. The piezoelectric strain coefficient, d_{33}, effective dielectric constant, ε, capacitance, C, and resistivity were measured and compared according to poling process, volume fraction of constituent phases and Al surface treatment. The maximum values of d_{33} were ~3.475 and ~1.0 pC/N for Corona and contact poled samples respectively, for samples with volume fractions of 0.40 and 0.13 of PZT and Al (surface treated) respectively. Also, the maximum dielectric constant for the surface treated Al samples was ~411 for volume fractions of 0.40 and 0.13 for PZT and Al respectively. The percolation threshold was observed to occur at an Al volume

fraction of 0.13. The composites achieved a percolated state for Al volume fractions >0.13 for both contact and corona poled samples. In addition, a comparative time study was conducted to examine the influence of surface treatment processing time of Al particles. The effectiveness of the surface treatment, sample morphology and composition was observed with the aid of SEM and EDS images. These images were correlated with piezoelectric and dielectric properties. PZT-epoxy-aluminum thick films (200 μm) were also fabricated using a two-step spin coat deposition and annealing method. The PZT volume fraction were varied from 0.2, 0.3 and 0.4, wherein the Aluminum volume fraction was varied from 0.1 to 0.17 for each PZT volume fraction, respectively. The two-step process included spin coating the first layer at 500 RPM for 30 seconds, and the second layer at 1000 RPM for 1 minute. The piezoelectric strain coefficients d_{33} and d_{31}, capacitance and the dielectric constant were measured, and were studied as a function of Aluminum volume fraction.

Acknowledgments

First and foremost, I would like to thank my advisor Dr. Kimberly Cook-Chennault for her endless support and for guiding me every step of the way. She has not only served as my mentor but has also been an inspiration to me towards becoming a better researcher with her limitless enthusiasm and undying compassion.

I would also like to thank my committee members, Dr. Haim Baruh and Dr. Aaron Mazzeo for their time, encouragement and for providing insight towards better shaping my research work.

I would like to show my appreciation to the former and present HESML lab members, Dr. Sankha Banerjee, Wanlin Du, Eric Bickford, Andrew Tang, Rui Wang and James Palmer for all the fun times and the several discussions that we have had that have helped me towards improving this thesis. I am also much obliged to fellow MAE graduates Abhimanyu Kamat, Sandesh Gopinath and Thomas Hansen for helping me get through all those tough times.

Last but not least, I would like to thank my parents and my sister who have provided me with a robust support system which has laid the foundation of my professional career, and I will always be indebted to them.

Udhay Sundar

May 2016

Table of Contents

List of Figures

List of Tables

Chapter 1

Introduction

1.1. Research goal

The inclusion of electrically conductive particles within a two-phase piezoelectric composite (PZT and epoxy) results in enhanced piezoelectric and dielectric properties (in comparison to the two-phase composite), with corresponding increases in dielectric loss of the material and reduction in the breakdown field strength [1-3]. It is well known that the dielectric and piezoelectric properties observed in materials such as these are a function of electrically conductive filler size, particle distribution, and the particle to matrix bond. These parameters influence the particle to matrix interfaces and subsequent efficacy of the polarization process, yet less is about their effect on the macroscopic dielectric and piezoelectric properties of the bulk and thick film forms of these composites. In this thesis, the materials of focus include two-phase piezoelectric-epoxy composites that incorporate semi-spherical and ellipsoidal aluminum inclusions as the electrically conductive third phase. Both bulk and thick films were fabricated and analyzed to understand the effects constituent volume fraction, composite polarization type, and particle surface treatment had on the bulk and thick film composite dielectric and piezoelectric properties.

Aluminum forms an aluminum oxide (Al_2O_3) shell around its core when exposed to air. As a result, the aluminum particle instantaneously establishes positive charges in the core and negative charges around the shell due to the charge transfer from aluminum to absorbed oxygen (O_2) [4]. The aluminum oxide shell affects the properties of the interface between the aluminum and epoxy matrix, and consequently the piezoelectric and dielectric properties of the composite.

This thesis includes a time study of the surface treatment of aluminum particles to understand how the particle to matrix interfacial properties influence the bulk composite piezoelectric and dielectric properties. Also, the piezoelectric and dielectric properties of the bulk and thick film PZT-aluminum-epoxy composites were observed as functions of frequency, composition and polarization method to gain an understanding of the variability of properties observed with the reduction in the aspect ratio of the samples.

1.2. Research motivation and background

Piezoelectricity can be defined as the electric polarization produced by mechanical strain in crystals belonging to certain classes, where the polarization is proportional to the strain, and changes sign with it. In other words, if the pressure is replaced by a stretch (i.e., a reversal in sign of the pressure) the sign of the electric polarity becomes reversed too [5]. Piezoelectric materials exhibit a non-centrosymmetric structure in the tetragonal phase, i.e., there is no crystalline inversion symmetry. As such, these materials have a linear relationship between mechanical and electrical energy of the material [6].

Piezoelectric materials are primarily used as transducers to convert mechanical energy into electrical energy, or vice versa. To this end, they are employed in structural health monitoring applications for civil structures [7-10], and as industrial sensors and actuators [11-13]. Materials such as these are also used in passive devices such as embedded capacitors [14-17], and vibration based energy harvesting applications due to their ability to convert mechanical energy to electrical energy [11, 18, 19].

Research and innovation in piezoelectric and dielectric materials are currently motivated by the *Internet of Things* (IoT) [11, 18, 20] - namely devices, vehicles, buildings, etc. that are wirelessly connected via electronics, software, sensors and network connectivity. The realization of devices such as these that can transmit information, communicate wirelessly, and self-power themselves requires the development and optimization of advanced piezoelectric and dielectric materials. Also, systems such as these that employ sensors are powered using conventional batteries; which limit their operation cycle. Also, replacement of the batteries can prove problematic, especially if they are positioned in remote locations, such as structural sensors on a bridge or as tracking devices on moving objects [21]. Hence, it is desirable to use self-powered sensors in such applications. Piezoelectric energy harvesting devices provide an alternative to traditional battery powered systems, where they can be used to self-power themselves and other components within micro-electromechanical systems (MES), where they could be integrated into hybrid power systems [11, 22, 23].

Many materials express the piezoelectric effect, such as quartz, ceramics ($Pb(Zr_xTi_{1-x})O_3$, $BaTiO_3$) and various polymers (PVDF, P(VDF-Tr-FE). In most practical cases, however, ceramics are used because of their high piezoelectric strain

coefficient or d values [18]. For example, ceramic materials such as lead zirconate titanate (PZT) (d_{33} ~ 630 pC/N [24]) and barium titanate ($BaTiO_3$) (d_{33} ~191 pC/N [25]) have been widely used in several applications due to their high d_{33} values [26]. Polymers such as poly(vinylidene difluoride) (PVDF) have been used in place of ceramics due to their large g_{33} voltage coefficient (g_{33} ~ 0.14-0.22 V.m/N [27]), which make it a more sensitive material, i.e. requiring less force to prompt a piezoelectric response. However, PVDF possesses a much lower piezoelectric strain coefficient (d_{33} = 33 pC/N) [18, 25] in comparison to other ceramic piezoelectric materials (d_{33} = 630 PZT Navy VI [24])).

Homogenous ceramic piezoelectric materials have relatively high d_{33} constants but are limited in their application because of their high stiffness (51-59 GPa for PZT [24] and 1.6-2.2 GPa for PVDF [27]), poor mechanical properties, brittle nature and high processing temperature [18, 28]. Many applications, e.g. actuators [12, 13, 26] and sensors [29, 30], require compliant and flexible materials with lower mechanical impedance. Researchers have thus found that using polymer-ceramic composites that utilize the individual properties of both materials can alleviate some of the challenges associated with homogenous ceramic materials [31-33].

The composite piezoelectric materials of interest for this thesis incorporate lead zirconate titanate ($(Pb(Zr_xTi_{1-x})O_3$) particles within an epoxy polymer matrix forming a 0-3 connectivity pattern. However several challenges exist with 0-3 composites (1) it is difficult to uniformly disperse the ceramic particles within the polymer matrix, especially at higher filler volume fractions, (2) there is increased porosity within the composite due to the formation of voids which leads to premature dielectric breakdown and ineffective

polarization, and (3) a reduction in the overall dielectric properties (despite having increased flexibility and compliance). In order to overcome these obstacles, researchers have investigated adding an electrically conductive filler to the conventional 0-3 composite, thereby creating a 0-3-0 connectivity pattern [34-37]. All have reported an increase in the polymer matrix conductivity due to the addition of the electrically conductive fillers. However less is known about the morphology of the composite and surface properties of the electrically conductive particles, which influence the dielectric and piezoelectric properties of the composite. In this work we investigate the surface interactions between the surfaces of the particles such as agglomerations within the composite with the aid of scanning electron microscopy (SEM) and energy dispersive X-ray spectroscopy (EDS).

1.3. Research hypotheses

Piezoelectricity in ferroelectric ceramics in induced when an electric field is externally applied to switch the polar axis of the crystallites to the symmetry along the direction of the applied electric field, in a process called poling [38]. The most conventional form of poling, *parallel-plate contact poling*, requires the piezoelectric material have electrodes placed at the top and bottom surfaces of the material, and placed within an oil bath while applying an external direct current electric field. However this process poses many inconveniences: (1) the sample sides must have electrodes applied on each surface prior to application of electric field and (2) this process is limited to samples of small area [38]. Another disadvantage is, for porous samples, the air voids create an area of reduced electrical resistance within the composite which in turn leads to weak zones that are

vulnerable to dielectric breakdown, which facilitates the formation of conductive pathways through the material, which eventually impedes further poling.

An alternative poling approach that makes use of a corona discharge from a needle to pole the samples has been developed. The corona discharge technique aims at quashing these disadvantages by creating a contact free poling method. Furthermore the corona poling technique is not limited to small sample surface area and surface do not need to have electrodes and thereby eliminating shorting of the samples at the weak zones.

This thesis is motivated by two hypotheses. The first hypothesis is that the corona polarization process is more effective than the parallel plate polarization process in these three phase bulk composites. Less literature is available for application of the corona polarization technique to bulk materials. The second hypothesis is that the functionalization of the conductive aluminum inclusions will enhance the interfacial layer between the matrix and the particle, which will result in increased piezoelectric and dielectric properties.

Hence, the objectives of the thesis were to fabricate three phase PZT-Aluminum-Epoxy bulk composites and thick film and to study their dielectric and piezoelectric properties such as piezoelectric strain coefficients d_{33} and d_{31}, capacitance, dielectric constant and conductivity as a function of the volume fraction of the spherical inclusion. The influence of two different polarization techniques, the conventional contact poling method and the corona discharge technique on the dielectric and piezoelectric characteristics, was also studied. The effect of functionalizing of the spherical inclusion prior to its addition to the composite and its distribution was investigated with the help of scanning electron microscopy (SEM) and energy dispersive X-ray spectroscopy.

1.4. Overview of the structure of the thesis

The structure of the thesis is as follows: In Chapter 1 the background, research goal and motivation are provided. It also provides the objective of the thesis. Chapter 2 introduces the concept of dielectric, ferroelectric and piezoelectric materials while also providing a historical background of these materials, from their discovery to their evolution. Chapter 2 also explains the basic of composite piezoelectric materials and various connectivity patterns and different types of poling namely, contact and corona poling technique. Chapter 3 provides an overview of the literature review of PZT-Epoxy composites both two-phase and three-phase in the form of bulk form and films. This chapter aims at tracing the development of these materials over time. Chapter 4 provides the methodologies used for the fabrication and characterization of the bulk composite and thick film. It then delves into materials characterization followed by explaining the surface treatment of the aluminum inclusions. Chapter 5 outlines the results and their discussion from the experiments for bulk composites and thick film composites, and how varying aluminum inclusion influences the properties of the overall composite.

Chapter 2

Definitions and History of Dielectric Materials

2.1. Dielectric Materials

A dielectric material is one that is electrically insulating (nonmetallic) and exhibits or may be processed to exhibit an electric dipole structure, i.e. there is a separation of positive and negative electrically charged particles on a molecular or atomic level. The dielectric materials exhibit one of the following types of polarization, electronic, ionic and dipolar or orientation. The process of dipole formation, or alignment of already existing permanent or induced dipoles under the influence of an external electric field, is called polarization [39]. Dielectric materials can also exhibit interface or space charge polarization. The various polarization mechanisms are explained.

Within each atom or ion there is a positively charged nucleus surrounded by a negative electron cloud. The applied field causes the electron cloud to distort in one direction while the nucleus moves in the other direction. Since the center of the electron cloud no longer coincides with the nucleus, a dipole moment develops. This polarization mechanism is known as electronic polarization as shown in Figure 2.1 [40].

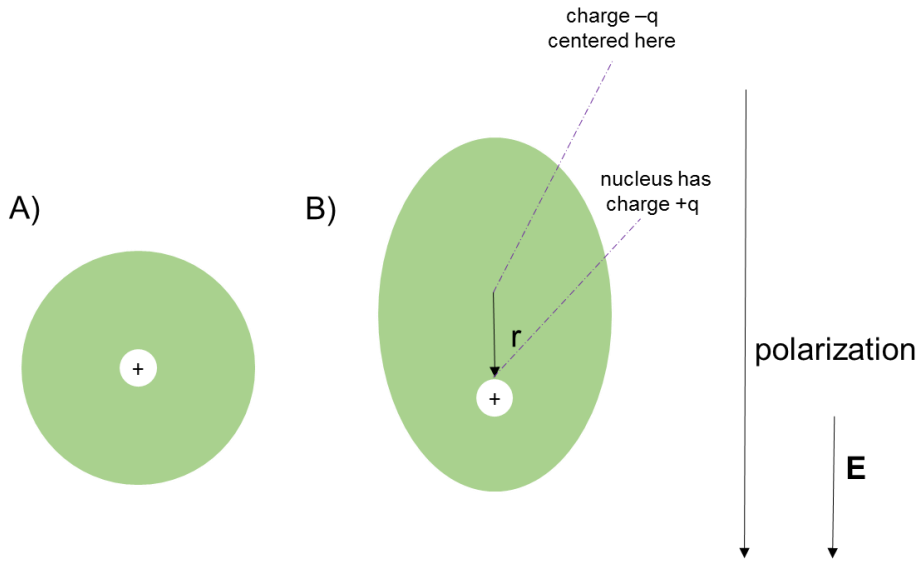

Figure 2.1: Schematic diagram of an A) atom or ion that has a positively charged nucleus surrounded by a negative electron cloud. B) The application of an electric field, *E* causes the electron cloud to distort in one direction while the nucleus moves in the other direction.

To undergo ionic polarization, a material must have an ionic structure that is it must be composed of cations and anions, as shown in Figure 2.2.

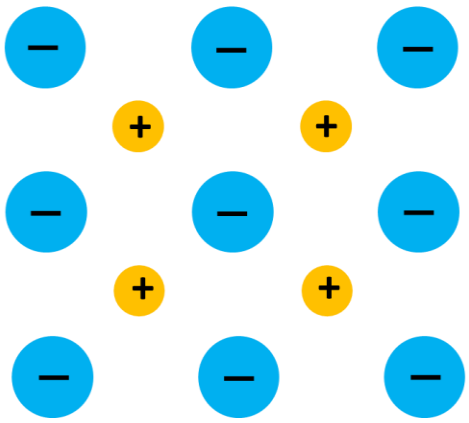

Figure 2.2: Representation of an ionic structure that is a structure composed of cations and anions, which is critical for a material to undergo ionic polarization.

Consider a cation and anion, of equal and opposite charges, held together by an ionic bond. This ion pair already possesses a dipole moment before the application of an electric

field, however the sum of dipole moments over the entire material, that is net polarization may still be zero. The applied field causes the ionic bond to stretch. If the material possessed a spontaneous polarization before the application of the field, this will cause it to increase by increasing the magnitude of the individual dipole moments. Similarly, if we reverse the direction of the field this causes a compression of the bond and thus decreases the dipole moment. This mechanism of ionic polarization is shown in Figure 2.3 [40].

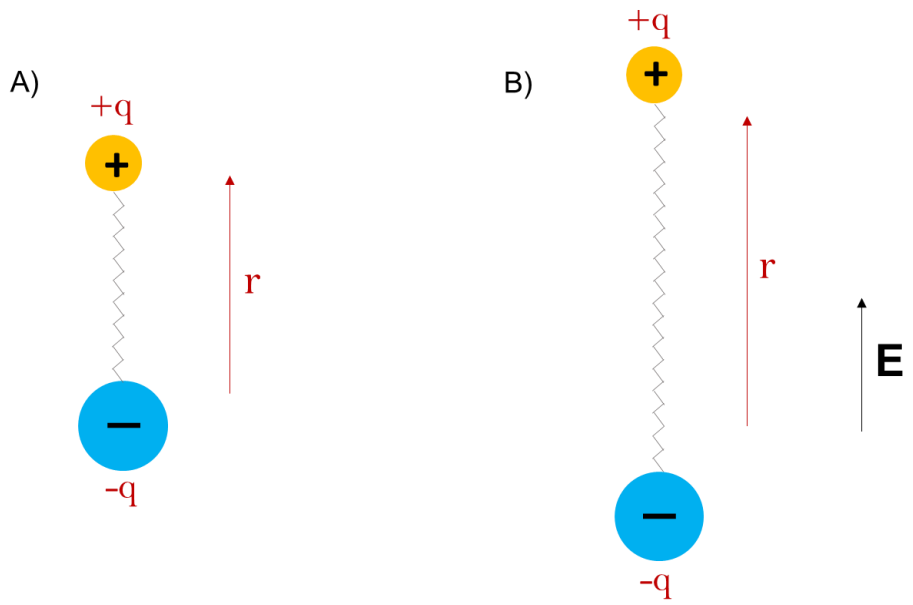

Figure 2.3: A) a simple case of a cation and an anion of equal and opposite charges, held together by an ionic bond, with a distance *r* between them. **B)** The application of an electric field causes the ionic bond to stretch thereby increasing the value of *r*.

Some molecules, such as H_2O possess a permanent dipole moment that is there is always a separation of charge within the molecule, even in the absence of an electric field as shown in Figure 2.4. Such permanent dipoles may also exist within ionic structures, such as crystals in which the cations are off-centered within the unit cells and do not coincide with the center of the negative charge [40].

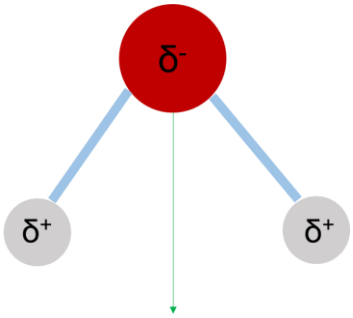

Figure 2.4: An example of H_2O, a molecule that possesses a permanent dipole that is there is always a separation of charge within the molecule even in the absence of an electric field. The permanent dipole is represented by an arrow for convenience.

These dipoles may be randomly arranged as a result of thermal motion, therefore the dipole moments from different molecules cancel out and the net polarization is zero as shown in Figure 2.5.

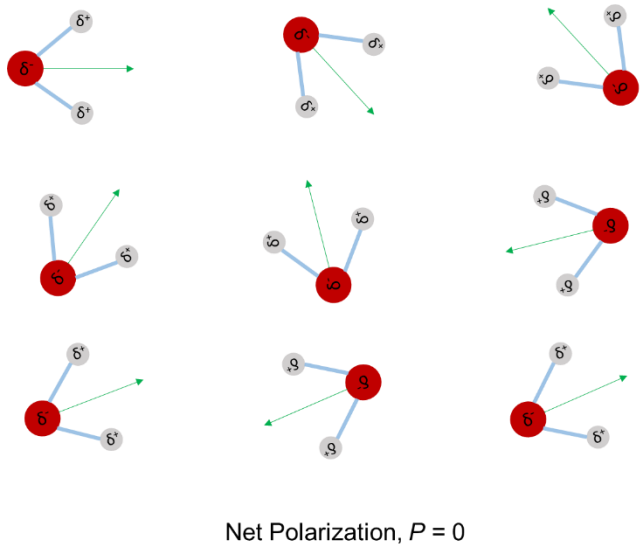

Figure 2.5: Molecules of water containing many dipoles randomly oriented resulting in a cancelation of the dipole moments leading to zero net polarization.

If an electric field is applied along a particular direction, then the dipoles rotate in order to align with the applied field. As a result, they also align with each other, thus the material develops a net polarization. This mechanism is explained in Figure 2.6.

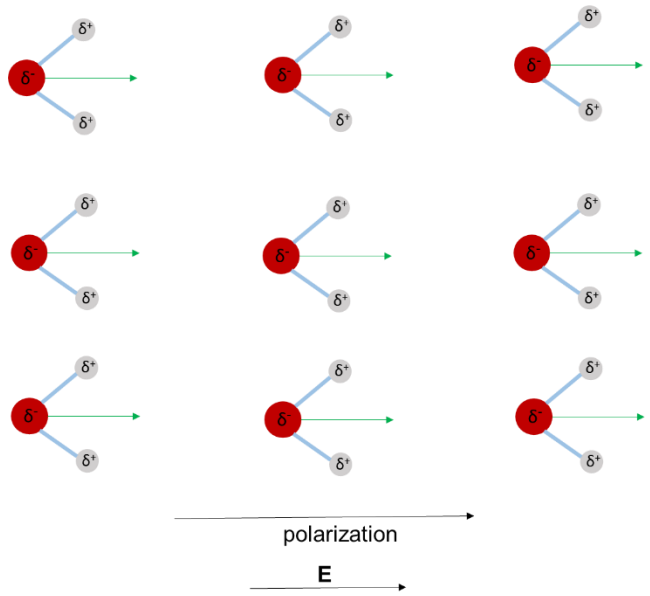

Figure 2.6: The dipoles rotate in order to align with the electric field as a result they align with each other. The dipole moments no longer cancel out leading to a net polarization.

Interface or space charge polarization involves limited movement of charges resulting in the alignment of charge dipoles under an applied electric field. This usually happens at the grain boundaries or any other interface such as an electrode-material interface [41]. This type of polarization occurs when there is an accumulation of charge at an interface between two materials or between two regions within a material because of an external field. This can occur when there is a compound dielectric, or when there are two electrodes connected to a dielectric material. This type of polarization is different from oriental and ionic polarization because instead of affecting bound positive and negative charges i.e. ionic and covalent bonding, interfacial polarization affects free

charges as well. As a result interfacial polarization is usually observed in amorphous or polycrystalline solids. This polarization mechanism is shown in Figure 2.7 [41].

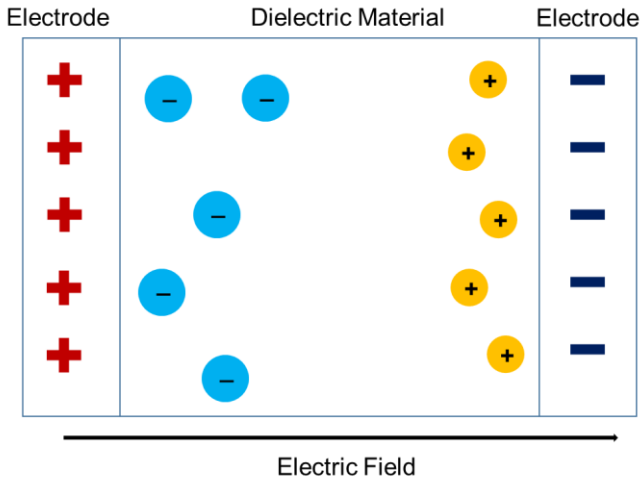

Figure 2.7: A schematic diagram showing how free charges can accumulate in a field, causing interfacial polarization. The electric field will cause a charge imbalance because of the dielectric's insulating properties.

There are two types of dielectrics, polar and non-polar dielectrics Polar dielectrics have a permanent electric dipole moment, i.e. the centers of the positive and negative charges are not overlapped. When an electric field E is applied to polar dielectrics, a torque is created, which causes the molecules to align in the direction of applied electric field, shown in Figure 2.8 [39].

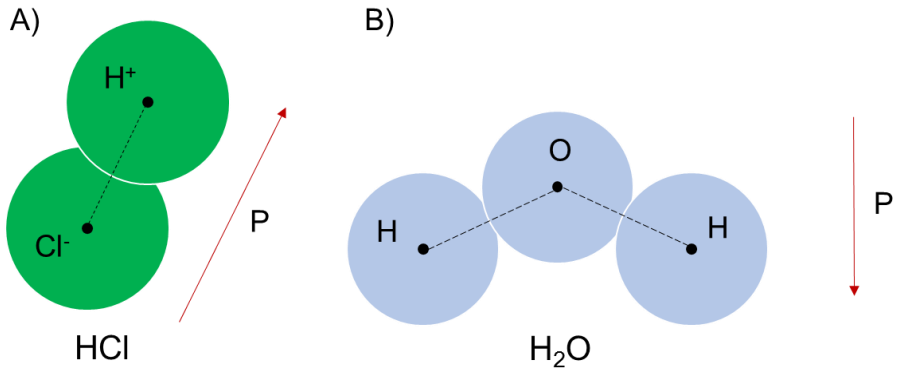

Figure 2.8: Molecules of **A)** HCl and **B)** H_2O both polar dielectrics, i.e. they exhibit permanent dipole moments. Upon application of an electric field a torque is created causing the molecules to align in the direction of the applied field.

Non-polar dielectrics are dielectrics that do not possess a permanent dipole moment, i.e. the centers of the positive and negative charges overlap each. Dipole moments can be induced in non-polar dielectrics when they are subjected to an external electric field as shown in Figure 2.9. The ability to polarize dielectric materials with the application of an electric field makes these materials useful for application in the capacitor industry because of their ability to increase charge storing capabilities [39].

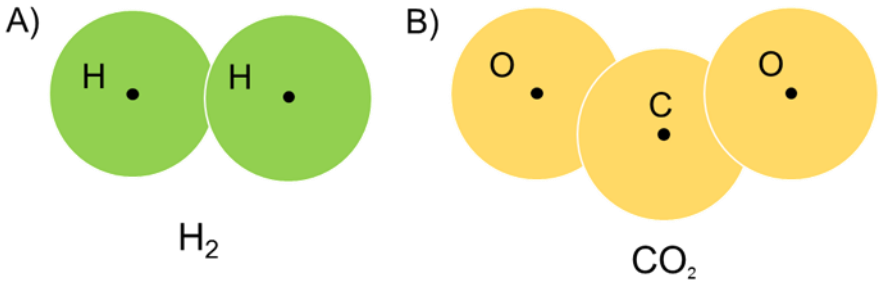

Figure 2.9: Two molecules **A)** H_2 and **B)** CO_2 both represent non-polar dielectrics, i.e. they do not possess a permanent dipole moment because the centers of the positive and negative charges overlap each other.

The relative complex permittivity (ε_r) is a dimensionless quantity, which compares the complex permittivity of a material (ε) to the permittivity of the free space ($\varepsilon_o = 8.854 * 10^{-12}$). It describes the interaction of a material with the electric field and consists of a real part ε_r', which represents the storage, and an imaginary part ε_r'', which represents the losses [42]. The real part of the permittivity (ε_r') is a measure of how much energy from an external electric field will be stored by the material and it is referred to as the dielectric constant. The imaginary part of the relative permittivity (ε_r'') is called the loss factor. It is a measure of how dissipative or lossy a material can be to an external electric field. When the relative complex permittivity is drawn as a vector diagram, the real and imaginary components are 90° out of phase, as can be seen in Figure 2.10. The vector sum ε_r forms an angle δ with the real axis (ε_r') [42].

$$\varepsilon_r = \varepsilon_r' - j.\varepsilon_r'', \tag{2.1}$$

$$\varepsilon_r = \frac{\varepsilon}{\varepsilon_o}. \tag{2.2}$$

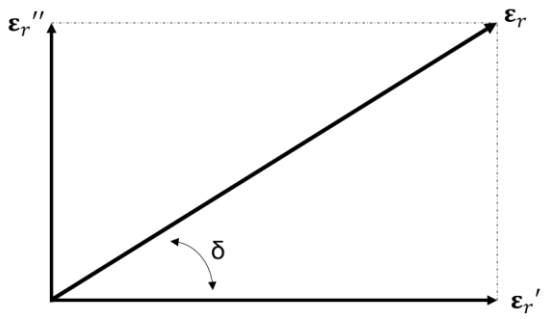

Figure 2.10: The complex relative permittivity vector diagram. The real part of permittivity, $\boldsymbol{\varepsilon_r'}$, and the imaginary part of permittivity, $\boldsymbol{\varepsilon_r''}$ are 90° out of phase. The vector sum forms an angle $\boldsymbol{\delta}$ with the real axis.

The tan δ, for a ceramic material is the tangent of the dielectric loss angle δ, and is determined by the ratio of effective conductance to effective susceptance in a parallel circuit [12]. The dielectric loss, *tan δ*, represents the damping capacity of the material, and describes the ability of the material to convert mechanical energy into electrical and heat energy, when subjected to an external load. It can be represented in the form of an equation,

$$\boldsymbol{\tan\delta = \frac{|E|\sin(\delta)}{|E|\cos(\delta)} = \frac{E''}{E'}}\ , \qquad (2.3)$$

where δ is the phase angle between the stress and strain, while E' and E" are the elastic storage modulus and elastic loss modulus, respectively [12]. The storage modulus represents the amount of mechanical energy stored during deformation while the loss modulus denotes energy lost as heat during the same deformation cycle.

Dielectric constants range over about four orders of magnitude in insulator materials (ε_r' of silicon dioxide, SiO_2 ~ 3.9 [43] up to ε_r' of calcium copper titanate, $CaCu_3Ti_4O_{12}$ ~> 250,000 [44])[31]. Gases, due to their low density have dielectric constants that are nominally equal to one (ε_r' for Propane ~ 1.00992 at 472.392 kPa and at 22.5 °C [45]) [31]. At one atmosphere, the dielectric constant of air is 1.0006 [31] . Most common ceramics and polymers have dielectric constants in the range between 2 and 10. Polyethylene is 2.3 and silica glass is 3.8. More ionic materials like sodium chloride (NaCl) and aluminum oxide (Al_2O_3) have slightly higher real relative permittivity (ε_r') values in the 6-10 range [31].

2.2. Ferroelectric Materials

Ferroelectrics are a class of dielectrics that exhibit spontaneous polarization i.e. polarization in the absence of an electric field. The spontaneous polarization of ferroelectric materials can be switched or reversed by applying an electric field in the opposite direction, this is known as ferroelectric switching. Ferroelectric materials undergo a structural phase transition to cubic phase at Curie temperature, thereby becoming paraelectric. All ferroelectric materials exhibit a P-E hysteresis loop [46].

Some of the major applications of ferroelectric ceramics are in dielectric applications which make use of their high permittivity, low dispersion and wide frequency range of response for compact multilayer capacitors, bulk, thick and thin film forms [47]. Its nonlinear hysteretic response is of interest in thin film nonvolatile semiconductor

memory [28, 48], and high permittivity films are also of interest in Dynamic Random Access Memory (DRAM) and chip packaging applications [49].

Ferroelectric ceramics was discovered in the 1940s in perovskite Barium titanate ($BaTiO_3$) ceramics where unusually high permittivity values (>1100) were observed and this was attributed to the phenomenon of ferroelectricity [50, 51]. The idea that $BaTiO_3$ exhibited ferroelectric nature proved invaluable when Gray *et al.* [52] discovered that an external electric field could orient the domains within the grains, thus resulting in a ceramic material that acted very similar to a single crystal possessing both ferroelectric and piezoelectric properties. This electrical aligning was termed as poling [46]. The poling process essentially converted in an inert ceramic into an electromechanically active material, and this led to the end of the notation that ceramics could not be piezoelectrically active because the randomly oriented crystallites would cancel out each other [46].

All ferroelectric materials exhibit a P-E hysteresis loop, i.e. polarization (P) versus applied electric field (E). As the applied electric field is increased, we can see a polarization also increase, almost linearly initially. Upon further application of electric field, the polarization starts to become nonlinear and eventually saturates, P_{sat} at a particular value of E. Increasing the electric field beyond this point would yield no greater polarization value. The P_{sat} value eventually drops to a value known as P_r or remnant polarization, this happens because some of the aligned diploes return to their original orientation. Now if the field is applied in the reverse direction, we see that the dipoles switch or reverse towards the direction of the field. This is known as ferroelectric switching, as the dipoles can be aligned in the opposite direction.

2.3. Piezoelectricity

Walter Guyton Cady defines Piezoelectricity as electric polarization produced by mechanical strain in crystals belonging to certain classes, the polarization being proportional to the strain and changing sign with it. That is if the pressure is replaced by a stretch (i.e. a reversal in sign of the pressure) the sign of the electric polarity becomes reversed too [5]. The 'piezo' in piezoelectricity, is derived from Greek, meaning 'to press', hence piezoelectricity is the generation of electricity as a result of mechanical stress.

Piezoelectricity was discovered in 1880 by Jacques and Pierre Curie whilst studying the effect of pressure on the generation of electrical charge by crystals, such as quartz, zincblende and tourmaline [53]. Their discovery was no mere coincidence; the Curie brothers were previously trying to study the relation between pyroelectric phenomena and crystal symmetry. This led them to not only look for electric charges but to also know in which direction pressure needs to be applied [54]. In 1881, the converse piezoelectric effect (that is the change of crystal shape upon application of an electric field) was mathematically predicted by Lipmann using thermodynamic principles and empirical data [55] The converse piezoelectric effect was later experimentally verified by the Curie brothers the following year [54]. In 1972, Paul Langevin, the French physicist, made use of quartz crystal to locate German submarines by creating a depth sounding device, and then after the war the same instrument was used to locate the debris caused by the ships he was trying to find [56]. In 1954, lead zirconate titanate ($Pb(Zr_{1-x}Ti_x)O_3$,,PZT)was discovered by Jaffe *et al.* which showed very strong piezoelectric activity near the morphotropic phase boundary (MPB), and to this day remains one of the most widely used piezoelectric ceramics [57].

All crystals can be classified into 32 crystal class or point groups, of which 21 are non-centrosymmetric and 20 of them are potentially piezoelectric, as shown in Figure 2.11. Of these 20 point groups, ten are polar, that is they exhibit a permanent dipole moment. Such materials have a spontaneous polarization. Thus these materials are also pyroelectric. Ferroelectric materials are a subset of pyroelectric materials in which the spontaneous polarization can be reoriented between crystallographically defined direction by application of an electric field [58]. Non-centrosymmetric crystals lack a center of symmetry, which is critical for the presence of piezoelectricity, because when the material lacks a center of symmetry, there will be a net displacement of the positive and negative ions with respect to each other (as a result of the stress) thereby producing electric dipoles, i.e., polarization [46]. The poling process defined as the process that electrically aligns the internal dipoles of the crystallites within the material by applying an external field.is an important technique that makes use of the piezoelectric effect in ferroelectric ceramics otherwise the ceramic would be inactive [46].

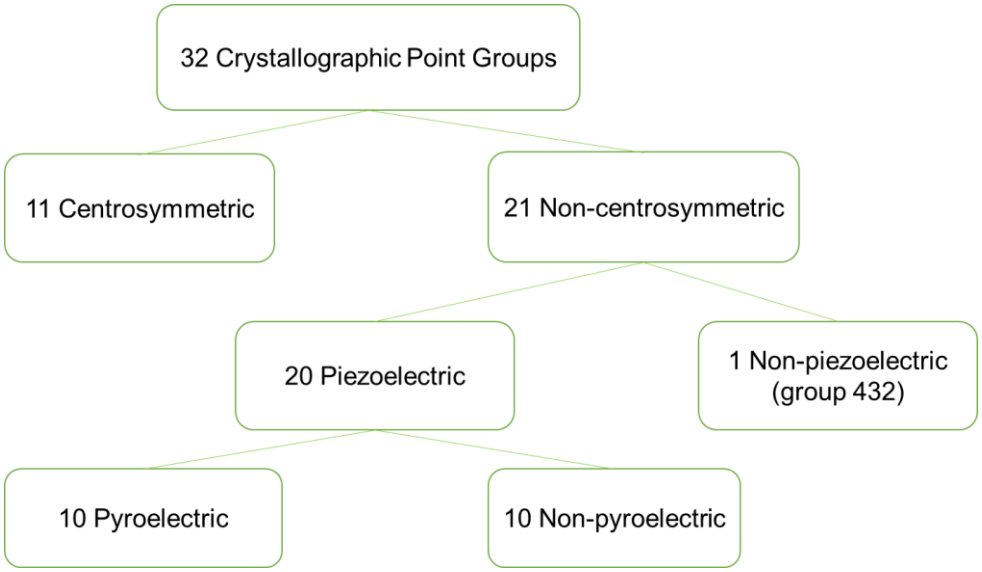

Figure 2.11: Symmetry hierarchy for materials exhibiting piezoelectricity. All crystals can be classified into 32 point groups, of which 21 are non-centrosymmetric. Of the non-centrosymmetric, 20 point groups are piezoelectric. 10 of these point groups are polar, which makes them a function of temperature, and hence they are pyroelectric.

The Heckmann diagram [39] which is depicted in Figure 2.12 is a triangle that explains the relation between different physical phenomena. In the three vertices we have field, stress and strain. The phenomena that yields and electric field upon applied stress is called piezoelectricity. But when this stress leads to polarization of charges on the surface, it is the dielectric piezoelectric effect. Applied electric field yielding a polarization is known as permittivity. When an applied field causes a material to strain then it is known as the converse piezoelectric effect.

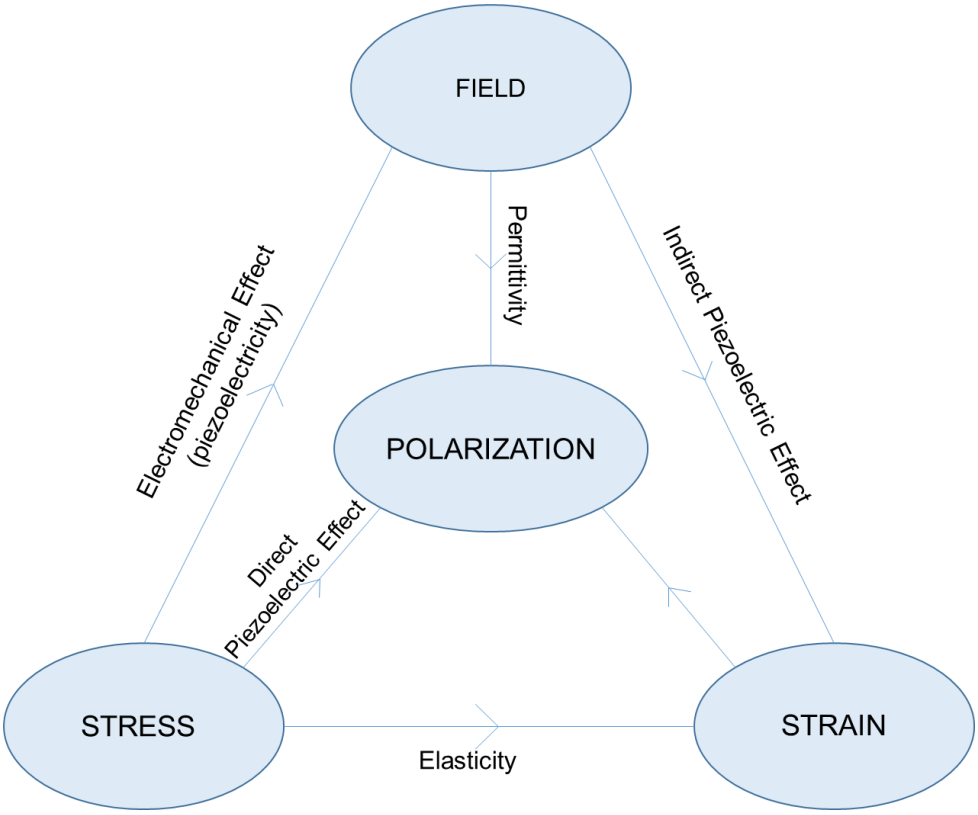

Figure 2.12: Heckmann diagram showing the interrelationship between various physical phenomena

There are primarily two effects in piezoelectricity, the direct piezoelectric effect (generator) and the converse or indirect piezoelectric effect (motor). The direct piezoelectric effect is the phenomenon where electrical charge is generated upon applied mechanical stress, whereas the converse effect is associated with the strain created upon application of an electric field [46].

$$D = dE + \varepsilon^T E, \quad (2.4)$$

$$S = s^E T + dE, \quad (2.5)$$

Where D is the dielectric displacement, T is the stress, E is the electric field, S is the strain, d is a piezoelectric coefficient, d is the material compliance, and ε the dielectric constant (relative permittivity) [59].

These physical properties also contain directional components and are usually followed by numerical subscripts to denote this. The piezoelectric strain coefficient d_{31} indicates that the polarization in the perpendicular direction i.e. 3 and the strain is developed in the lateral direction i.e. the 1 direction.

$$D_3 = d_{33}T_3 \quad (2.6)$$

$$S_3 = d_{33}E_3 \quad (2.7)$$

Piezoelectric materials have garnered interest in energy harvesting application due to their ability to withstand large amounts of strain. Large strains can potentially lead to greater mechanical energy, which in turn converts it to usable electrical energy. To create more available energy, it is essential that we use an effective coupling mode. There are two practical coupling modes, the *-31* mode and the *-33* mode. In the *-31* mode, a force is applied in a direction perpendicular to the poling directions, whilst in the *-33* mode the force is applied in the same direction as the poling direction. Although the *-33*

mode is more robust and has a higher coupling coefficient, the *-31* mode yields a higher overall power output [21].

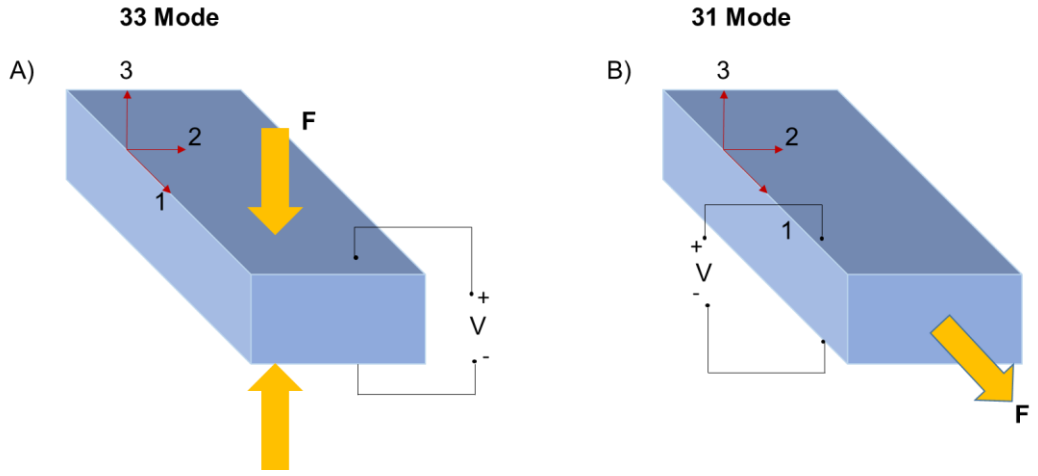

Figure 2.13: Two coupling modes are shown **A)** -33 mode in which the force applied in the same direction as the poling direction. **B)** -31 mode in which the force is applied in a direction perpendicular to the poling direction.

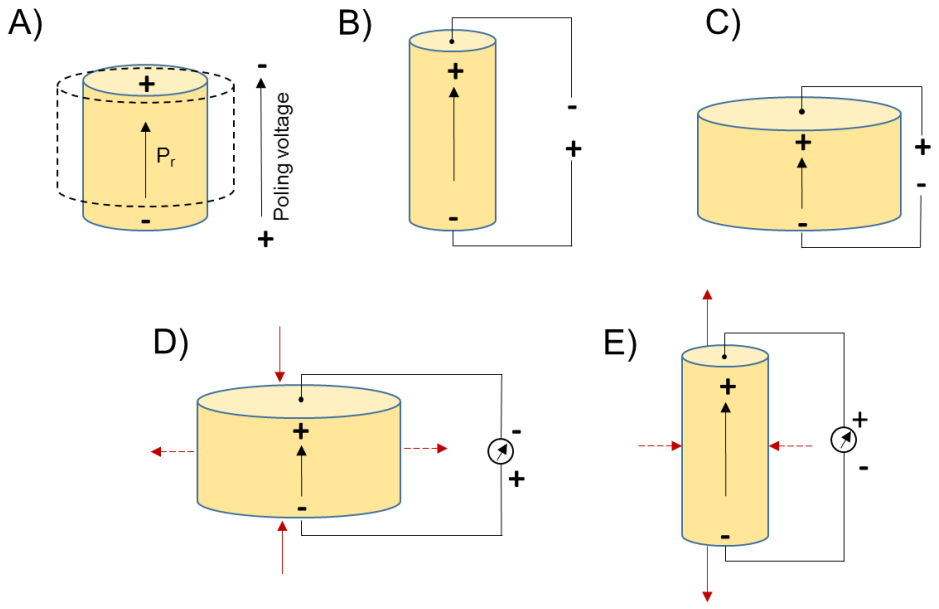

Figure 2.14: A) Piezoelectric material before (dotted) and after poling **B)** strain in material upon applied electric field **C)** strain upon changing polarity of applied field **D)** generated voltage with polarity similar to poling **E)** generated voltage with polarity opposite to poling voltage.

A Venn diagram is used to summarize the above definitions and to help in understanding the interrelationship between these materials as shown in Figure 2.15: [60]. From this we can conclude that all ferroelectric materials are pyroelectric, all pyroelectric materials are piezoelectric and all piezoelectric materials are dielectrics, but their converse is not true.

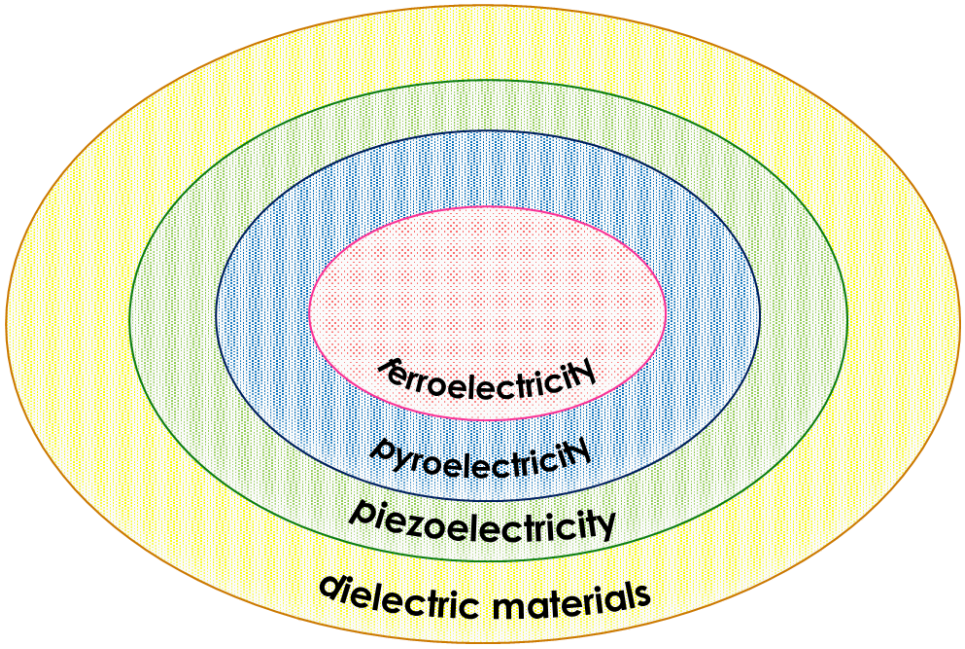

Figure 2.15: Venn diagram describing the interrelationship between different types of materials [19]

2.4. Perovskite Structure

Oxygen octahedron structures exhibit strong ferroelectric properties and have are consistent in high temperature ranges. One of the simplest models of this type of structure is the perovskite structure, denoted as ABO_3, as shown in Figure 2.16. Perovskite electroceramics are primarily used bulk capacitors, piezoelectric transducers and are increasingly being used in thin film applications.

In a cubic array, a perovskite structure shows high symmetry (m3m), and the larger cation is 12-fold coordinated with respect to oxygen, while the smaller cation is octahedrally coordinated with oxygen. Once the perovskite structure distorts, a phase transition occurs and leads to the development of a spontaneous polarization i.e. ferroelectricity. It is evident that polarization occurs when the centers of the positive and negative charges within the unit cell are no longer coincident. In the case of $BaTiO_3$, which shows a perovskite structure, at room temperature polarization occurs when the Ti^{4+} ion moves along the <001> of the cubic lattice towards the oxygen ions.

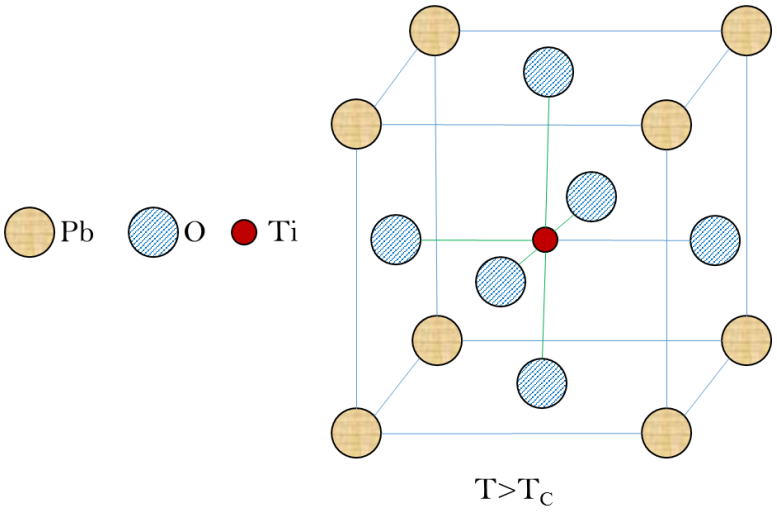

Figure 2.16: Unit cell for a typical cubic perovskite Lead zirconate titanate (PZT) in the cubic Pm3m phase above T_c [8]

In ferroelectric materials, it is possible to orient the direction of the domain walls within the grain or the spontaneous polarization with the aid of an applied electric field, this is termed as poling. When the electric field is removed the polarization does not return to its original orientation as there is no restoring force. The larger the applied field, the orientation becomes more parallel to the electric field and this leads to larger

piezoelectric coefficients. When polarization occurs, the material will elongate in the direction and will contract in the transverse direction as shown in Figure 2.17.

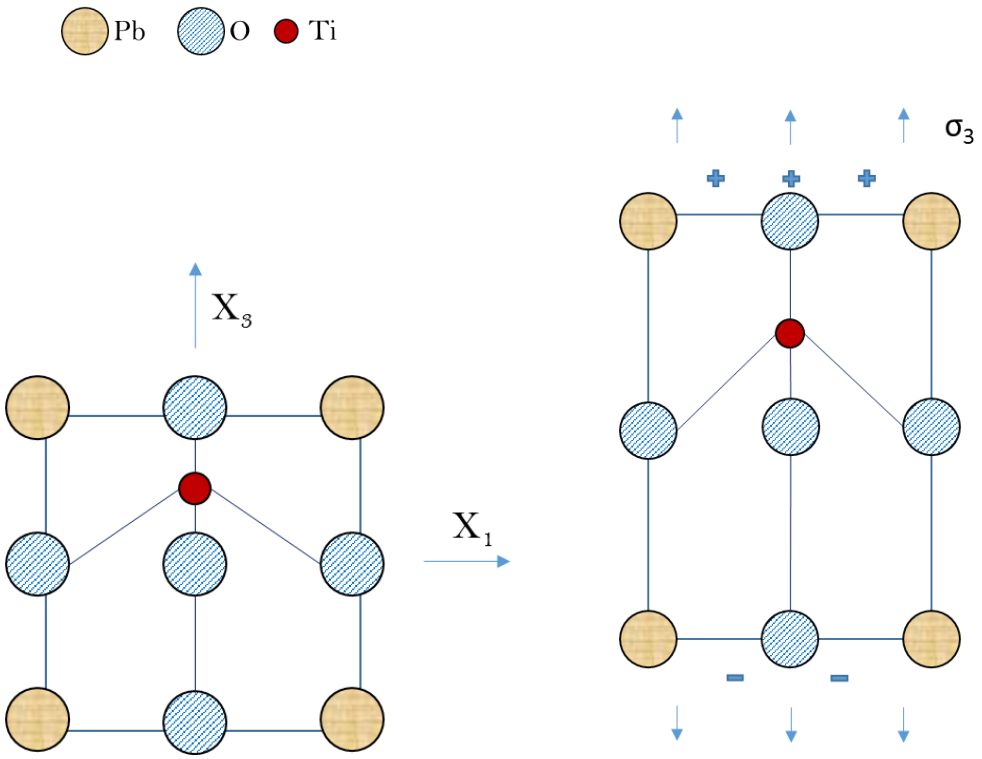

Figure 2.17: Piezoelectric response in a single domain PbTiO3 crystal (a) when there is no field (b) shift of the Ti^{4+} cation away from its original position upon application of stress

Lead zirconate titanate, $PbZr_{1-x}Ti_xO_3$ or PZT is the most widely used piezoelectric material and the most commercially important ceramic [58] because it boasts very high relative permittivity values and possesses strong piezoelectric coefficients[61-63]. PZT is formed by the solid solution of $PbTiO_3$, which is anti-ferroelectric and $PbZrO_3$, which shows limited piezoelectric characteristics. So it came as a surprise to most researchers that their combination yielded a material that displays significant piezoelectric properties and it remains an interesting case right from its discovery [64], to its development [57]

and to this day [58]. The $PbZr_{1-x}Ti_xO_3$ (PZT) solid solution is a perovskite system as can be seen in the phase diagram of PZT is shown in Figure 2.18:

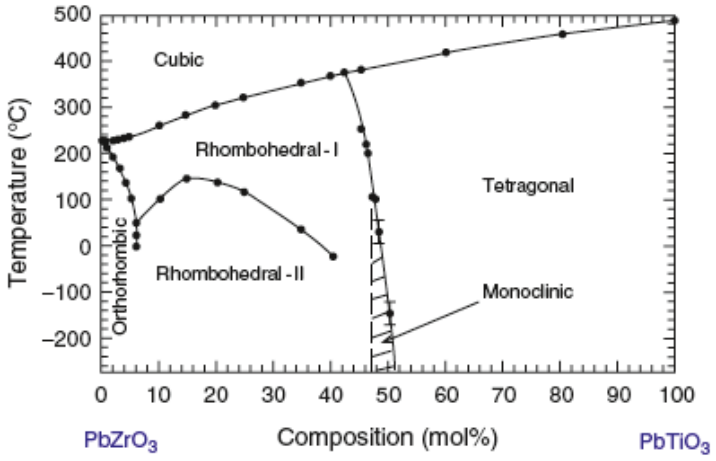

Figure 2.18: PZT phase diagram showing different phases with varying temperature, also we can see the Morphotropic Phase Boundary (MPB) as Ti4+ concentration becomes 48 mol% [20, 25, 26].

PZT possesses a rhombohedral structure at high temperatures, but once it begins to cool below the Curie temperature, it takes up a tetragonal structure, as can be seen in Figure 2.19 In this form the center zirconium or titanium atom is displaced out of the geometric center, giving rise to a permanent charge displacement giving rise to piezoelectricity [18, 62].

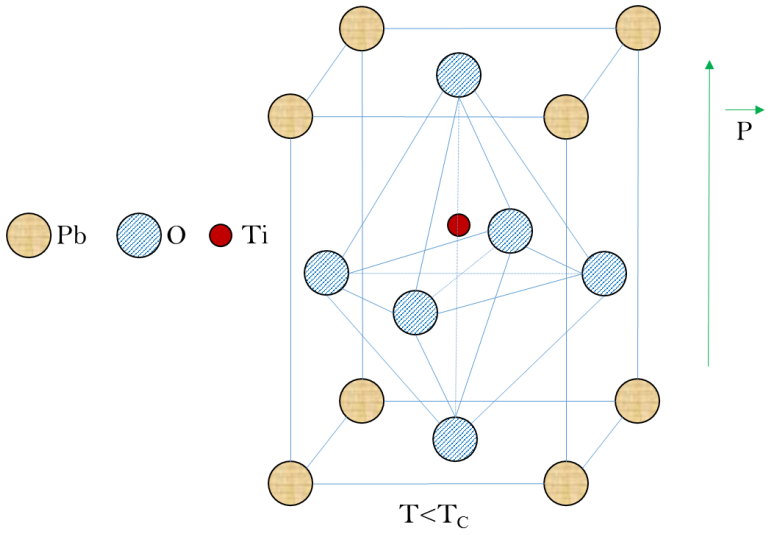

Figure 2.19: A schematic diagram of PZT which shows a tetragonal structure below the Curie temperature i.e. for T<Tc. The displacement of the Ti^{4+} cation yields in a net dipole moment and leads to polarization.

2.5. Poling Process

The aligning process discovered by Gray *et al.* [52] that orients the domains within a grain by applying an external electric field is termed as poling i.e. it's a process that induces piezoelectricity in ferroelectric ceramics by applying an electric field to switch the [polar axis of crystallites to the symmetry-allowed directions nearest to the applied field [38]. Poling is the process that converts inert ceramics into electromechanically active materials [46]. Poling is an important step in obtaining the desired piezoelectric properties of the material. In composites that are polymer based poling is carried out at its glass transition temperature, by gradually heating it and by placing it in a strong static external electric field [65, 66]. The temperature at which poling takes place and the applied field strength are critical parameters in defining the electromechanical properties of the poled material. Both the temperature and the applied field are required to reduce the energy band gap in order to orient the domains in the direction of the field. Most

multiphasic composites have been traditionally poled using the contact poling method. In this poling method, the material is in direct contact with the poling electrode/needle. However there are some disadvantages with this technique as it can cause dielectric breakdown of the composite material, especially when the composite has conductive inclusions [65, 66]. Also in this method the samples are required to place inside a silicone oil bath for uniform heating of the sample. In order to overcome the challenges of this method, researchers [38] have developed the corona discharge poling method where a high poling voltage is applied to the air molecules above the sample, thereby eliminating physical contact. Researchers have also shown that higher voltages can be achieved by the corona poling method in comparison to traditional contact poling method [66, 67].

2.5.1 Contact Poling

This is the conventional poling method by which piezoelectric ceramics and composites are poled by applying a large dc voltage. This poling method requires physical contact of the live electrode with the sample electrode and with the application of a very large electric field the sample will be poled. However application of large dc fields to polymer matrix composites often cause dielectric breakdown of the sample. The samples are placed in a silicone oil bath and uniformly heated throughout up to its glass transition temperature as shown in Figure 2.20:. The samples need to be coated with a top electrode for this method in addition to a bottom electrode and poling is usually limited to samples of smaller area [38]. One of the major drawbacks of this method in addition to the dielectric breakdown is the local breakdown at weak spots, such as pinholes, short-circuits the electrodes and prevents further poling. In order to improve this form of poling the corona discharge technique was developed [38].

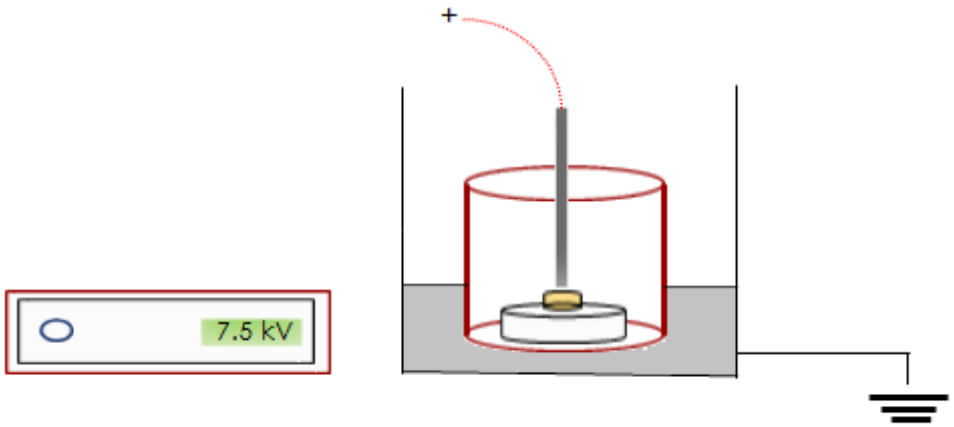

Figure 2.20: Contact poling setup for electrically aligning samples. The poling electrode is in contact with the sample top electrode. The base plate on which the sample rests is grounded.

2.5.2 Corona Poling Method

In the corona poling technique, charge from the corona point/needle is sprayed onto the surface that has no electrode, creating an electric field between the sample surfaces. Because of the absence of electrodes there is no shorting of the sample at weak spots, further higher poling voltages can be achieved. This method also allows samples of larger area to be poled and may be adapted to a continuous process for mass production. Here the live wire is connected to the corona discharge needle, and the base plate upon which the sample is rests is grounded as shown in Figure 2.21:. The fine tip of the corona needle ensures that nearby air molecules are ionized. The entire poling setup is placed inside a protective casing. This ensures that the ionized air molecules do not make contact with surrounding objects. The distance between the needle and sample is a critical experiment variant and studies have shown that different distances can influence the poling procedure significantly [38]. So for these experiments the corona needle distance from the sample was kept constant at 10 mm to ensure experiment repeatability and eliminate experiment variability.

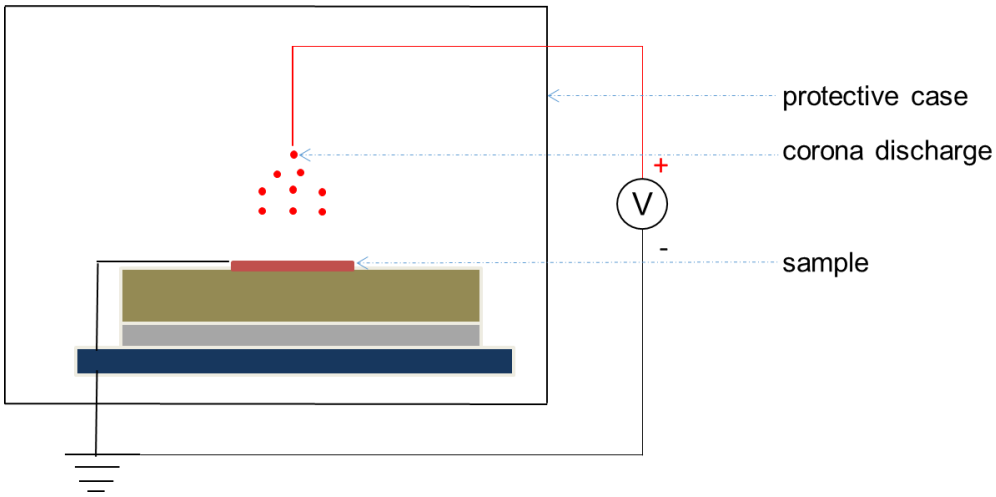

Figure 2.21: Corona discharge technique, the live wire ionizes the surrounding air molecules onto the sample surface without the electrode. There is no physical contact between the corona needle and the surface of the sample.

2.6 Composite Piezoelectric Materials

Piezoelectric ceramic/polymer composites, also known as piezocomposites have been developed over the past few decades mainly because they have shown superior properties when compared to single-phase materials [68]. Piezocomposites especially combine high coupling, low impedance, low mechanical quality factor and an intermediate dielectric constant, thereby proving to be excellent candidates for electromechanical transducers, in addition to better flexibility [68]. A summary of the advantages and disadvantages of using polymer/ceramic composites is listed in Table 2.1

The connectivity which is the microstructural arrangement of the individual components was first reported by Newnham *et al.* [69] and later modified by Pilgrim *et al.* [33], it can be defined as the number of dimensions in which a phase within the composite is self-connected [68]. Within passive polymer matrices, they randomly

distributed ceramic particles. By virtue of doing this they were able to establish multiple connectivity patters between the polymer and ceramic materials giving rise to distinct properties. A polymer matrix with ceramic fillers would represent a 0-3 connectivity pattern, with the digit representing the number of dimensions of that phase within the composite. The connectivity is a critical parameter that determines the electromechanical performance of the composite. For a composite that contains two phases, there are a total of sixteen different connectivity patterns that can be accomplished. For example, if we have a 0-0 composite, then neither phase is self-connected, if we have a 3-3 then each phase is self-connected in three dimensions. In this representation, the first digit refers to the dimension of the piezoelectric ceramic, also known as the active phase and the second digit represents the dimension of the polymer or inactive phase. A schematic representation is shown in Figure 2.22.

Most research has been limited to the 0-3 connectivity, where randomly dispersed ceramic particles are embedded into a three dimension polymer matrix. 0-3 composites have gained popularity owing to their flexibility, ease of processing and use in embedded passive devices [14, 17, 70]. Two phase, or diphasic composites, such as metal/polymer and ceramic/polymer have been extensively investigated [71-74].

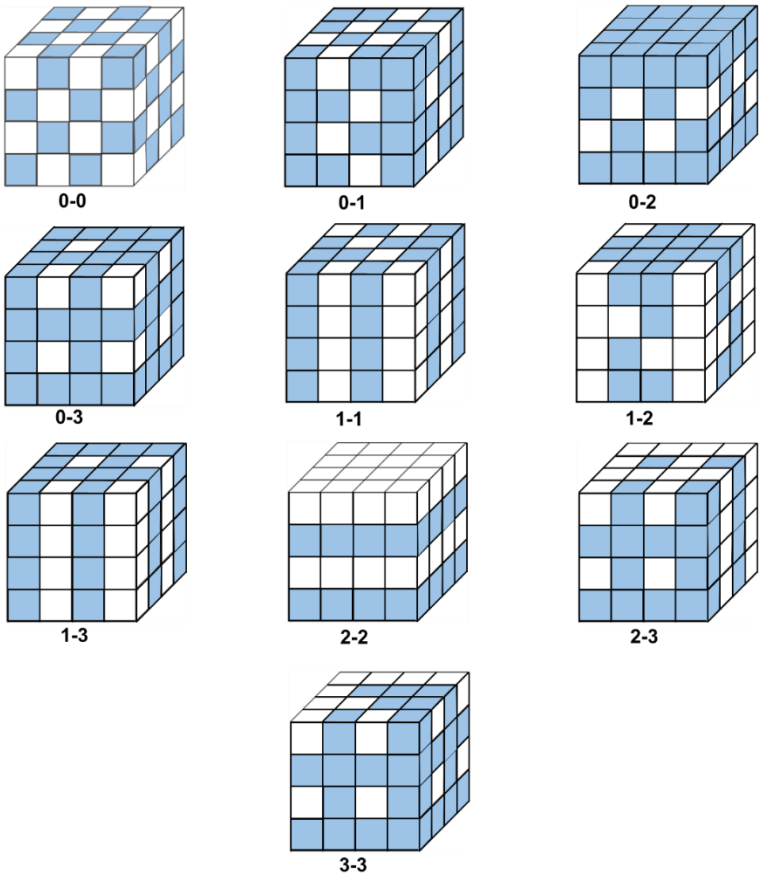

Figure 2.22: Ten different connectivity patterns of diphasic composites, the digits represent the number of dimensions in which the phase within the composite is self-connected. In this representation, the first digit refers to the dimension of the piezoelectric ceramic, also known as the active phase and the second digit represents the dimension of the polymer or inactive phase.

This convention can also be extended to accommodate a third phase by incorporating a third digit, so we can have a 0-3-0 composite that will have a two phases as particles dispersed within a matrix. Several researchers have looked at introducing conductive fillers into the composite as a third phase, and have reported an increase in the conductivity of the polymer matrix [75, 76].

Table 2.1: Advantages and Disadvantages of Piezoelectric Ceramic, Polymers, and Composites [32, 68]

Parameter	Ceramic PZT	Polymer PVDF	Ceramic/polymer
Acoustic Impedance, Z 10^6 kg/m^{2}s	High 33.7 [77]	Low 3.9 [77]	Low
Coupling Factor, k_p	High 0.68 [24]	Low 0.2 [77]	High
Piezoelectric strain coefficient d_{33}/-d_{31} pF	High 630/276 [24]	Low 30/18 [27]	Medium
Dielectric constant, ε_r	High 3300 [24]	Low 11.5 [27]	Medium
Flexibility/Brittleness Modulus of elasticity (GPa)	Stiff 51-59 [24]	Flexible 1.6-2.2 [27]	Flexible

2.7 History of industrial application of piezoelectric materials

The number one technique for medical imaging and non-destructive evaluation (NDE) is ultrasound. There have been several innovation in ultrasound, such as stimulated elastography, magnetic resonance imaging (MRI) and ultrasound therapy [32, 58]. These techniques can only come to fruition if specific transducers are designed and developed. The performance of a transducer can be evaluated using (1) electrical input impedance, (2) electroacoustic response and (3) radiation pattern. Piezoelectric materials are the most common materials that are used to develop transducers for these applications, and the geometry and size of these materials are of significant importance, since they influence all the properties. Lead zirconate titanate (PZT) based compositions such as PZT-polymer composites are the most efficient compromise for the vibration modes used in medical diagnosis and NDE applications [58]. The design of these transducers essentially consist of an active material, i.e. the piezoelectric material and a

rear face or the backing material. The backing material not only acts as a mechanical support for the active material, but also is a filter for acoustic energy to flow by the rear face and thus induces damping of the transducer, and the closer to the acoustic impedance is between the two materials the lower the efficiency. Which is why the active material is usually PZT based material and the backing layer is a high loss polymer, such as epoxy resins. Even today a combination of these two materials possesses the best performance trade-off that no material can achieve [58].

An electroacoustic transducer is a device that converts acoustic energy (sound) into electrical energy (voltage or current) or vice versa. When the transducer is used to generate sound, it is known as a transmitter. When it is used to detect sound, it is called a receiver. When these receivers are used to detect sound underwater, then they are known as hydrophones. The purpose of the hydrophone is to measure extremely weak hydrostatic pressure waves using large area sensors. For hydrostatic pressure, the normal stress values are all equal as shown in equation 2.8.

$$X_{11} = X_{22} = X_{33} = -p. \tag{2.8}$$

The change in polarization is given by,

$$P_3 = d_{33}(-p) + d_{31}(-p) + d_{31}(-p), \tag{2.9}$$

$$= (d_{33} + 2d_{31})(-p), \tag{2.10}$$

$$= d_h(-p), \tag{2.11}$$

where d_h is called the hydrostatic piezoelectric charge coefficient. The voltage generated by the hydrophone, is given by 2.12, and the figure of merit is the product of $d_h g_h$ and is given by equation 2.13.

$$g_h = \frac{(d_{33} + 2d_{31})^2}{\varepsilon_{33}}, \quad (2.12)$$

$$d_h g_h = \frac{(d_{33} + 2d_{31})^2}{\varepsilon_{33}}. \quad (2.13)$$

For a high sensitivity PZTs (PZT 5A) [28], there is a near cancellation between $d_{33} \approx -2d_{31}$, and hence the PZT alone is not a good enough hydrophone material. On the other hand, if we create a composite with dielectric constant approximately in the region of 10, we can enhance the voltage coefficient, due to the reduced overall dielectric constant. This is how industrial hydrophones are manufactured [28].

2.8 Use of spin coat and deposition for films in industry

The spin coating technique is currently the predominant technique employed to produce uniform thin films with thickness of the order of micrometers and nanometers [78]. The pioneering analysis of spin coating was performed over fifty years ago my Emslie *et al.* [79] who proposed the spreading of a thin axisymmetric film of Newtonian fluid on a planar substrate rotating with constant angular velocity. In most common scenarios, the coating material is polymeric and is applied in the form of a solution from which the solvent evaporates [78].

This process is widely used in the manufacture of integrated circuits [80], optical mirrors, television screens and as a magnetic discs for DRAM applications and data storage [81]. The centrifugal force drives the liquid radially outward, and the viscous force and surface tension causes a thin residual film to be retained on the flat substrate. Spin coating has also been widely used in the semiconductor industry [82]. Circuit

designs are generally imprinted on the silicon by the process of photolithography, where circular semiconductor wafers are coated with thin polymeric photoresist films that are then exposed through masks to transfer the circuit design to the silicon. The process of layering this photoresist material onto the wafer is achieved by spin coating. Compared with other nano-surface-texturing techniques, spin coating possesses several advantages for controlling the mechanical and tribological properties such as adjustable nano-texture surfaces, size and density [83].

Chapter 3

Literature Review

3.1. Bulk Composite

Two-phase piezoelectric composites, *so-called* 0-3 connectivity composites comprised of piezoelectric particles embedded within a continuous polymer matrix, have attracted much attention due to their flexibility and ease of processing [84, 85], and applications to dielectric [1, 75], sensing/actuating [12, 23, 86], energy harvesting [11, 84, 87] and acoustic damping [88-90] applications. However, these materials suffer from relatively low values of piezoelectric and dielectric properties due to the inherent insulative properties of the polymer matrix phase [71, 72, 91, 92], which is associated with difficulties in poling of these materials [93] and contact resistance at the particle/matrix interface [1, 2]. Hence, researchers have begun to investigate three-phase materials comprised of piezoelectric and electrically conductive particles embedded with a continuous polymer matrix [94]. In some cases, these *so-called* three-phase (0-3-0 connectivity) composites have demonstrated enhanced dielectric, piezoelectric and acoustic dampening when close to the percolation threshold [95, 96].

In this thesis, the influences of three entities on the piezoelectric and dielectric properties are observed: volume fractions of constituent phases (PZT and Al), poling technique (contact and contactless - Corona) and surface treatment of the electrically conductive phase. The volume fractions of PZT and Al were varied from 0.1 to 0.3 and

0.01 to 0.17, respectively. Composites were independently contact and Corona poled. Also, composites that included non-surface treated Al particles were compared to those that included surface treated Al particles. A detailed time study was conducted to elucidate the optimal time for surface treatment of the Al particles. The piezoelectric strain coefficients and effective dielectric constants were observed to identify the percolation threshold of the Al particles with the piezoelectric polymer composites.

Many researchers have studied the influence of conductive fillers on 0-3 composite materials and the formation of percolated networks of these fillers. However, less is known about the role that poling technique (contact and Corona) plays on the piezoelectric and dielectric properties of three-phase materials. For example, several researchers have studied the influence of electrically conductive inclusions on piezo-damping and related it to the electrically conductive network (percolation) formed by the inclusions. Piezo-damping is the conversion of mechanical vibration energy to electrical energy (in piezoelectric materials), and subsequent conversion of electrical energy to heat. Zhang *et al.* and Ding *et al.* [97, 98] fabricated two-phase chlorinated polyethylene (CPE) barium titanate and CPE and 2'-methylene-bis-(4-methyl-6-cyclohexylphenol) composites and compared the piezo-damping of these materials to those where electrically conductive vapor-grown carbon fibers (VGCF) were added. It was concluded that the piezo-damping effect was directly related to the electro-conductive network formed by the carbon fibers within the polymer matrix. It was found that the this network contributed to increased loss factors, *tan δ*, and more efficient damping [99]. Liu et al. [100-102] prepared composites using a hot press technique that were comprised of lead zirconate titanate (PZT), polyvinyl chloride (PVC) and additives such as graphite, carbon

nanotubes and carbon black. It was also shown that the optimal longitudinal piezoelectric strain coefficient, d_{33} (22 pC/N for graphite, 20 pC/N for carbon black), was obtained close to the percolation threshold values (volume fraction = $v_g = 0.005$ for graphite, $v_c = 0.5$ for carbon black) of the electrically conducting additive. It was also concluded that the addition of graphite, carbon black or carbon nanotubes reduced the coercive field of the composite. Choi *et al.* [95] prepared composites, which were comprised of barium titanate, polymethyl methacrylate (PMMA) and nickel using a two-step mixing and hot-molding process. It was found that the size of the nickel particles played a role in the dielectric constant, wherein composites that contained smaller sized nickel particles (4 μm) had higher dielectric constants and dielectric loss near the percolation threshold, in comparison to composites that contained larger sized particles (40 μm).

Similarly, Banerjee *et al.* explored the dielectric properties of two-phase composites that incorporated a third electrically conductive phase (aluminum [1, 2, 12, 75] and multi-walled carbon nanotubes [3]). It was found that the inclusion of electrically conductive particles within a two-phase piezoelectric composite (PZT and epoxy) resulted in enhanced piezoelectric and dielectric properties, with corresponding increases in dielectric loss of the material. Also, it was concluded that the electrically conductive filler size, distribution and particle-matrix resistance play key roles in the dielectric and piezoelectric properties of the composites. It is well known that aluminum, when exposed to air forms an Al_2O_3 shell around the Al core. As a result, the Al particle instantaneously forms positive charges in the core and negative charges around the shell due to charge transfer from Al to absorbed O_2 [4], which affects the properties of the interface

between the Al and the epoxy matrix and consequential piezoelectric and dielectric properties of the composite.

Hence in this thesis, a time study of the surface treatment of Al particles was conducted. This study was performed to understand the role of the particle/matrix interfacial properties on composite piezoelectric and dielectric properties. In addition, the piezoelectric and dielectric properties of bulk PZT-Al-epoxy composites are observed as functions of frequency and poling method.

Table 3.2 Dielectric and piezoelectric properties of the PZT polymer composites and comparison with those of previous workers [100-106].

Sample	Volume Fraction % PZT/Epoxy/ Al	Dielectric constant, εr	d33 (pC/N)	Reference
PZT/DEGBA Epoxy/Al (Control 2)	40/47/13	~270	0.99	This work
PZT/DEGBA Epoxy (data set G)	40/60/0	~134	1.36	This work
Control 2, PZT/DEGBA Epoxy/Al (data set H)	40/47/13	~305	2.32	This work
PZT/DEGBA Epoxy/Al (data set I)	40/47/13	~420	3.48	This work
PZT/PVC	50/50/0	43.7	13.0	Liu et al. (2005)
PZT/PVDF	50/50/0	68.1	14.0	Liu et al. (2005)
PZT/PVDF/C	50.0/0.5/49.5	47.8	20.0	Liu et al. (2005)
PZT/PVDF	50/50	56.0	14.0	Wang et al. (2000)
PZT/PVDF	50/50	95.0	13.8	Venkatragavaraj et al. (2001)
PZT/Polyester	50/50	52	18	Nhuapeng et al. (2002)
PZT/epoxy resin	37/63	15	25.3	Thamjaree et al. (2005)

3.2. Thick Composite Films

Interest in ferroelectric films has increased over the last 20 years because of the exciting possibility of using them for non-volatile memory applications [14, 107], MEMS [11, 23, 26] and ultrasonic devices [26, 108]. The properties if piezoelectric films cannot be compared directly with those of the bulk materials because their processing and electrical properties differ from their bulk counterparts. Ferroelectric films are part of a hybrid structure (ferroelectric film and non-active substrate), wherein the strain across the film-substrate interface must be continuous, i.e. perfectly affixed to the substrate in the film plane, and also free to move in the off-plane direction [26]. Previous work on preparation of piezoelectric films involved techniques such as RF planar magnetron sputtering [109, 110], ion beam sputtering [111] or DC magnetron sputtering [112]. Most recently, researchers have succeeded in fabricating films using various chemical methods of deposition such as; metal-organic-chemical vapor deposition (MOCVD) [113-115], chemical solution deposition [116, 117], metal-organic decomposition (MOD) [118, 119], and also pulsed laser deposition (PLD) [120-122]. Of all these methods sol-gel method is preferred in applications because it offers compositional control, reduced temperature processing of highly uniform, dense, crack-free films and low cost of fabrication [123, 124]. These methods of processing ferroelectric films have been used with notable success to produce piezoelectric ceramic films comprised of Lead-Zirconate-Titanate ($PbZr_xTi_{1-x}O_3$ also known as, PZT). PZT has a high dielectric constant, ferroelectric, piezoelectric, and pyroelectric properties. The aforementioned ideal properties of PZT have made its application to transducer, sensor and actuator devices ubiquitous. However, the poor mechanical strength of these devices has limited their life

cycle and performance. Therefore, interest in polymer-ceramic [1, 2, 12, 75] (and ceramic-ceramic [125, 126]) composites has emerged as an area of interest for industrial companies because polymers are flexible, low cost, easily processed [37, 127] and able to be polarized under the influence of an external electric field [128].

Piezoelectric ceramic/polymer composites possessing various connectivity patterns have been the focus of much study over the past several years [69, 72, 125, 126, 129, 130]. Among the composites examined, the simplest types are those with 0-3 connectivity [129]. Piezoelectric composites with 0-3 connectivity consist of piezoelectric ceramic particles dispersed in a three dimensionally connected polymer matrix. The advantages of these composites lie in the ease in which they may be processed into fairly complex shapes, including but not limited to thin sheets, molded shapes and extruded bars and fibers [129]. The most documented of piezoceramics used in composites such as these is PZT [26, 38, 72, 116, 131-133]. For example, Thongsanitgarn *et al.* [134] fabricated PZT-polymer composites with 0-3 connectivity, where the volume fraction of PZT was varied from 0 to 1 in increments of 0.1. The polymer matrix used was the ferroelectric polyvinylidene flouride (PVDF). In this work, it was reported that the composites with higher ceramic content yielded higher dielectric constant values. The dielectric constant varied from ~9 to ~958 for PZT volume fractions of 0 and 1, respectively, where the PZT particles ranged from single particles to agglomerated clusters that had mean diameters from 3 to 64 μm. The individual grain sizes were nominally 5 μm. Similarly, Hanner *et al.* [129] fabricated 0-3 PZT-polymer composite paints, where the PZT particles were randomly distributed within two different polymer matrices to understand the behavior of the particles with the polymer.

The polymers examined were acrylic and polyurethane as the two polymer matrices. The PZT particles were randomly dispersed within the polymer matrix at a volume fractions from 60 to 70%. The ceramic filler was loaded into the polymer mixture and allowed to stir at room temperature for approximately two hours. The fabricated composites were deposited onto brass plate substrates. The films were initially dried in air at room temperature for 24 hours and then placed in a vacuum oven at 110 ^{o}C for an additional 24 hours, which resulted in the formation of films thicknesses that ranged from ~ 200 - 500 μm. The PZT-acrylic composites were poled at ~150 kV/cm and the PZT-polyurethane composites were poled at ~120 kV/cm and at 75° C. The reported piezoelectric strain, d_{33} and dielectric constant were 26 pC/N and 29 for 60% PZT in acrylic and 25 pC/N and 51 for 60% PZT in polyurethane, respectively. In order to enhance the dielectric constant, Zhen et al. [108] inserted PZT pillars within an epoxy matrix to create a 1-3 PZT-polymer composite thick films, which were fabricated using a modified dice and fill method. The dimension of the PZT pillars were 40 μm sectional width and 40 μm spacing. They recorded high piezoelectric strain coefficient, $d_{33,}$ ~332 pC/N and dielectric constant ~ 105.

Banerjee *et. al* [125]studied the influence of aluminum inclusion on the dielectric properties of three-phase PZT-cement-aluminum composites, where the aluminum and PZT particles were dispersed in a Portland cement matrix. The fabricated samples were nominally 6 mm in thickness and were poled at a low poling voltage of 0-6 kV/mm at a temperature of 160° C in air. It was reported that three-phase composites possessed a higher piezoelectric strain coefficient (d_{33}) than two-phase composites. The highest value of d_{33} observed for the three-phase composite was 8.1 pC/N for volume fractions equal to

0.7 and 0.2 for PZT and Al, respectively. This d33 value for the three-phase piezoelectric composite was 1.64 times the value measured for the two-phase composite.

Banerjee *et. al* [2] also investigated the influence of micro and nano sized aluminum inclusions in a three-phase PZT-Epoxy-Al bulk composite. The fabricated composite was ~ 6 mm thick. The composites that were comprised of micron sized aluminum particles and PZT had higher dielectric constants that the composites that incorporated nano-sized aluminum particles (both sets of samples were polarized at the same value: 0.2 kV/mm in air) due to interfacial effects and increased agglomeration. Specifically, for composites with PZT volume fractions equal to 0.20, 0.30 and 0.40 and micron-sized aluminum particles, the dielectric constants were equal to 405.7, 661.4, and 727.8 (pC/N), respectively. On the other hand, the dielectric constants for composites that were comprised of nano-sized aluminum particles the (the same PZT volume fractions) dielectric constants were equal to 233.28, 568.81, and 657.41 (pC/N), respectively. They concluded that samples that contained micron sized aluminum inclusion yielded higher dielectric constant values compared to the nano sized aluminum inclusions

Pascariu *et al.* [135] fabricated two-phase 0-3 composites by a gravity casting method where the volume fraction of PZT was varied from 0 to 0.15 in an epoxy resin polymer matrix. The thickness of the composite films varied between 160 μm- 340 μm. The PZT mean diameter size was ~1-2 microns. They studied the role of the filling factor and of the gradient composition on the effective dielectric properties using a finite element method. They reported that the maximum dielectric constant was ~18 for 0.075 volume

fraction of PZT, which yielded the highest dielectric loss tangent below a volume fraction of PZT equal to 0.03. Nguyen *et. al* [127] also fabricated PZT-Epoxy two-phase composites where the volume fraction of PZT was varied from 0 to 0.2, and the mean diameter of the PZT particles was the 50 nm. The nanocomposites thicknesses ranged from60 - 160 μm. They observed an increase in the glass transition temperature from 164 ^{o}C to 178 ^{o}C for PZT volume fractions of 0.0 (pure epoxy) and 0.2, respectively. The dielectric properties were studied for a frequency range between 10 Hz to 100 kHz. The dielectric constant increased from 5.56 to 6.29 at 1 kHz (at 60 ^{o}C), for PZT volume fraction 0 and 0.2, respectively. James *et. al* [136] fabricated structured PZT-epoxy composites using dielectrophoresis. They effect of poling voltage on piezoelectric properties for various volume fractions of PZT were studied in this work. The PZT-Epoxy composite was prepared by applying an alternating 1kV/mm voltage across the suspension of ceramic particles in the epoxy matrix. This resulted in the formation of circular disk shaped samples. They observed that the d_{33} value increased with increasing poling field and they achieved saturation at 15kV/mm. The maximum d_{33} value observed was 9 pC/N for 0.5 volume fraction of PZT.

Chapter 4

Experimental Methods

4.1. Materials and Methodology

PZT-Al-Epoxy composites were fabricated where the volume fractions of PZT and Al were varied from 0.20 to 0.40 and 0.0 to 0.17, respectively. A minimum of three samples of each were fabricated for each of the studies described herein. An overview of the samples/powders prepared and/or surface treated are provided in Table 4.3.

Table 4.3: Overview of the data sets prepared for the time study of the aluminum surface treatment and poling studies. Control 1 is the aluminum powder subjected to no ethanol treatment. Control 1 is compared to aluminum powders that were surface treated with ethanol (data sets A, B, C, D, E and F) for 0.25, 0.5, 1, 2, 3 and 4 hours, respectively. Control 2 is the three-phase composite that was fabricated with aluminum that was not surface treated and contact poled. Data sets G, H and I are compared to Control 2.

Data Set *Composition (Description)*	**Poling Technique**	**Surface Treatment of Aluminum**	**Volume Fractions** *A minimum of 3 samples prepared for each volume fraction.*
Control 1 Aluminum powder ONLY	n/a	0 hours	n/a
A, B, C, D, E, F Aluminum powder ONLY	n/a	0.25, 0.5, 1, 2, 3 and 4	n/a
Control 2 PZT - Epoxy – Al Composite	Contact poled	None	v_{PZT}: 0.20 – 0.40 v_{Al}: 0.0 to 0.17
G PZT-Epoxy Composite	Corona poled	None	v_{PZT}: 0.20 – 0.60 v_{Al}: 0.0
H PZT - Epoxy – Al Composite	Corona Poled	None	v_{PZT}: 0.20 – 0.40 v_{Al}: 0.0 to 0.17
I PZT - Epoxy – Al Composite	Corona poled	Ethanol treatment of Aluminum for 4 hours	v_{PZT}: 0.20 – 0.40 v_{Al}: 0.0 to 0.17

The control samples/powders were prepared as detailed in Figure 4.23 and Figure 4.24. A minimum of six samples were prepared for each volume fraction and poling scenario analyzed.

4.2. Materials

The materials used in all experiments were PZT-855 (Navy Type VI) [24] powder (APC International); DGEBA, Epofix TM Cold-setting embedding resin (Electron Microscopy Sciences), and aluminum - 99.97% , 200 mesh i.e. ~ 75 μm (Acros Organics). The piezoelectric and physical properties of the materials are provided in Table 4.4. Homogenous samples of the epoxy and PZT were prepared to obtain the electrical and physical properties presented in Table 4.4, while the Al properties were obtained from the manufacturer.

Table 4.4: Physical, dielectric and piezoelectric properties of the PZT, epoxy and aluminum (Al).

Property	PZT 855	Epoxy	Al
Relative dielectric constant, ε_r	3300	2.9-3.7	1.6 - 1.8
Dielectric dissipation, tan δ	$\leq$ 2.50	~0.02 – 0.04	--
Electromechanical coupling, k_p/k_{33}	0.68 / 0.76	--	--
Piezoelectric charge constant, d_{33} (10^{-12} C/N)	630*	12.28*	1.6-1.8
Young's Modulus, Y_{11}^E / Y_{33}^E (10^{10} N/m^2)	5.9 / 5.1	0.15 –0.20	6.89
Density (g/cm^3)	7.6	(in the wet-state) 1.16 g/cm^3	2.7
Electrical Resistivity (ohm-cm)	49.27* @ 1kHz	0.15 @1kHz	3.99e-6

* Experimental values

4.3. Surface Treatment of Aluminum: A Time Study

The bond strength between the embedded particles and polymer matrix play a key role in the interfacial properties and subsequent macroscopic properties of the composite. Also, the processing of the aluminum influences the composition of the outer shell of the aluminum. Hence, a time study of the surface treatment of the aluminum with ethanol was conducted. An overview of this processing technique is depicted in Figure 4.23. In this process, Al powder was weighed and placed in a beaker with 15 ml of ethanol. A paraffin film was placed at the top of the beaker to prevent evaporation of the ethanol into the air. Several mixtures (data sets: A – F, described in Table 4.3) were prepared and sonicated for 0.25, 0.5, 1, 2, 3 and 4 hours, respectively. The particle size, morphology and distribution of the Al particles were observed with the aid of a Zeiss Sigma Field Emission scanning electron microscope (SEM) and an Oxford INCA PentaFETx3 8100 energy dispersive X-ray spectroscopy (EDS). The surface treatment that minimized the agglomeration of the Al powder was selected for use in fabrication of composites observed for data set I (described in Table 4.3).

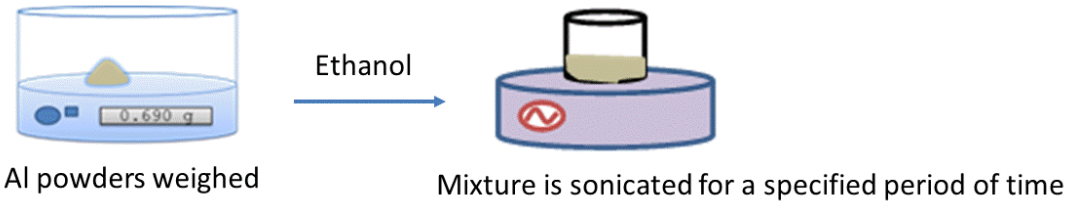

Figure 4.23: Al powder data sets A – F were sonicated in 15 mL of ethanol for 0.25, 0.5, 1, 2, 3 and 4 hours. The size, morphology and distribution (agglomeration) of the particles was observed with the aid of SEM and EDS.

4.4. Bulk Composite Preparation

An overview of the fabrication process for the three-phase composites is provided in Figure 4.24. First, the PZT, Al and epoxy were weighed to achieve the desired volume fraction and combined. The Al was surface treated with ethanol for 4 hours for data set I (described in Table 4.3) prior to mixing with the PZT and Al. The mixture was subsequently hand stirred and sonicated in an ultra sonicator for 30 minutes. Ethanol was then added to the mixture, which was then sonicated for an additional 30 minutes. The epoxy hardener was then added to the mixture. The final compound was poured onto a mold and cured in air for 8 hours at 75°C. The surfaces of the samples were then polished and coated with colloidal silver solution. The volume fractions of PZT and Al were varied from 0.20 to 0.40 and 0.0 to 0.17, respectively. A minimum of six samples were prepared for each volume fraction. All samples were poled at 12-15kV/mm at 65°C for 15 minutes. The samples prepared for Control 2 were contact poled, and the samples prepared for data sets G, H, and I were Corona poled. The duration of poling remained constant for both contact and corona poling, however the contact poling was performed in a silicon bath to ensure uniform heating of the sample.

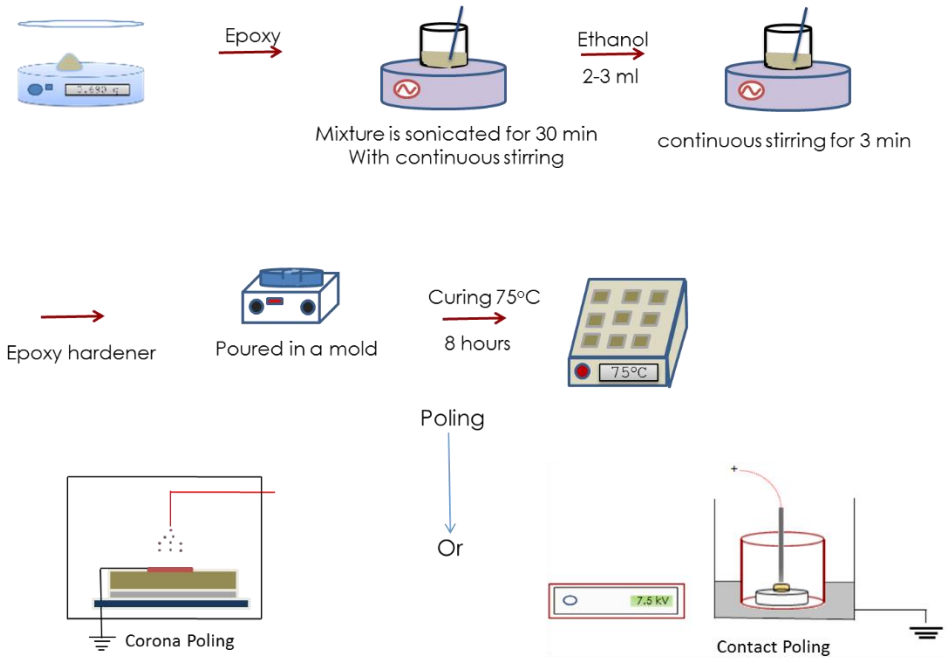

Figure 4.24: PZT and Al powders are weighed and processed accordingly. The powder mixture was then combined with epoxy, mixed by hand and sonicated for 30 minutes. The mixture was then combined with ethanol, stirred and then poured into a mold. Once in the mold, the mixture was cured in air for 8 hours at 75°C. Subsequent samples were either contact or Corona poled.

4.5. Dielectric and Piezoelectric Characterization

The longitudinal piezoelectric strain coefficient, d_{33}, and capacitance, C, were measured using a Piezo Meter System manufactured by Piezo Test, Piezoelectric Materials & Device Testing Company, while the resistance was obtained using an Impedance/Gain Phase Analyzer (HP4194A).

The dielectric constant was calculated using the expression,

$$\varepsilon_r = \frac{Ct}{A\varepsilon_o}. \tag{4.1}$$

In equation [14], C is the capacitance in Farads, A is the area of the sample, ε_o is the permittivity of free space ≈ 8.854×10e-12 F m^{-1}); and t is the thickness of the sample. The impedance analyzer was used to measure the real part of the resistance, R, of each sample, and the resistivity was determined from equation [15],

$$\rho = \frac{RA}{t}. \tag{4.2}$$

4.6. Composite Thick Film: Materials and Methodology

PZT-aluminum-epoxy thick film composites were fabricated where the volume fractions of PZT and Al were varied from 0.20 to 0.40 (increments of 0.10) and 0.0 to 0.17, respectively. A minimum of three samples were fabricated for each of the studies. In addition, the dielectric and piezoelectric properties resulting from samples that had two different types of top electrodes (sputtered gold and silver paint), were compared. The change in the piezoelectric and dielectric properties with respect to time was observed over a five-day period.

4.7. Materials

The materials used in all experiments were PZT powder (READE), DGEBA Epofix TM Cold-Setting embedding resin (Electron Microscopy Sciences) [137], and aluminum - 99.97%, 200 mesh i.e. ~ 75 μm (Acros Organics) and 0.0254 mm stainless steel substrates (Alfa Aesar). The piezoelectric and physical properties of the materials are presented in Table 4.5 and Table 4.6, respectively. The properties for the aluminum were obtained from the manufacturer website [138].

Table 4.5: Physical and dielectric properties of PZT powder were provided by the manufacturer [139].

PZT Properties	
Average particle diameter	6-7 microns
Density	7.75 – 8.0
Young's Modulus	5.8 – 9.0
Curie Temperature	170 – 360
Relative Dielectric Constant	1000 - 4100

Table 4.6: Physical, dielectric and piezoelectric properties of the epoxy and aluminum [137, 138].

Property	**Epoxy**	**Al**
Relative dielectric constant, ε_r	2.9-3.7	1.6 - 1.8
Dielectric dissipation, *tan* δ	~0.02 – 0.04	--
Electromechanical coupling, k_p/k_{33}	--	--
Piezoelectric charge constant, d_{33} (10^{-12} C/N)	12.28*	1.6-1.8
Young's Modulus, Y_{11}^E / Y_{33}^E (10^{10} N/m^2)	0.15 –0.20	6.89
Density (g/cm^3)	1.16 g/cm^3 (in the wet-state)	2.7
Electrical Resistivity (ohm-cm)	0.15 @1kHz	3.99e-6

* Experimental values

4.8. Composite Thick Film Preparation

PZT-Epoxy-Al thick composite films were deposited onto stainless steel substrate using a spin coat and deposition technique. The stainless steel squares were 25 mm x 25mm and 0.0254 mm thick. An overview of the fabrication process for the three-phase composites is provided in Figure 4.25. The volume fraction of the PZT and aluminum was varied from 0.20 to 0.40 and 0.01 to 0.17, respectively.

The PZT, aluminum and epoxy were weighed to achieve the desired volume fraction, and combined in a beaker. The contents in the beaker were hand stirred for 5 minutes and 5 ml of ethanol was added to this mixture. The mixture was subsequently sonicated in an ultra sonicator for 1 hour, while being hand stirred every 15 minutes. The epoxy hardener was then added to the mixture. The final compound is then poured onto the stainless steel substrate via a dropper, during this time the spin coater is rotated from 100 - 500 rpm for 30 seconds, followed by 1000 rpm for 60 seconds. The initial low rpm enables even distribution of the compound over the substrate. The spin coat and deposition system was then brought back to 0 rpm.

After the spin coating process, the samples are removed and cured on a hot plate in air for 8 hours at 75^{o}C. The samples were subsequently cooled for 24 hours and were coated with colloidal Samples were prepared with colloidal silver paint as the top electrode. They were then contact poled at a voltage of 2.2 kV/mm at 65^{o}C in a silicone oil bath for 15 minutes. An additional set of samples were prepared, where the volume fractions of PZT and aluminum were 0.3 and 0.05, respectively.

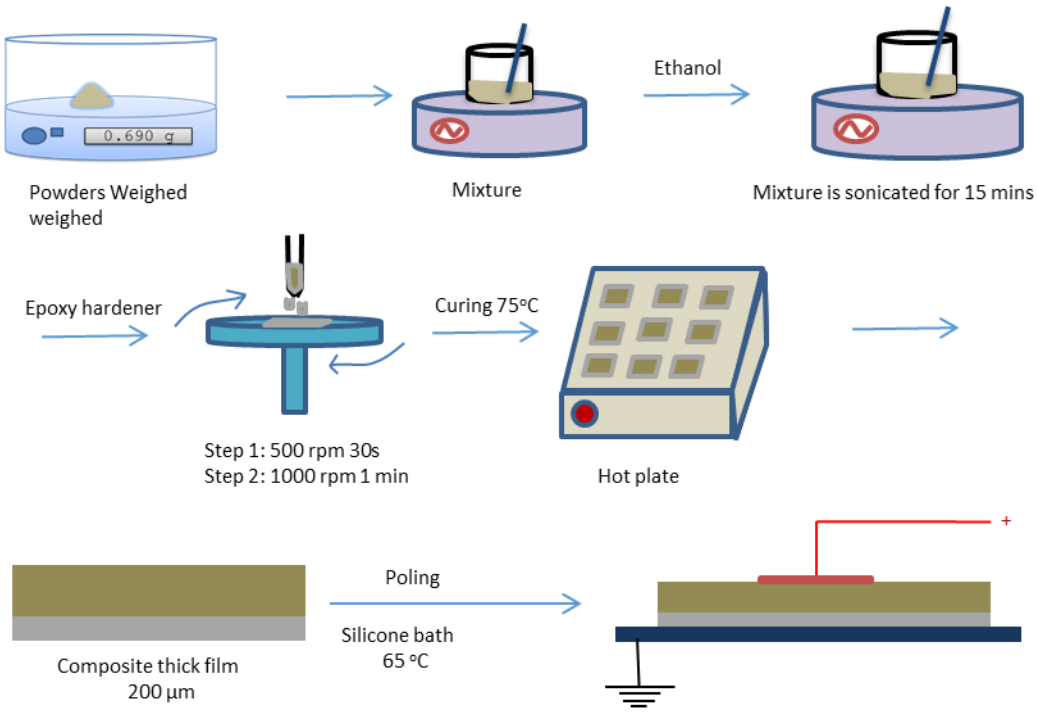

Figure 4.25: A schematic diagram explaining the stages in the preparation of the composite film. The mixture was spin coated by a two-step process, 500 rpm for 30 seconds and 1000 rpm for 60 seconds, followed by curing at 75°C, and then contact poling in a silicone bath for 15 minutes at 65°C.

Sputtered gold was used as the top electrode for these samples instead of colloidal silver paint. All samples were then wrapped in aluminum foil and stored at room temperature in the air for 24 hours to remove any remaining residual charges that may be on the samples.

4.9. Material Morphology and Surface Characterization

The surface morphology of the individual phases and the composite was examined using scanning electron microscopy (SEM) micrographs. Two types of images were gathered for these composites, one was from the top surface of the sample, which provides information about the distribution of the individual phases within the polymer matrix, and the other was the cross-sectional image along the thickness of the sample. The cross-

sectional image represents how the particles are distributed along the thickness and a macroscopic view of the composite substrate interface.

Chapter 5

Results and Discussion

5.1 Bulk Composite

Aluminum powder was surface treated with ethanol for time periods of 0.25, 0.5, 1, 2, 3 and 4 hours to determine the appropriate sonication time required for minimal agglomeration of the particles. PZT-epoxy composites were fabricated using the Corona poling technique for data set G. PZT- Al-epoxy composites were fabricated using Al powder that was not surface treated and contact (Control 2) or Corona poled (data set H). PZT- Al-epoxy composites were fabricated using Al powder that was surface treated for 4 hours (data set I). The volume fractions of PZT and Al were varied from 0.2 to 0.4 and 0 to 0.17, respectively. The longitudinal piezoelectric strain coefficient, d_{33} was measured at 110 Hz while the dielectric constant, ε, and resistance were measured as a function of frequency.

5.1.1 Surface Treatment of Aluminum: A Time Study and Surface Morphological Characterization

The size, shape, surface morphology and degree of agglomeration of the aluminum powder was observed using a scanning electron microscope (SEM) and Energy Dispersive X-ray Spectroscopy (EDS). SEM images were coupled with software packages; ImageJ and Photoshop CS5.1 to ascertain the average particle size. The aluminum powder was surface treated with ethanol using an ultrasonicator for time

periods of 0.25, 0.5, 1, 2, 3, and 4 hours to determine the sonication time that would render the minimal degree of agglomeration and most consistent particle size of the aluminum. In Figure 5.26 and Figure 5.27, micrograph SEM and EDS images are presented for Al powder that was surface treated with ethanol for 0.0 and 4 hours, respectively. The average size of the non-treated aluminum was ~13.43 μm, while the average size of the aluminum that was ultra-sonicated with ethanol for 4 hours was 5.05 μm. The SEM images indicate that the exposure of the aluminum to ethanol over extended periods of time diminished the agglomeration of the aluminum particles and reduced the size of the aluminum particle, as seen in Figure 5.26. In theory, this was achieved when the ethanol chemically reacted with the Al_2O_3 shell to form ethane, where oxygen molecules in Al_2O_3 combined with hydrogen molecules of ethanol, thereby reducing the oxide layer around the Al particle [140, 141].

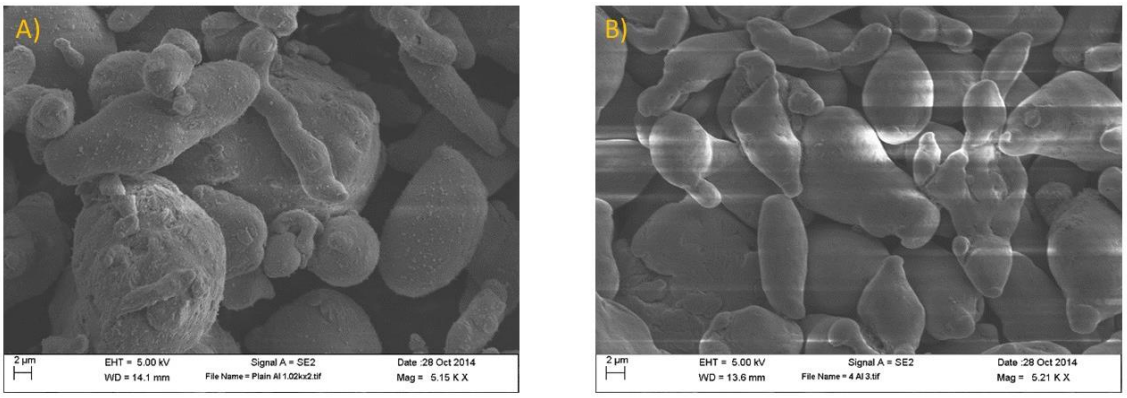

Figure 5.26: SEM micrograph images of aluminum powder that was A) not surface treated with ethanol (5.15X magnification). The average aluminum particle size is~13.43 μm, and B) ultra-sonicated with the solvent, ethanol, for 4 hours (5.21X magnification), where the average particle size was observed to ~5.05 μm.

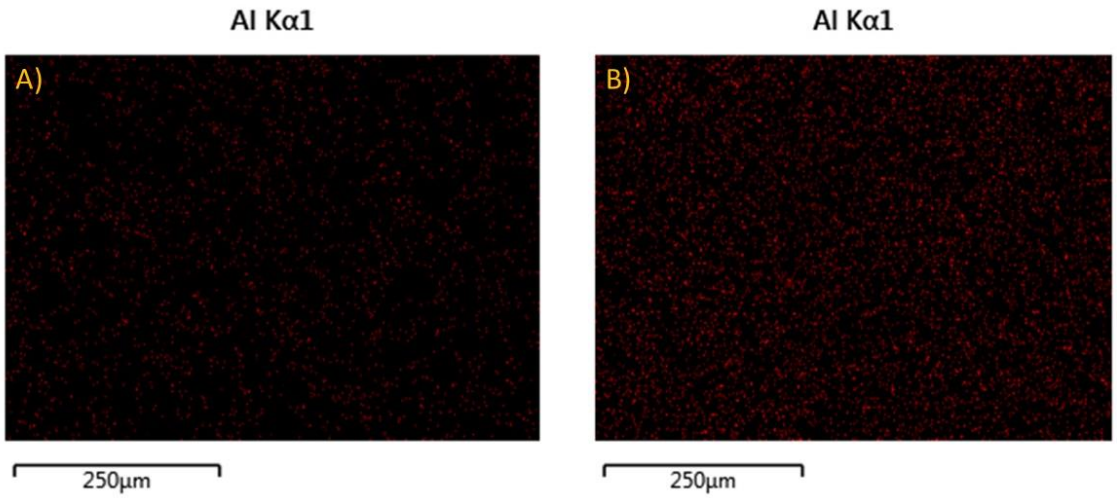

Figure 5.27: EDS micrograph images of aluminum powder that was A) not surface treated with ethanol and B) surface treated with ethanol for 4 hours. The images indicate that the surface treated Al powder was more evenly distributed across the matrix, in comparison to the Al powder that was not surface treated.

5.1.2 Piezoelectric and Dielectric Characterization

In Figure 5.28, the piezoelectric strain coefficients of the two-phase composites, data set G, (Corona poled at 15kV/cm) are plotted as a function of PZT volume fraction (from 0.2 to 0.6). As expected, the piezoelectric strain coefficient increases with the volume fraction of PZT content. The piezoelectric strain coefficients for Control 2 (contact poled at 12 kV/cm, non-surface treated Al), data set H (Corona poled at 15 kV/cm, non-surface treated Al) and data set I (Corona poled at 15 kV/cm, Al surface treated in ethanol for 4 hours) are plotted as a function of aluminum volume fraction, for PZT volume fractions of 0.2, 0.3 and 0.4, in Figure 5.29, Figure 5.30, and Figure 5.31, respectively. The piezoelectric strain coefficients increase with PZT and aluminum content up to an aluminum volume fraction of 0.13, beyond which there is a sharp decline in d_{33} values. This increase in d_{33} values is consistent with the observations of [72, 92, 105, 142-146], who measured increases in d_{33} as PZT content increased within piezoelectric polymer composite. The particle size and relative density of the composites influence the effective

piezoelectric strain and dielectric constants of the composite piezoelectric materials. In this work, the d_{33} values are relatively small in comparison to some values reported by others Table 5.7. The small piezoelectric strain values are most likely due to the use of small size and volume fraction of PZT particles, which were ~3 μm, in comparison to the works of [105, 147] where piezoelectric particles sizes were ~160 μm and 875 μm respectively. In particular, [74] concluded that in two phase composites, ceramic powder particles with larger particle sizes have a higher degree of surface energy than smaller powder particle sizes, which could be due (in part) to the fact that the contacting surface area between the bigger ceramic powder particles and the polymer, is larger than that of smaller ceramic particles and the polymer matrix. Hence, [74] concluded that larger size powder particles achieve more effective poling in the composite than smaller powder particles in a polymer matrix. The range of d_{33} depicted in Figure 5.28 is consistent with the work of [74] where the active particle size was less than 34 μm (poling voltage at 10 kV/mm and room temperature), which is consistent with the poling voltages used in this work.

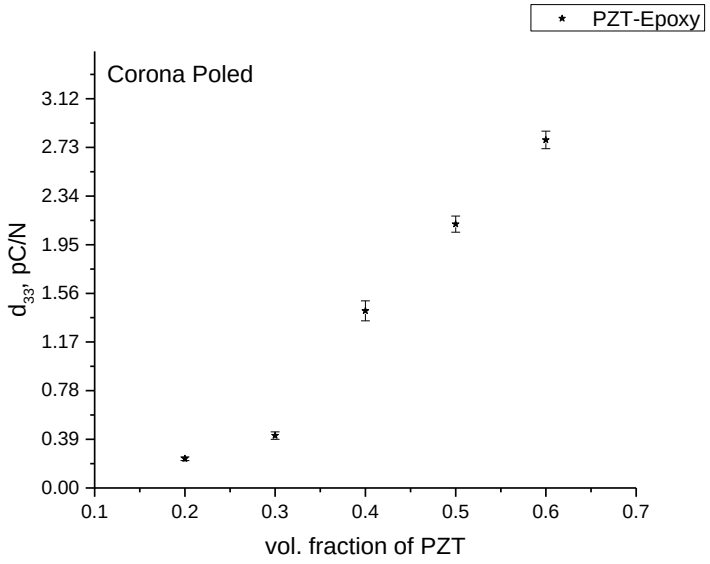

Figure 5.28: The piezoelectric strain coefficient, d_{33}, for the PZT-epoxy composites (data set G) that were Corona poled at 15kV/cm are plotted as a function of PZT volume fraction. The maximum d_{33} value occurs 2.73 pC/N at a PZT volume fraction equal to 0.6

There is a difference in the trends observed between the two-phase corona and the three-phase contact poled samples (where Al was not surface treated), where at 0.2 and 0.3 volume fractions of aluminum, the contact poled three-phase composites exhibit higher d_{33} values than data set G. On the other hand, at the higher PZT volume fraction, 0.4, the corona poled two-phase composite (data set G) is higher than Control 2 (PZT volume fraction equal to 0.4). The contribution of the aluminum inclusions are not clearly observed at higher PZT volume fractions in contact poled samples, as shown in Figure 5.29, Figure 5.30, and Figure 5.31. This observation is most likely due to problems associated with the difficulty of achieving the desired poling voltage of ~12kV/cm for contact poled samples. This was not the case for data sets H and I, which were Corona poled. In corona poling, charged ions adhere to the surface of an electrode sample, thereby creating an electric potential between the top sample surface and grounded plate [93]. Thus, samples with defects and electrically conductive inclusions can be poled at higher

voltages using the Corona poling process, wherein the effectiveness of the poling process is enhanced. In both the Corona and contact poled samples, d_{33} ceased to increase beyond an aluminum volume fraction of 0.13. This is most likely because electrical percolation occurred at or near a volume fraction of 0.3 for the aluminum. The percolation volume fraction is slightly smaller than the theoretical prediction range, 0.15 to 0.17 [148], which is valid for spherical particles, where percolation occurs by way of particle contact. However, the mechanism of percolation can also be achieved by way of electrical conduction through inter-particle tunneling [149], which can diminish percolation threshold values in a continua composite.

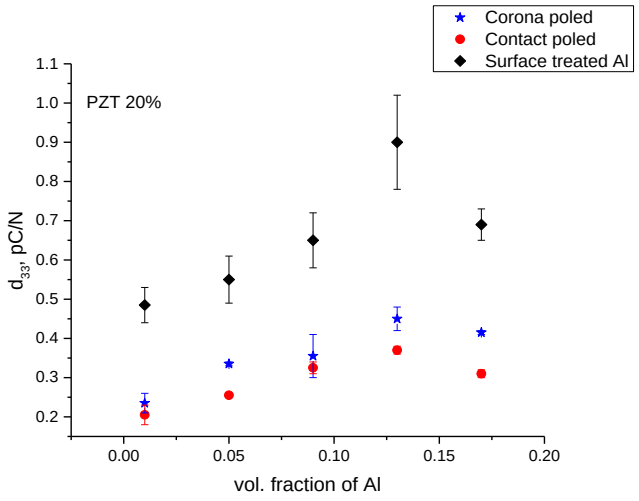

Figure 5.29: The piezoelectric strain coefficient, d_{33}, for Control 2 (contact poled at 12 kV/cm and non-surface treated Al), data set H (Corona poled at 15 kV/cm and non-surface treated Al) and data set I (Corona poled at 15 kV/cm and surface treated Al for four hours) as a function of aluminum volume fraction for a constant PZT volume fraction equal to 0.2. The maximum d_{33} values are 0.37, 0.45 and 0.9 pC/N for Control 2, data set H and data set I, respectively. The maximum d_{33} values occur when the volume fraction of aluminum is equal to 0.13.

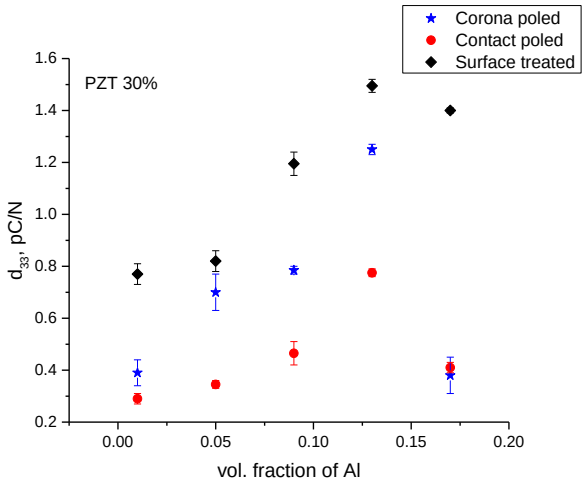

Figure 5.30: The piezoelectric strain coefficient, d_{33}, for Control 2 (contact poled at 12 kV/cm and non-surface treated Al), data set H (Corona poled at 15 kV/cm and non-surface treated Al) and data set I (Corona poled at 15 kV/cm and surface treated Al for four hours) as a function of aluminum volume fraction for a constant PZT volume fraction equal to 0.3. The maximum d_{33} values are 0.78, 1.25 and 1.50 pC/N for Control 2, data set H and data set I, respectively. The maximum d_{33} values occur when the volume fraction of aluminum is equal to 0.13.

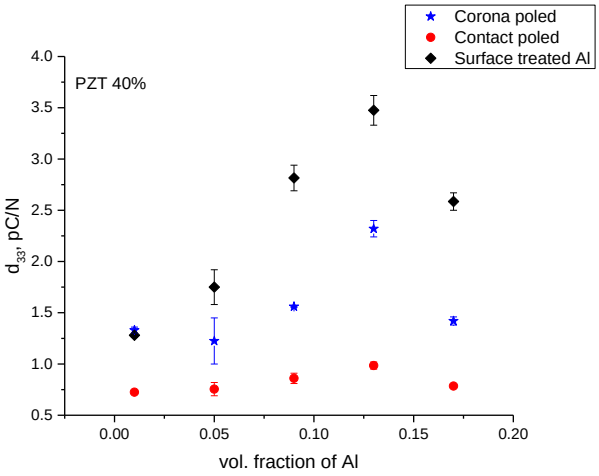

Figure 5.31: The piezoelectric strain coefficient, d_{33}, for Control 2 (contact poled at 12 kV/cm and non-surface treated Al), data set H (Corona poled at 15 kV/cm and non-surface treated Al) and data set I (Corona poled at 15 kV/cm and surface treated Al for four hours) as a function of aluminum volume fraction for a constant PZT volume fraction equal to 0.4. The maximum d_{33} values are 0.99, 2.32 and 3.48 pC/N for Control 2, data set H and data set I, respectively. The maximum d_{33} values occur when the volume fraction of aluminum is equal to 0.13.

The dielectric constants for the two-phase composite (PZT-epoxy, data set G) are plotted as a function of PZT volume fraction in Figure 5.32. The dielectric constant for the two-phase composite does not appear to vary with frequency. The dielectric constant was found to increases with PZT content, where the average values of were ~68.2, ~96.9 and ~131.7 for PZT volume fractions of 0.2, 0.3 and 0.4 respectively. These values were found to be slightly higher than those of [71,74,147,150], who fabricated PZT-polymer 0-3 composites with PZT volume fractions of 50% (values sin Table 3).

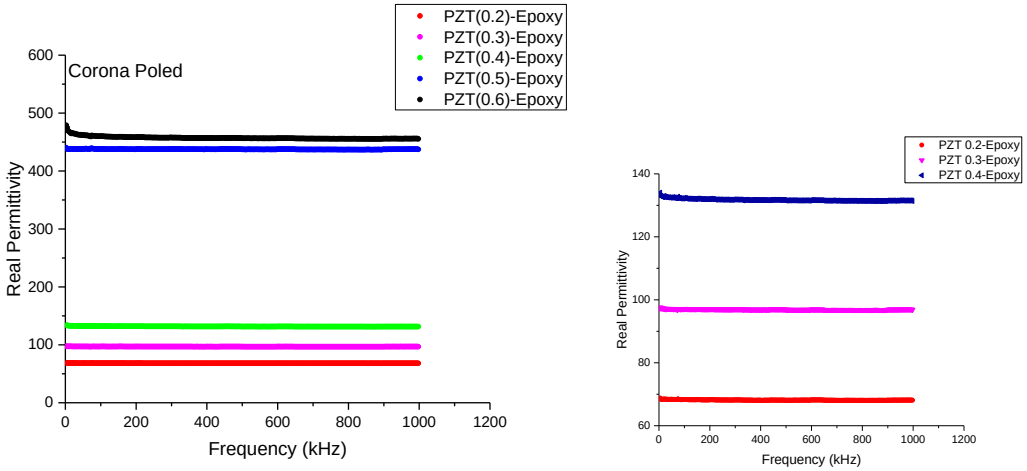

Figure 5.32: The real permittivity (dielectric constant, calculated from Equation [1]) for data set G (PZT-Epoxy) composite is plotted as a function of frequency. Data set G composites were corona poled at 15kV/cm. As expected, the real permittivity is nearly constant over the frequency range and the maximum value occurs when the volume fraction of PZT is equal to 0.6.

Table 5.7: Dielectric and piezoelectric properties of the PZT polymer composites and comparison with those of previous workers [100-102,104-106,133].

Sample	Volume Fraction % PZT/Epoxy/Al	Dielectric constant, ε_r	d33 (pC/N)	Reference
PZT/DEGBA Epoxy/Al (Control 2)	40/47/13	~270	0.99	This work
PZT/DEGBA Epoxy (data set G)	40/60/0	~134	1.36	This work
Control 2, PZT/DEGBA Epoxy/Al (data set H)	40/47/13	~305	2.32	This work
PZT/DEGBA Epoxy/Al (data set I)	40/47/13	~420	3.48	This work
PZT/PVC	50/50/0	43.7	13.0	Liu et al. (2005)
PZT/PVDF	50/50/0	68.1	14.0	Liu et al. (2005)
PZT/PVDF/C	50.0/0.5/49.5	47.8	20.0	Liu et al. (2005)
PZT/PVDF	50/50	56.0	14.0	Wang et al. (2000)
PZT/PVDF	50/50	95.0	13.8	Venkatragavaraj et al. (2001)
PZT/Polyester	50/50	52	18	Nhuapeng et al. (2002)
PZT/epoxy resin	37/63	15	25.3	Thamjaree et al. (2005)

The dielectric constants (real permittivity) for the Control 2 and data sets H and I are presented as a function of frequency for PZT and aluminum volume fractions of 0.2 to 0.4 and 0.01 to 0.17, in Figure 5.33, Figure 5.34, and Figure 5.35, respectively. The dielectric constants for all samples increase with volume fraction of PZT and Al. The results indicate that all samples containing aluminum particles (corona and contact poled) had higher values of dielectric constant that the two phase counterparts. Furthermore, the dielectric constant for Control 2 (for volume fractions equal to 0.2 and 0.13 for PZT and

Al, respectively), ~156.7 is higher than composite samples comprised of 20% $BaTiO_3$ (80 nm particles) and 15% nickel [95], whose dielectric constant was ~100.8. In general, the dielectric constant values of this work were found to be slightly higher than those in other works with similar volume fractions of PZT [100, 104], and others that included carbon black [100]. In Table 3, a comparison of dielectric constant values are presented.

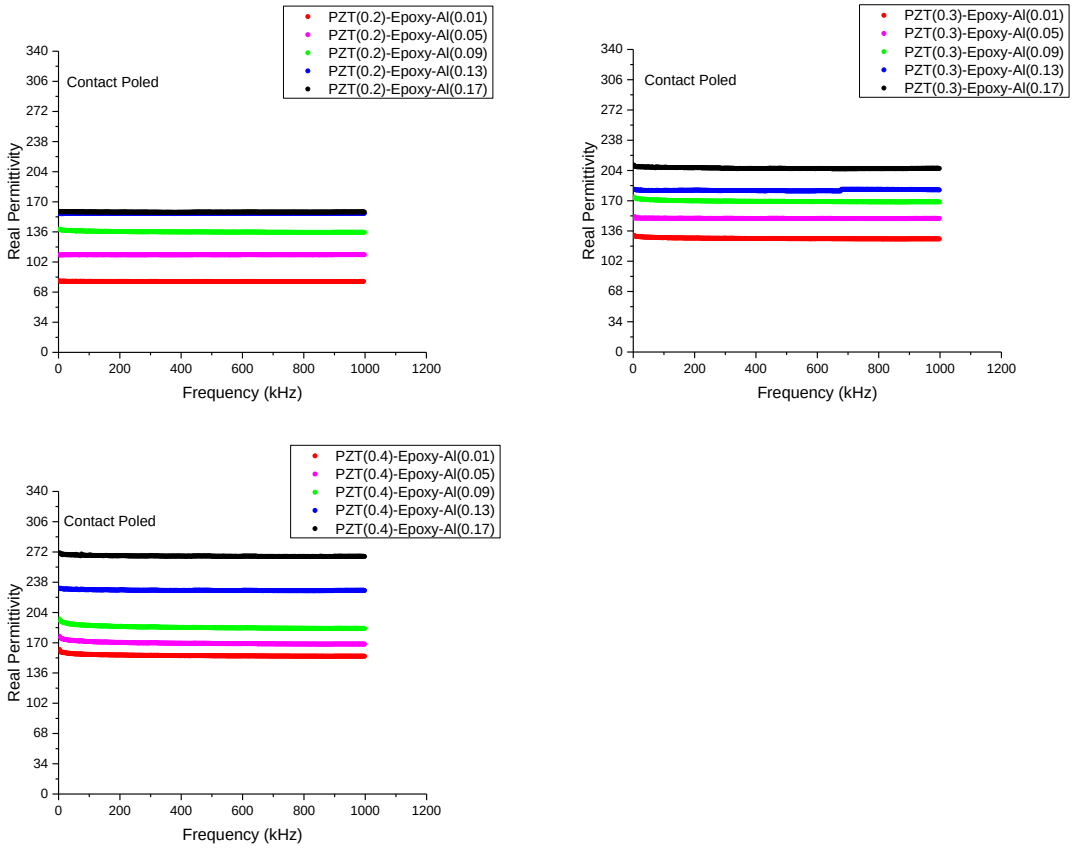

Figure 5.33: The real permittivity (dielectric constant, calculated from Equation [1]) for Control 2 (PZT-Epoxy-Al, contact poled at 12kV/cm) is plotted as a function of frequency for A) 0.2, B) 0.3 and C) 0.4 volume fraction of PZT. The maximum values of dielectric constant occur at 0.17 volume fraction of Al for 0.2, 0.3 and 0.4 volume fractions of PZT.

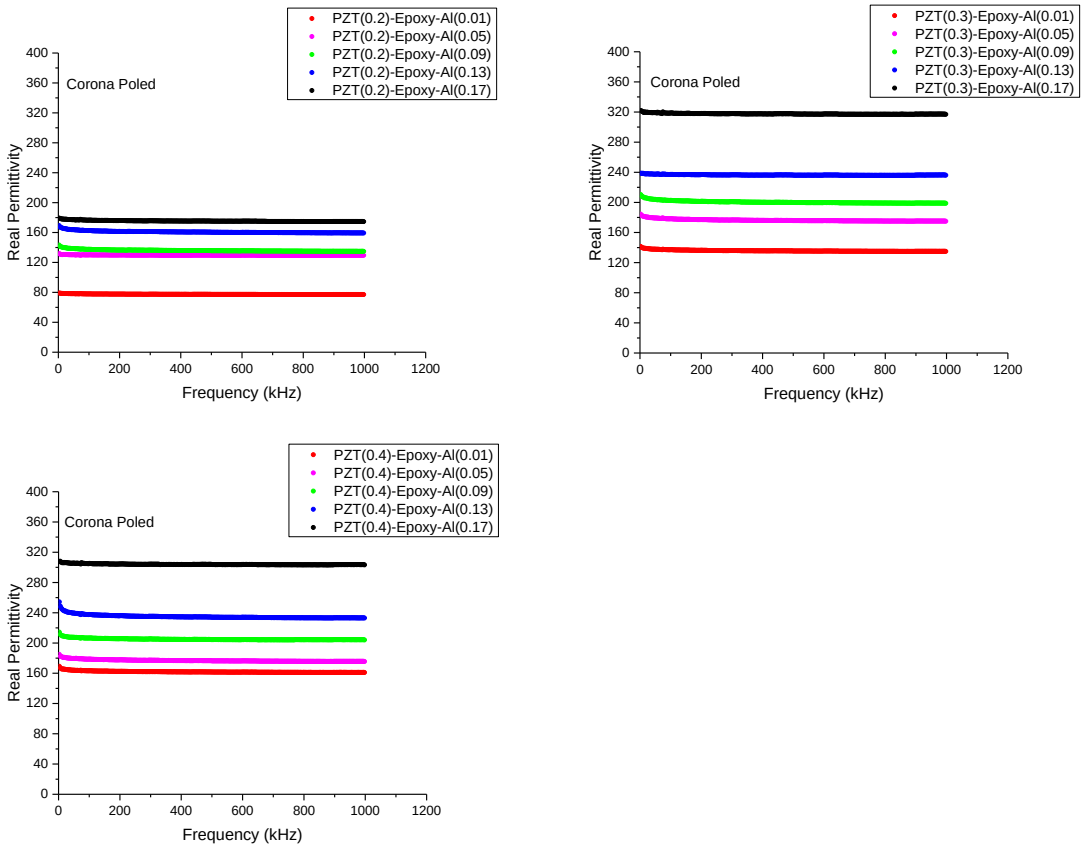

Figure 5.34: The real permittivity (dielectric constant, calculated from Equation [1]) for data set H (PZT-Epoxy-Al, non-surface treated Al, Corona poled at 15kV/cm) is plotted as a function of frequency for A) 0.2, B) 0.3 and C) 0.4 volume fractions of PZT. The maximum values of dielectric constant occur at 0.17 volume fraction of Al for 0.2, 0.3 and 0.4 volume fractions of PZT.

The maximum dielectric constant values observed were for samples that were surface treated and Corona poled (data set I) with PZT at 40% volume fraction and Al at 13% volume fraction. The influence of Corona poling on dielectric constant is somewhat of an issue of debate, where some scholars have found no difference in dielectric constants poled contact and corona poled [74]. On the other hand, Waller et al. [38] have found that poling by the Corona method produced higher dielectric constants than the conventional method. Based on the increases in dielectric constant and decrease in d_{33} at 0.13 volume fraction of PZT (in Control 2 and data sets H and I), it is believed that the percolation

threshold was achieved at the volume fraction of 0.13. This is confirmed via observation of resistivity plots of these composites as a function of frequency for PZT and aluminum volume fractions equal to 0.2 to 0.4 and 0.01 to 0.17, respectively in Figure 5.35, Figure 5.36, and Figure 5.37. The dielectric characteristics of most materials are a function of ferroelectricity, charge density wave formation, hopping charge transport, the metal insulator transition and interface effects [151]. In Figure 5.33, Figure 5.34, and Figure 5.35 the dielectric constants increased as a function of aluminum volume fraction, which could be the result of hopping transport and interface effects. This could be validated by decreased resistivity in samples with aluminum content as demonstrated in Figure 5.36, Figure 5.37 and Figure 5.38.

The maximum value of dielectric constant was observed to be 411 for samples that were surface treated and corona poled at PZT 40% and Al at 13%. The surface treated samples also displayed higher resistivity values, as can be seen in Figure 5.38. Exposing the aluminum powder to ethanol for 4 hours, resulted in smoother surface morphology of the aluminum particles and de-agglomeration of aluminum particles cluster, which may have contributed to better aluminum particle distribution within the composite (as shown in Figure 5.27). Exposure of the aluminum to ethanol over extended periods of time in theory results in the self-passivation of aluminum and formation of an Al_2O_3 shell outside the metallic sphere. This outer shell allows electrons in the metallic core to tunnel through it, which causes the composite to have a higher dielectric constant as a percolated system. The Al_2O_3 shell around the Al particle also inhibits electron tunneling between successive Al particles, thereby leading to enhanced dielectric constant [4, 152, 153].

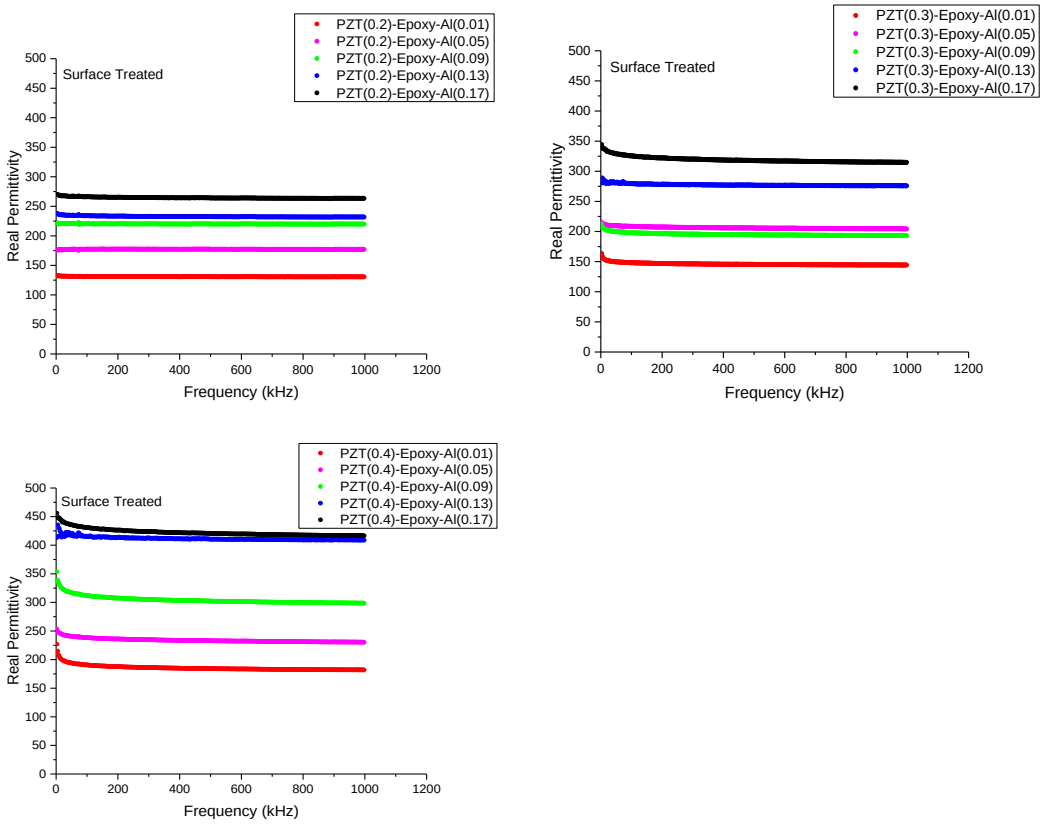

Figure 5.35: The real permittivity (dielectric constant, calculated from Equation [1]) for data set I (PZT-Epoxy-Al, surface treated Al, Corona poled at 15kV/cm) is plotted as a function of frequency for A) 0.2, B) 0.3 and C) 0.4 volume fractions of PZT. The maximum values of dielectric constant occur at 0.17 volume fraction of Al for 0.2, 0.3 and 0.4 volume fractions of PZT.

A thinner Al_2O_3 layer on an Al particle leads to a higher dielectric constant, as it more closely resembles a percolative system [154]. This interfacial polarization, the so-called Maxwell-Wagner, effect is responsible for the enhancement of dielectric constant [34]. The dielectric constants increase near the percolation threshold due to the presence of micro-capacitor networks, which in theory can be represented as shown in Figure 5.39.These networks are formed by neighboring conductive filler particles that sandwich PZT particles, which are insulated by the dielectric polymer matrix. Collectively the networks contribute to the increase in capacitance[155, 156] of the sample. The formation of the network creates results in an increase in the local electric field when the

conductive fillers are close together near percolation, this promotes migration and accumulation of charge carriers at the interfaces between the Al particles and the polymer matrix [34]. The charges generated are accumulated at the interfaces as a result of Coulomb blockade by the insulating matrix, until the conductive fillers approach each other and the charges are relaxed by tunneling or by ohmic conduction.

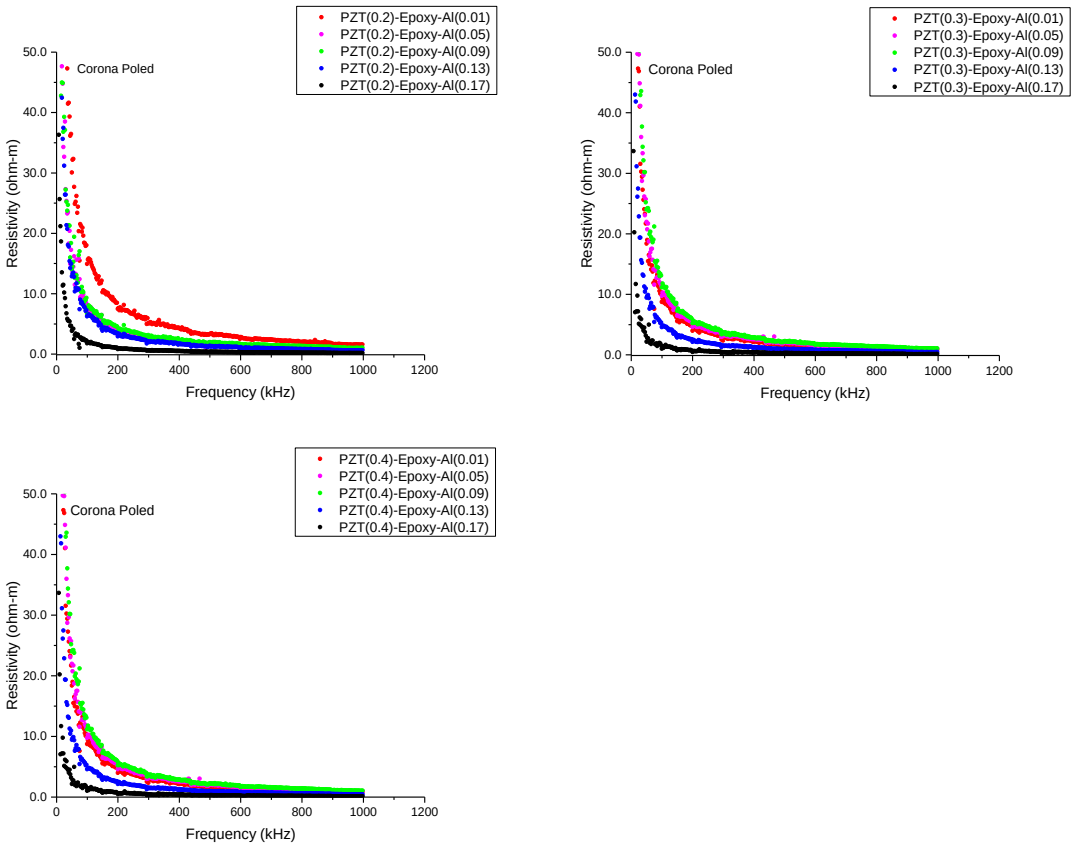

Figure 5.36: The resistivity for Control 2 (PZT-Epoxy-Al, contact poled at 12kV/cm) is plotted as a function of frequency for A) 0.2, B) 0.3 and C) 0.4 volume fraction of PZT. The minimum values of resistivity occur for 0.17 volume fraction of Al for 0.2, 0.3 and 0.4 volume fractions of PZT.

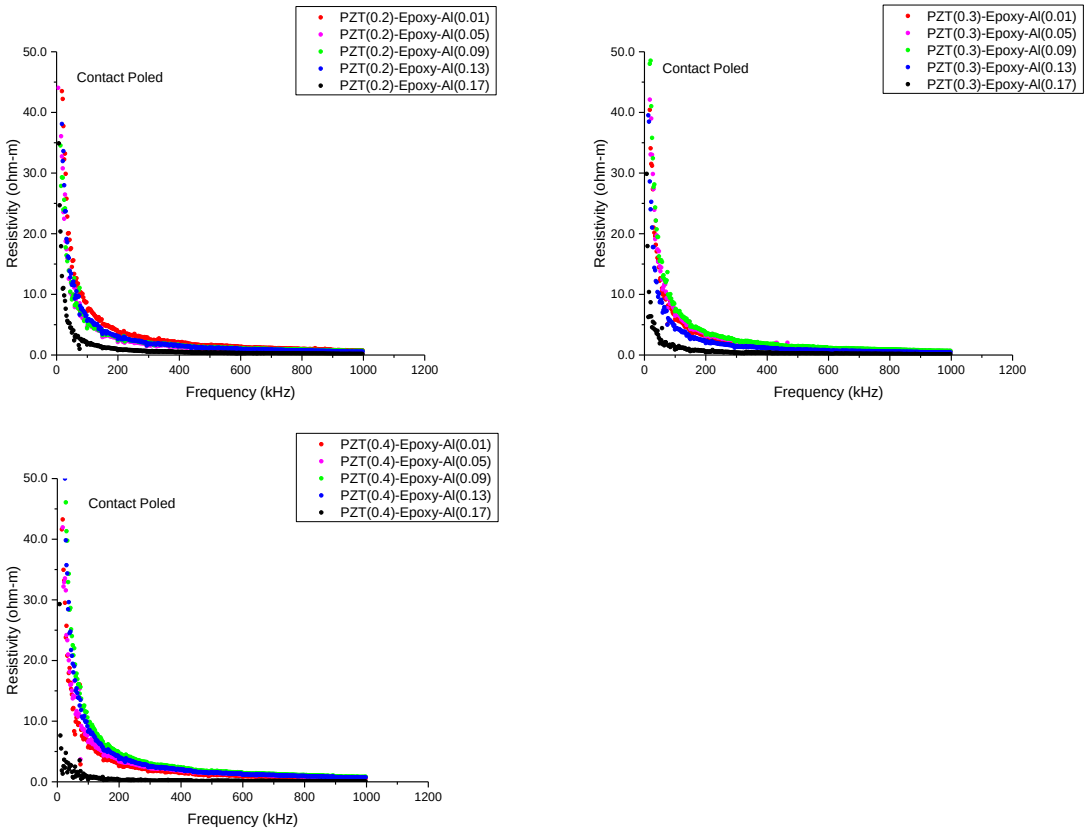

Figure 5.37: The resistivity for data set H (PZT-Epoxy-Al, non-surface treated Al, Corona poled at 15kV/cm) is plotted as a function of frequency for A) 0.2, B) 0.3 and C) 0.4 volume fractions of PZT. The minimum value of resistivity occurs for 0.17 volume fraction of aluminum for 0.2, 0.3 and 0.4 volume fractions of PZT.

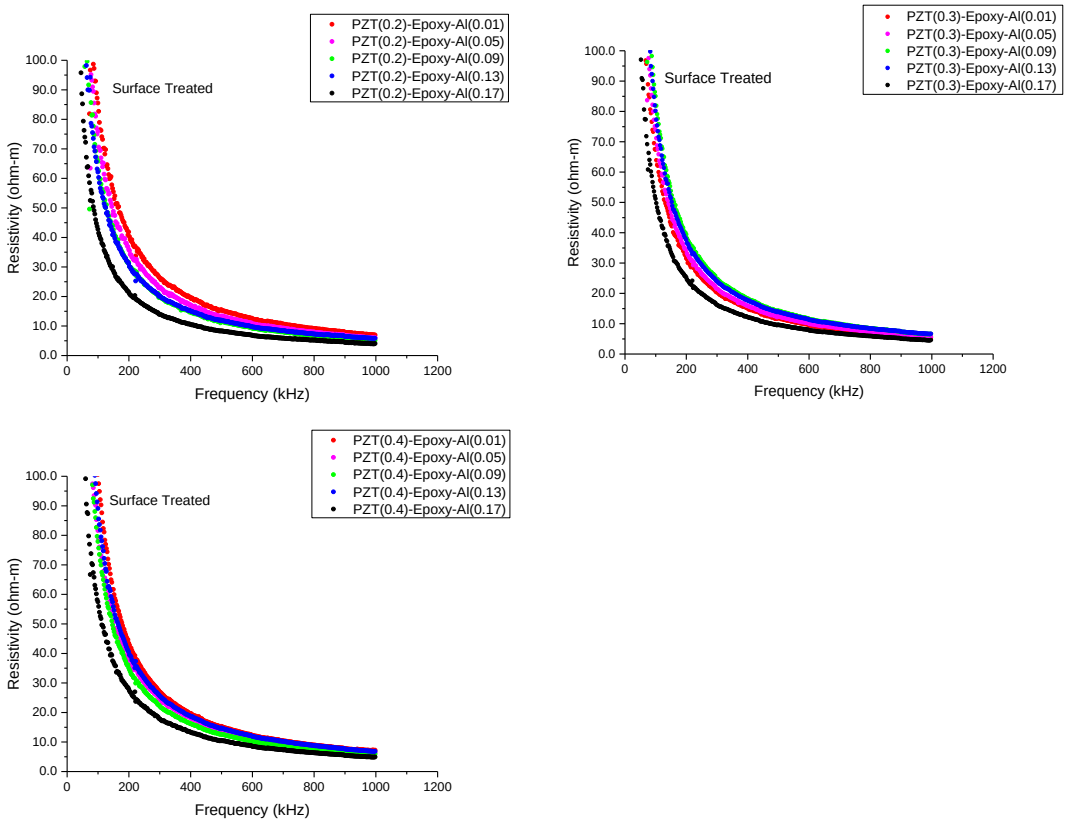

Figure 5.38: The for data set I (PZT-Epoxy-Al, surface treated Al, Corona poled at 15kV/cm) is plotted as a function of frequency for A) 0.2, B) 0.3 and C) 0.4 volume fractions of PZT. The minimum value for resistivity occurs for 0.17 volume fraction of aluminum for 0.2, 0.3 and 0.4 volume fractions of PZT.

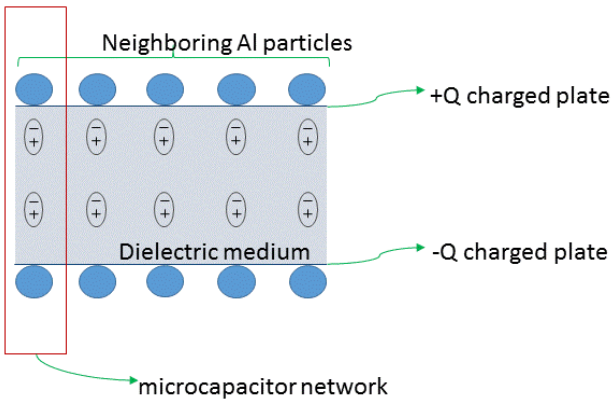

Figure 5.39: A schematic overview of a micro-capacitor network.

5.2 Composite Thick Film

5.2.1 Surface Morphology of the composite

The surface morphology and particle distribution were observed via scanning electron microscopy (SEM) and energy-dispersive X-ray spectroscopy (EDS) micrographs. PZT-epoxy-aluminum samples that were comprised of 0.30 PZT and 0.09 aluminum (by volume fraction) were observed. The cross-sections of the samples were obtained by cutting the sample using a blade and placing the samples onto the SEM stud to reveal the samples cross-sectioned thickness or surface morphology. In Figure 5.40, a SEM micrograph of the cross-section of the film is presented, where the imaged composites was at 467× magnification. There do not appear to be any microscopic pores or delamination points at the interface between the substrate and the film. The image in Figure 5.40 represents the fractured cross section as seen from the side, that is, along the thickness of the composite film with the stainless steel electrode at the top.

In Figure 5.41, the surface morphology of the composite film is depicted at a magnification of 520 X. PZT and aluminum particle agglomeration is observed in this SEM micrograph. The agglomeration may be attributed to several mechanisms of agglomeration: Brownian, gravitational, turbulent, and electrostatic, where the gravitational form is mitigated by the spin coating process. This can be validated Figure 5.40, where minimal coagulation of particles is observed at the interface of the substrate and the composite. The as-received PZT and aluminum powders tend to naturally form clusters that vary between 5-20 μm in the case of aluminum and 10-25 μm in the case of PZT as shown in Figure 5.42 A and B), where these agglomerations are most likely

attributed to electrostatic agglomeration. Addition of ethanol to the mixture did not effectively change the pH of the solution to negate the surface charge on the all of the particles which most likely diminished its effectiveness in counteracting the electrostatic forces between particles. The extent of the effectiveness of the ethanol on the pH of the solution was also a function of the number of particles within the colloidal sol gel.

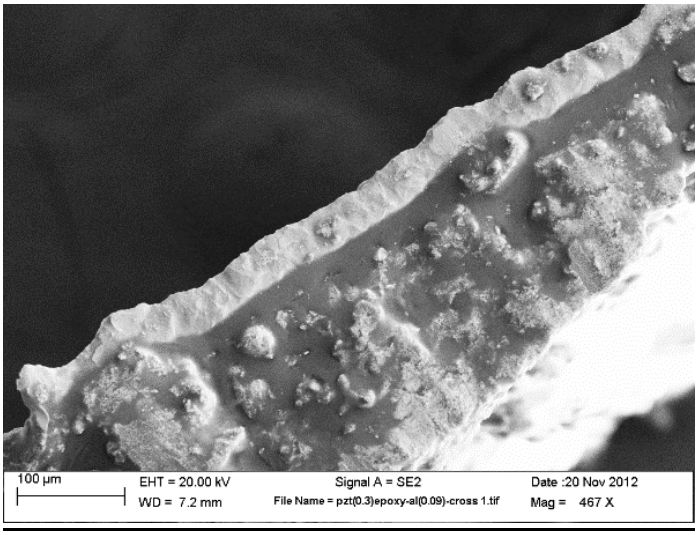

Figure 5.40: A cross-section view of the film thickness (thicknesses of the stainless steel and composite film were 25 and 150 µm, respectively). The film is comprised of 0.30 and 0.09 volume fractions of PZT and aluminum, respectively. No delamination at the interface between the film and substrate is observed at a magnification of 467× and EHT = 20.00 kV.

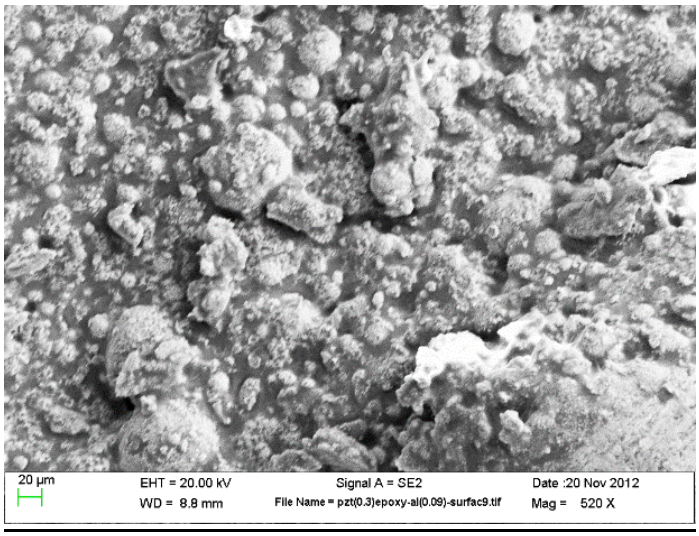

Figure 5.41: The surface morphology of the composite containing 30%PZT and 9% Al can been in the SEM micrographs where the magnification is 520 X and the EHT = 20.00 kV. We can see that the formation of PZT clusters or agglomerates occur within the composite. The aluminum particles are distributed around the PZT clusters, which could lead to aluminum-aluminum conductive pathways within the composite.

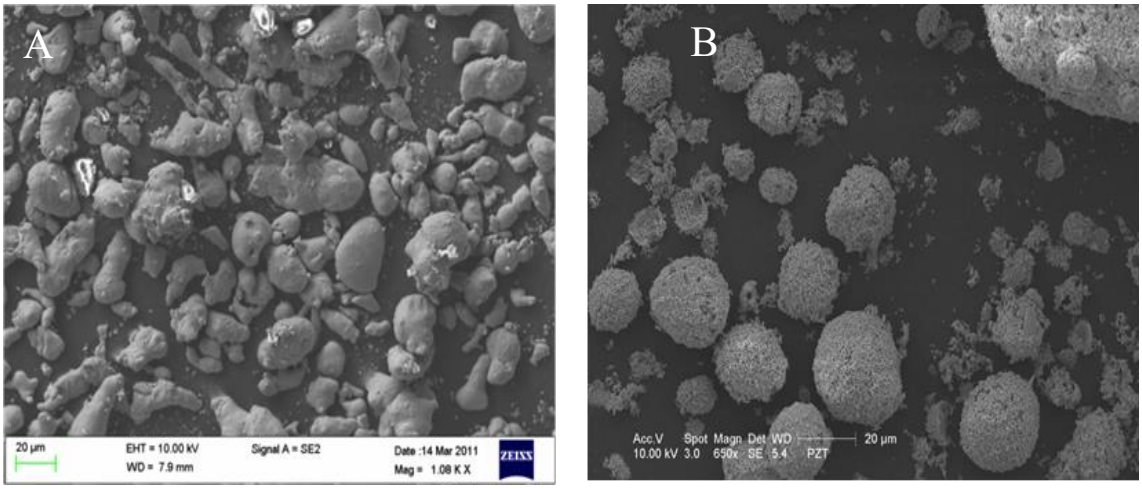

Figure 5.42: The surface morphologies of the A) micron sized Al inclusions (200 mesh) and B) PZT (EC-76 R8658) particles with average particle size ~6-7 µm. The SEM micrograph of the aluminum is magnified at 1080 X at EHT = 10.00 kV and the SEM micrograph of the PZT is magnified by 650 X at 10.00 kV.

5.2.2 Piezoelectric and Dielectric Characterization

In Figure 5.43 and Figure 5.45, the piezoelectric strain coefficients, d_{31} and d_{33}, for PZT-epoxy film composites are plotted as a function of PZT volume fraction. The films were fabricated in a similar manner as the 0-3-0 films, only they were Corona polarized at 15

kV/cm, instead of Contact Parallel Plated polarized. In Figure 5.44 the piezoelectric strain coefficients, d_{31} of the composites are plotted as a function of Al (0.0 to 0.17) for volume fractions 0.2, 0.3 and 0.4 of PZT, respectively. The samples that are PZT-epoxy were Corona polarized. As expected, the piezoelectric strain coefficients, d_{31} increase with PZT content and aluminum content up to 0.13, beyond which there is a steep decline in d_{31} values. The increase in d_{31} values is consistent with many researchers such as [72, 92, 131], who demonstrated increased values of d_{31} with increased PZT content within the piezoelectric polymer composite. A similar trend is expected for d_{33} values of the composite. However the magnitude of the d_{31} values is considerably higher than the d_{33} values owing to the higher strain in the direction along the 1-axis as compared to the strain in the 3-axis. The range of the d_{31} and d_{33} is consistent with [74, 131] where the active particle size was <34 μm with poling voltage at 10 kV/mm at room temperature, which is consistent with the data presented here. The differences in the d_{31} and d_{33} values for the 0-3 and the 0-3-0 composites are greater for lower volume fractions of PZT, but the advantage of Corona poling over Contact Parallel plate is evident at lower volume fractions of aluminum. However, at a higher volume fraction of the aluminum (0.15), the d31 values slightly surpassed those of the PZT-epoxy values for PZT volume fractions of 0.3 and 0.4.

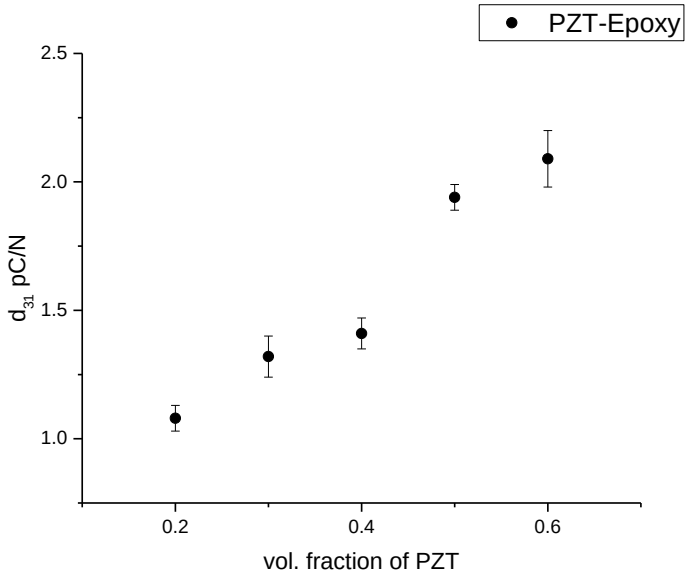

Figure 5.43: The piezoelectric strain coefficient, d31 for the PZT-Epoxy composite that are plotted as a function of volume fraction of PZT. The maximum value is 2.09 pC/N for PZT volume fraction of 0.6

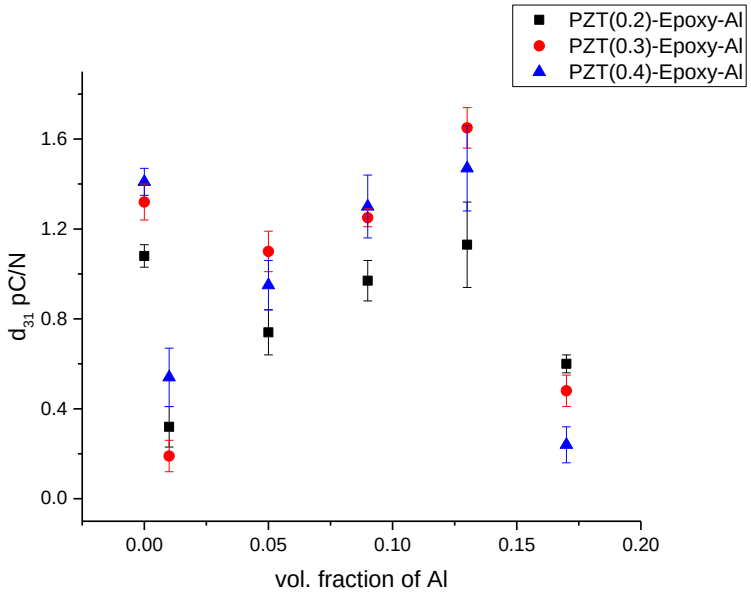

Figure 5.44: A comparison of piezoelectric strain coefficient d31 for the two-phase (PZT-Epoxy) composites plotted as a function of Al volume fraction for PZT at 20%, 30% and 40%

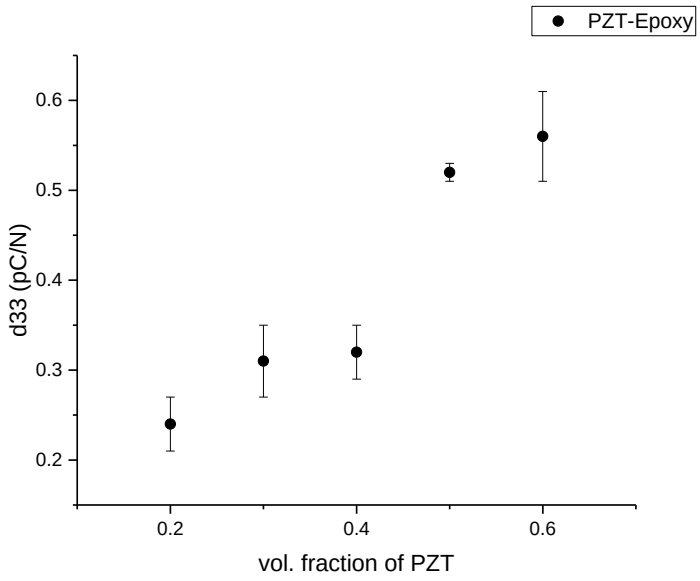

Figure 5.45: The piezoelectric strain coefficient, d33 for the PZT-Epoxy composite that are plotted as a function of volume fraction of PZT. The maximum value is 0.56 pC/N for PZT volume fraction of 0.6

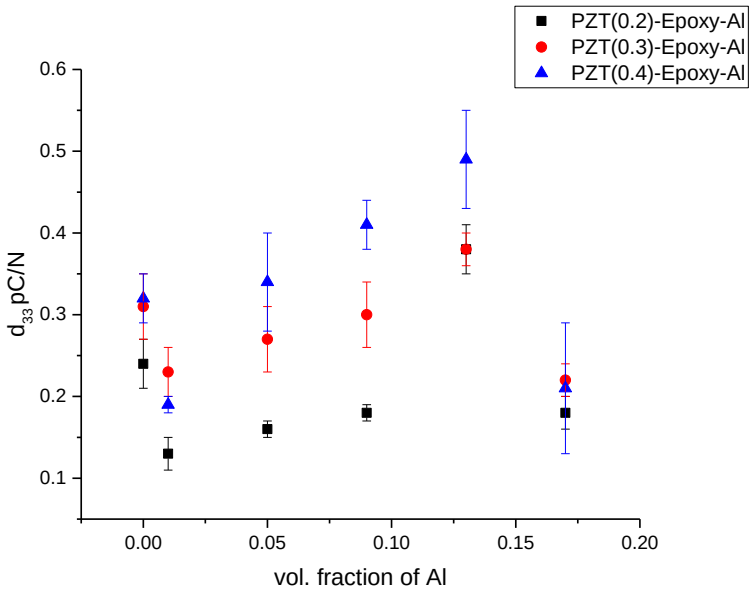

Figure 5.46: A comparison of piezoelectric strain coefficient d33 for the two-phase (PZT-Epoxy) composites plotted as a function of Al volume fraction for PZT at 20%, 30% and 40%

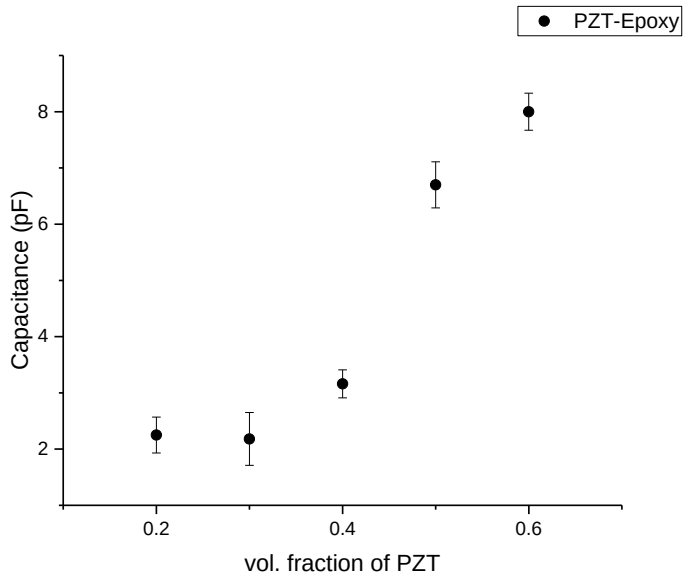

Figure 5.47: The capacitance for the PZT-Epoxy composite that are plotted as a function of PZT volume fraction. The maximum value is 8pF and occurs at 0.6 volume fraction of PZT

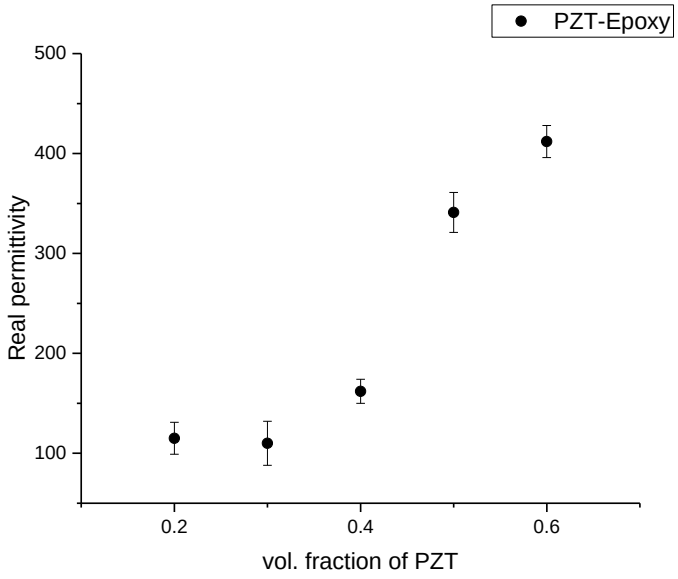

Figure 5.48: The real permittivity for the PZT-Epoxy composite that are plotted as a function of PZT volume fraction. The maximum value is 412 and occurs at 0.6 volume fraction of PZT

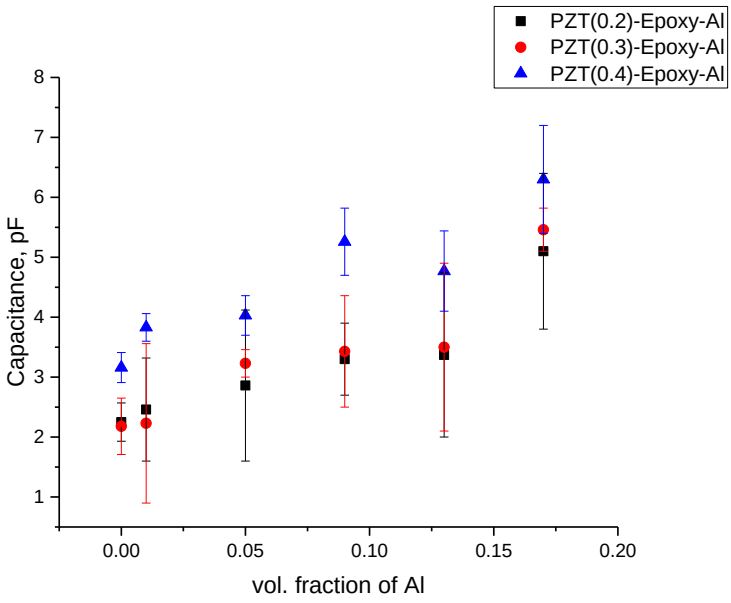

Figure 5.49: A comparison of capacitance values for the two-phase (PZT-Epoxy) composites plotted as a function of Al volume fraction for PZT at 20%, 30% and 40%

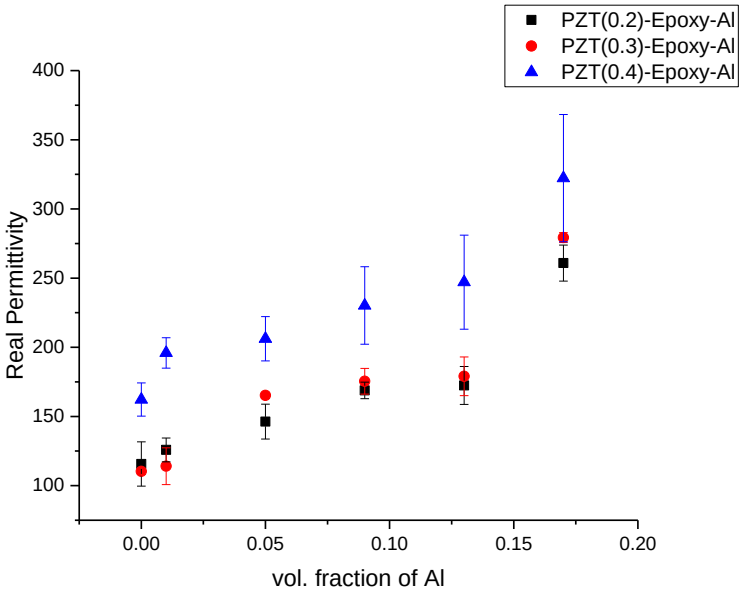

Figure 5.50: A comparison of real permittivity for the two-phase (PZT-Epoxy) composites plotted as a function of Al volume fraction for PZT at 20%, 30% and 40%

The dielectric constants of the two-phase composites are presented in Figure 5.48. The dielectric constant was found to increase with PZT content, where the maximum

value was ~412 for PZT volume fractions of 0.6. With increasing content of PZT the composite can be more easily polarized due to its inherent ferroelectric property, and hence this leads to a higher overall dielectric constant. The dielectric constants for the three-phase samples are presented in Figure 5.50 respectively. The dielectric constants for all samples increase with volume fraction of PZT and Al. The results indicate that all samples containing aluminum particles had higher dielectric constant than their two-phase counterparts. The maximum value of dielectric constant was observed for samples that contained 40% PZT and 17% Al.

5.2.3 Study comparing the effect of different top electrodes

Gold and silver top electrodes were applied to PZT (0.3)-Epoxy (0.05) samples to evaluate its influence on the electromechanical properties of the composite. Colloidal silver solution was applied as the top electrode with 5 µm thickness and 400 nm gold was sputtered on the sample using a sputtering machine.

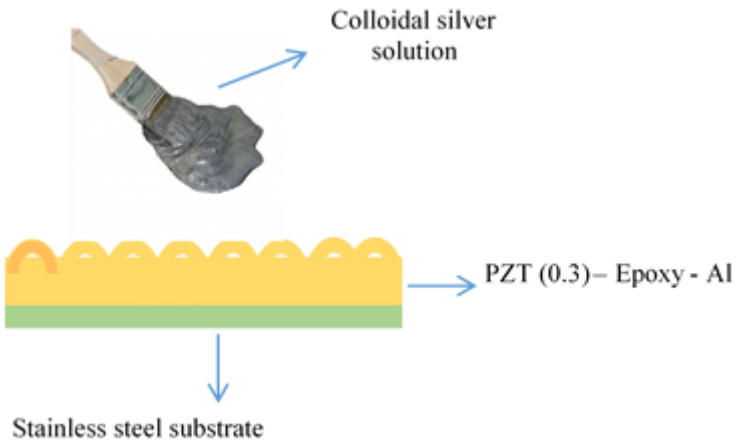

Figure 5.51: A schematic diagram of the application of the 5 µm thick colloidal silver electrode onto the surface of the film

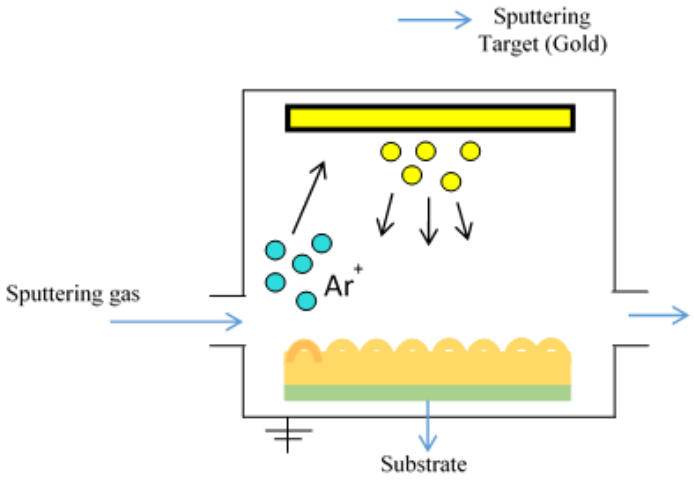

Figure 5.52: A schematic diagram describing the sputtering process of 400 nm gold layer onto the thick film. The molecules of the sputtering gas (Ar), strike the gold target thereby releasing gold molecules onto the surface of the film.

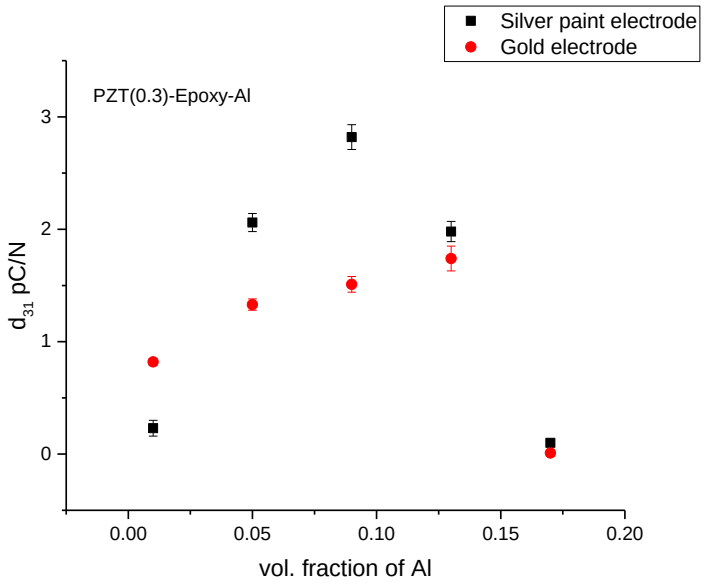

Figure 5.53: A Comparison of piezoelectric strain coefficient d_{31} for samples containing 30% PZT volume fraction and 5% Al volume fraction with silver and gold electrodes

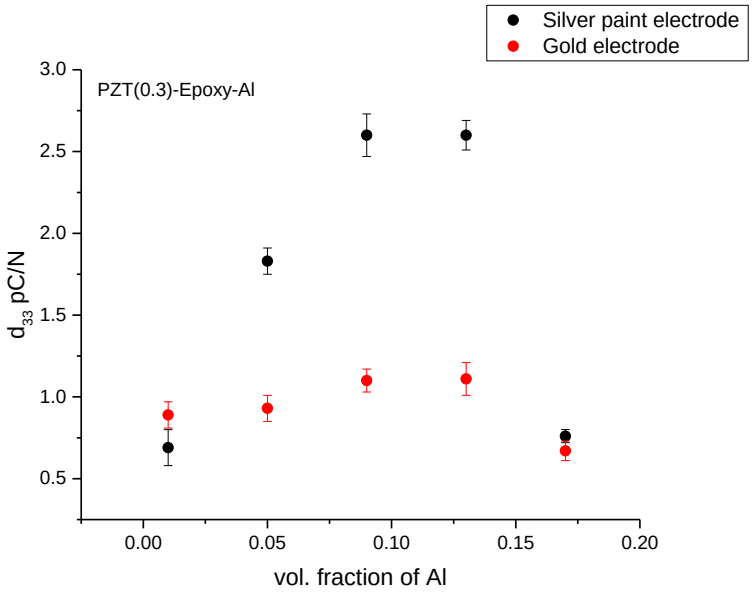

Figure 5.54: A Comparison of piezoelectric strain coefficient d_{33} for samples containing 30% PZT volume fraction and 5% Al volume fraction with silver and gold electrodes

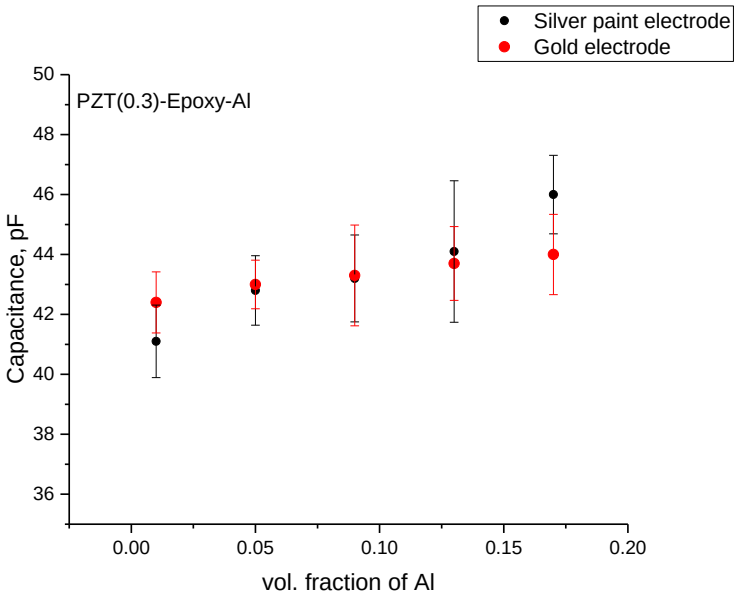

Figure 5.55: A Comparison of capacitance for samples containing 30% PZT volume fraction and 5% Al volume fraction with silver and gold electrodes

The electron transport properties at the interface of the composite thick film surface and the device electrode are influenced by the surface characteristics, such as the surface morphology of the thick films, the contact resistance and the total number of contact points connecting the thick film surface to the surface of the device electrode[12, 86, 157]. In order to draw a comparison between different top electrodes, the thick film were deposited with gold (Au) and silver (Ag) electrodes. The electrical resistivity and conductivity values are different for both materials. The variation in the piezoelectric strain coefficients d_{33} and d_{31} of the thick film are shown in Figure 5.53 and Figure 5.54. The values are enhanced by the addition of the metallic electrodes below the percolation threshold. This improvement in the d_{33} and d_{31} values is due to the decrease in the contact resistance and increase in the mobility of electrons at the interface between the film surface and the electrode due to the presence of the metallic layer[125]. We can see a maximum d_{31} and d_{33} values for the samples with silver electrode are 2pC/N and 2.5pC/N, respectively occur at ~13% Al. These values are higher than that of gold, d_{31} and d_{33} are ~1.8pC/N and ~1.2pC/N, respectively because of the decreased electrical resistivity of silver (Ag~0.00955 10^{-8} Ωm and Au~0.0502 10^{-8} Ωm)[158].

The capacitance values are enhanced by the addition of the top electrode. The top electrodes were applied to samples containing 30% PZT and 5% Al, and we can see that the capacitance for this sample with the gold electrode was ~43pF, with the silver electrode ~42.8pF and with no electrode was ~3.5pF. The enhancement of the capacitance could be due to several factors such as electron tunneling due to an increase in the intensity of local electric field[34]. Also, the conductive layer reduces the losses

due to metal insulator transition and other interface defects as compared to the composite without a conductive layer[125].

5.2.4 Effect of Aging of Samples: Data accumulated after 1day and 5days

The composites were also poled via contact poling method at the same poling voltage as the other samples (i.e. 2.2kV/mm). Once poled the data was measured on two separate occasions, after 1day and 5 days of poling, to study the effect of aging on the electromechanical properties of the composite. A comparison analysis was carried out to compare their respective values.

5.2.4.1 Samples with Silver Electrode

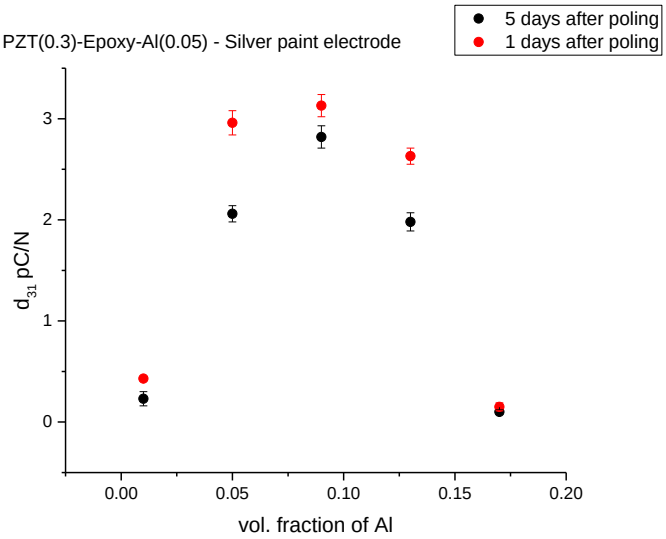

Figure 5.56: A comparison of the piezoelectric strain coefficient, d_{31} as a function of aging time i.e. time elapsed since poling the sample and recording the measurements, in this case a) one day and b) five days, for samples with 30% PZT and varying Al volume fraction with silver electrode.

5.2.4.2 Samples with Gold Electrode

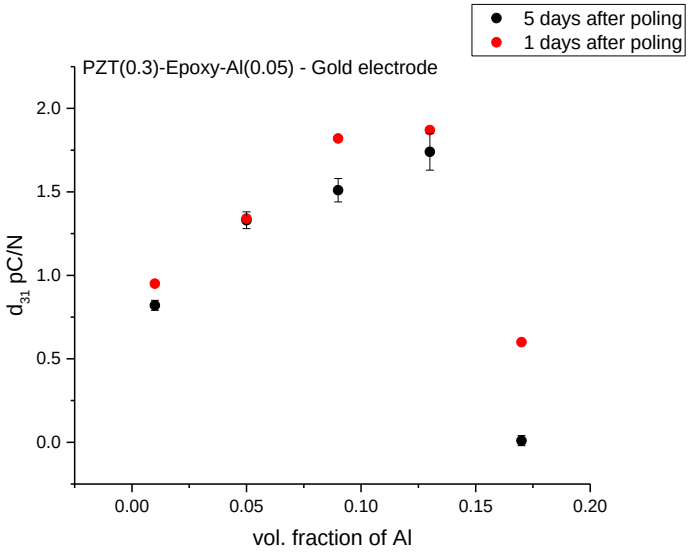

Figure 5.57: A comparison of the piezoelectric strain coefficient, d_{31} as a function of aging time i.e. time elapsed since poling the sample and recording the measurements, in this case a) one day and b) five days, for samples with 30% PZT and 5% Al volume fraction with gold electrode.

5.2.4.3 Samples with Silver Electrode

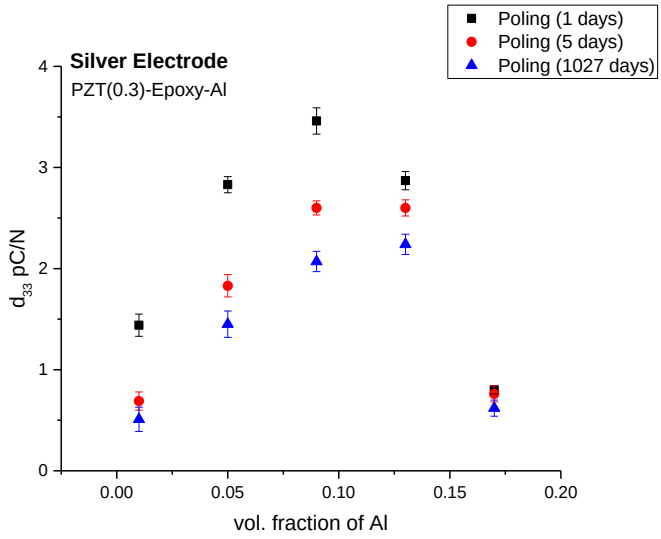

Figure 5.58: A comparison of the piezoelectric strain coefficient, d_{33} as a function of aging time i.e. time elapsed since poling the sample and recording the measurements, in this case a) one day and b) five days, for samples with 30% PZT and 5% Al volume fraction with silver electrode.

5.2.4.4 Samples with Gold Electrode

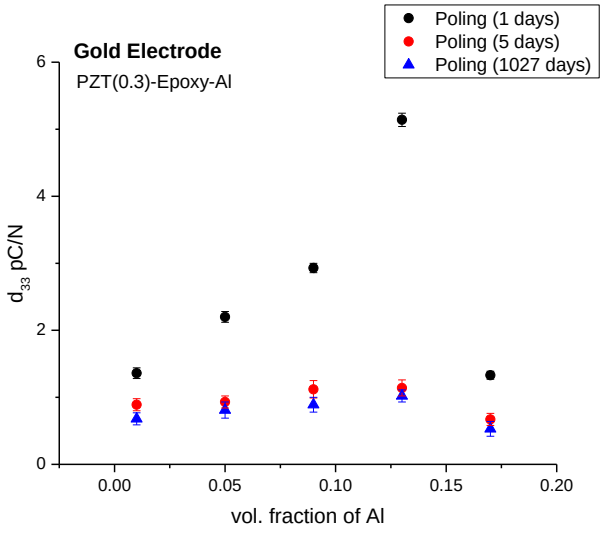

Figure 5.59: A comparison of the piezoelectric strain coefficient, d_{33} as a function of aging time i.e. time elapsed since poling the sample and recording the measurements, in this case a) one day and b) five days, for samples with 30% PZT and 5% Al volume fraction gold electrode.

The piezoelectric strain coefficient measurements d_{31} and d_{33} were measured after one and five days of poling the sample. The results that were recorded provided a brief insight into how the d_{33} and d_{31} values vary over time. As we can see from Figure 5.58 and Figure 5.59 the values measured after five days were slightly lower than the values of samples recorded after one day, and this happens because the sample reached remnant polarization gradually over time, and thus attains a lower d_{33} and d_{31} value as some of the dipoles that were forced to align return back to their natural position. The samples were measured again, 1027 days after poling, the d_{31} and d_{33} values reduced only slightly (10.5% - 23.5% less compared d_{33} of 5 days after poling), however they did observe a similar trend in values varying with aluminum volume fraction, as shown in Figure 5.58 and Figure 5.59.

Chapter 6

Conclusion and Future Work

6.1. Conclusion

Three phase piezoelectric PZT-Epoxy-Al composites have been fabricated and poled using corona and contact methods. The volume fraction of PZT and Al were varied from 0.2 to 0.4 and 0.0 to 0.17 respectively. The piezoelectric strain coefficient and the dielectric constant increased with PZT and Al volume content. However, the percolation threshold is believed to have been achieved for a volume fraction of 0.13 of Al, which was validated by observation of the resistivity of samples as a function of frequency and volume fraction. The resistivity of the samples decreased as a function of PZT and Al, where sharp decreases in resistivity were observed for the volume fraction above 0.13 of Al.

Surface treated aluminum was found to have better dispersion within the polymer matrix, and this was corroborated using the EDS images. The three phase composites, PZT-Epoxy-Al that contained surface treated aluminum inclusion yielded higher d_{33} and real permittivity values ε_r.

6.2. Future Work

Lead has recently been expelled from many commercial applications and materials e.g. from solder, glass and pottery glaze, owing to concerns regarding its toxicity. PZT contains more than 60 weight percent lead [159]. So despite PZT possessing high dielectric and piezoelectric properties ($\boldsymbol{\varepsilon}_r \sim 3300$ and $d_{33} \sim 630$ [24]), there has been interest in moving towards lead-free piezoceramics for use within composites.

Researchers have recently been looking at Barium Titanate ($BaTiO_3$) as an alternative material. $BaTiO_3$ was the first material used for manufacturing dielectric ceramic capacitors, multilayer capacitors etc. It is used for this application due to its high dielectric constant ($\boldsymbol{\varepsilon}_r \sim 4500$ at room temperature [160]) and low dielectric loss. $BaTiO_3$ is a member of a large family of compounds with the general formula ABO_3 which are called perovskites.

Therefore future work includes, but not limited to, embedding $BaTiO_3$ particles within a polymer matrix (epoxy resin) to create a composite with high dielectric constant and good piezoelectric characteristics. However a common problem associated with the inorganic-organic composites is the incompatibility of the two materials. In $BaTiO_3$ – Epoxy composites, the surface of $BaTiO_3$ with residue hydroxyl groups are hydrophilic in nature, while the epoxy resin and organic solvent are hydrophobic [161]. When these materials are mixed, the $BaTiO_3$ particles tend to agglomerate and separate from the organic solvent or resin, resulting in processing difficulties and inhomogeneous distribution of $BaTiO_3$ particles in the polymer. In order to ensure proper distribution of

$BaTiO_3$ particles within the composite there needs be surface treatment of the particles prior to mixing with epoxy. By using a silence coupling agent that possess different functional groups that can hydrolyze with the surface of $BaTiO_3$ [161] and which also has epoxy groups that can react with the polymer. By virtue of this, we can homogeneously distribute the $BaTiO_3$ particles within the composite.

However, Ramajo *et al.* [162] have identified that the amount of silane coupling agent added is critical to enhancing dispersion. Increasing the amount of coupling agent (>0.50 wt %) could be detrimental, as it increased porosity within the composite. Therefore it is paramount that an optimization study be conducted to determine the amount of coupling agent that needs to be used. In addition to enhancing dispersion, the dielectric and piezoelectric properties need to mimic that of the PZT composites to ensure that the composites of the latter can be substituted seamlessly in applications.

References

[1] S. Banerjee and K. A. Cook-Chennault, "An investigation into the influence of electrically conductive particle size on electromechanical coupling and effective dielectric strain coefficients in three phase composite piezoelectric polymers," *Composites Part a-Applied Science and Manufacturing,* vol. 43, pp. 1612-1619, Sep 2012.

[2] S. Banerjee and K. A. Cook-Chennault, "Influence of Al Particle Size and Lead Zirconate Titanate (PZT) Volume Fraction on the Dielectric Properties of PZT-Epoxy-Aluminum Composites," *Journal of Engineering Materials and Technology-Transactions of the Asme,* vol. 133, Oct 2011.

[3] S. Banerjee, R. Kappera, K. A. Cook-Chennault, and M. Chhowalla, "Multi Walled Carbon Nanotube based Flexible Multi-morph Composite Thick Films with Graphene Electrodes," *Science of Advanced Materials,* 2013.

[4] J. Xu and C. Wong, "Effects of the low loss polymers on the dielectric behavior of novel aluminum-filled high-k nano-composites," in *Advanced Packaging Materials: Processes, Properties and Interfaces, 2004. Proceedings. 9th International Symposium on*, 2004, pp. 158-170.

[5] W. G. Cady, *Piezoelectricity: An introduction to the theory and application of electromechanical phenomena in crystals*: McGraw-Hill, 1946.

[6] D.-I. E. G. Gautschi, *Piezoelectric sensors*: Springer, 2002.

[7] V. Giurgiutiu, *Structural health monitoring: with piezoelectric wafer active sensors*: Academic Press, 2007.

[8] V. Giurgiutiu, A. Zagrai, and J. J. Bao, "Piezoelectric wafer embedded active sensors for aging aircraft structural health monitoring," *Structural Health Monitoring,* vol. 1, pp. 41-61, 2002.

[9] G. Park, H. H. Cudney, and D. J. Inman, "Impedance-based health monitoring of civil structural components," *Journal of infrastructure systems,* vol. 6, pp. 153-160, 2000.

[10] W. Staszewski, C. Boller, and G. R. Tomlinson, *Health monitoring of aerospace structures: smart sensor technologies and signal processing*: John Wiley & Sons, 2004.

[11] K. A. Cook-Chennault, N. Thambi, and A. M. Sastry, "Powering MEMS portable devices - a review of non-regenerative and regenerative power supply systems with special emphasis on piezoelectric energy harvesting systems," *Smart Materials and Structures,* vol. 17, Aug 2008.

[12] S. Banerjee, W. Du, L. Wang, and K. A. Cook-Chennault, "Fabrication of dome-shaped PZT-epoxy actuator using modified solvent and spin coating technique," *Journal of Electroceramics,* vol. 31, pp. 148-158, Oct 2013.

[13] R. C. Buchanan, E. Park, R. Surana, H. Tennakone, and K. Tennakone, "High piezoelectric actuation response in graded Nd(2)O(3) and ZrO(2) doped BaTiO(3) structures," *Journal of Electroceramics,* vol. 26, pp. 116-121, Jun 2011.

[14] S. K. Bhattacharya and R. R. Tummala, "Epoxy nanocomposite capacitors for application as MCM-L compatible integral passives," *Journal of Electronic Packaging,* vol. 124, pp. 1-6, Mar 2002.

[15] P. Gonon and A. Boudefel, "Electrical properties of epoxy/silver nanocomposites," *Journal of Applied Physics,* vol. 99, Jan 2006.

[16] L. Li, A. Takahashi, J. J. Hao, R. Kikuchi, T. Hayakawa, T. A. Tsurumi*, et al.*, "Novel polymer-ceramic nanocomposite based on new concepts for embedded capacitor application (I)," *Ieee Transactions on Components and Packaging Technologies,* vol. 28, pp. 754-759, Dec 2005.

[17] S. Ogitani, S. A. Bidstrup-Allen, and P. A. Kohl, "Factors influencing the permittivity of polymer/ceramic composites for embedded capacitors," *Ieee Transactions on Advanced Packaging,* vol. 23, pp. 313-322, May 2000.

[18] C. Baur, D. J. Apo, D. Maurya, S. Priya, and W. Voit, "Advances in Piezoelectric Polymer Composites for Vibrational Energy Harvesting," 2014.

[19] M. Hori, T. Aoki, Y. Ohira, and S. Yano, "New type of mechanical damping composites composed of piezoelectric ceramics, carbon black and epoxy resin," *Composites Part a-Applied Science and Manufacturing,* vol. 32, pp. 287-290, 2001.

[20] A. Erturk and D. J. Inman, *Piezoelectric energy harvesting*: John Wiley & Sons, 2011.

[21] H. A. Sodano, D. J. Inman, and G. Park, "A review of power harvesting from vibration using piezoelectric materials," *Shock and Vibration Digest,* vol. 36, pp. 197-206, 2004.

[22] J. Kwon, W. Seung, B. K. Sharma, S.-W. Kim, and J.-H. Ahn, "A high performance PZT ribbon-based nanogenerator using graphene transparent electrodes," *Energy & Environmental Science,* vol. 5, pp. 8970-8975, 2012.

[23] K. A. Cook-Chennault, N. Thambi, M. A. Bitetto, and E. B. Hameyie, "Piezoelectric Energy Harvesting: A Green and Clean Alternative for Sustained Power Production," *Bulletin of Science Technology & Society,* vol. 28, pp. 496-509, 2008.

[24] A. International, "PHYSICAL AND PIEZOELECTRIC PROPERTIES OF APC MATERIALS," *A. International, Ed.,* 2013.

[25] S. Priya, R. Taneja, R. Myers, and R. Islam, "Piezoelectric energy harvesting using bulk transducers," in *Piezoelectric and Acoustic Materials for Transducer Applications*, ed: Springer, 2008, pp. 373-388.

[26] P. Muralt, "PZT thin films for microsensors and actuators: Where do we stand?," *Ultrasonics, Ferroelectrics, and Frequency Control, IEEE Transactions on,* vol. 47, pp. 903-915, 2000.

[27] Piezotech. (2012). *Piezoelectric Films Technical Information*.

[28] L. E. Cross, "Ferroelectric ceramics: tailoring properties for specific applications," in *Ferroelectric ceramics*, ed: Springer, 1993, pp. 1-85.

[29] M. Sunar and S. Rao, "Recent advances in sensing and control of flexible structures via piezoelectric materials technology," *Applied Mechanics Reviews,* vol. 52, pp. 1-16, 1999.

[30] L. E. Cross, R. E. Newnham, and D. P. Skinner, "Flexible piezoelectric composite transducers," ed: Google Patents, 1980.

[31] R. E. Newnham, *Properties of Materials: Anisotropy, Symmetry, Structure: Anisotropy, Symmetry, Structure*: OUP Oxford, 2004.

[32] R. E. Newnham, D. P. Skinner, K. A. Klicker, A. S. Bhalla, B. Hardiman, and T. R. Gururaja, "Ferroelectric ceramic-plasticcomposites forpiezoelectric and pyroelectric applications," *Ferroelectrics,* vol. 27, pp. 49-55, 1980.

[33] S. M. Pilgrim and R. E. Newnham, "3-0 - A new composite connectivity," *Ieee Transactions on Ultrasonics Ferroelectrics and Frequency Control,* vol. 33, pp. 805-805, 1986.

[34] C.-W. Nan, Y. Shen, and J. Ma, "Physical properties of composites near percolation," *Annual Review of Materials Research,* vol. 40, pp. 131-151, 2010.

[35] H. W. Choi, Y. W. Heo, J. H. Lee, J. J. Kim, H. Y. Lee, E. T. Park*, et al.*, "Effects of BaTiO3 on dielectric behavior of BaTiO3-Ni-polymethyl methacrylate composites," *Applied Physics Letters,* vol. 89, p. 3, Sep 2006.

[36] L. Qi, B. I. Lee, W. D. Samuels, G. J. Exarhos, and S. G. Parler, "Three-phase percolative silver–BaTiO3–epoxy nanocomposites with high dielectric constants," *Journal of applied polymer science,* vol. 102, pp. 967-971, 2006.

[37] X. Chao, Z. Yang, G. Li, and Y. Cheng, "Fabrication and characterization of low temperature sintering PMN–PZN–PZT step-down multilayer piezoelectric transformer," *Sensors and Actuators A: Physical,* vol. 144, pp. 117-123, 2008.

[38] D. Waller and A. Safari, "Corona poling of PZT ceramics and flexible piezoelectric composites," *Ferroelectrics,* vol. 87, pp. 189-195, 1988.

[39] R. S. Dahiya and M. Valle, *Robotic tactile sensing: technologies and system*: Springer Science & Business Media, 2012.

[40] U. o. Cambridge. (2012). *Dielectric Materials - Polarization Mechanisms*.

[41] C.-U. o. C.-. Davis. (2012). *Dielectric Polarization*.

[42] C. T. Dervos, C. D. Paraskevas, P. D. Skafidas, and P. Vassiliou, "A complex permittivity based sensor for the electrical characterization of high-voltage transformer oils," *Sensors,* vol. 5, pp. 302-316, 2005.

[43] P. R. Gray, P. J. Hurst, R. G. Meyer, and S. H. Lewis, *Analysis and design of analog integrated circuits*: John Wiley & Sons, 2008.

[44] S. Guillemet-Fritsch, T. Lebey, M. Boulos, and B. Durand, "Dielectric properties of CaCu 3 Ti 4 O 12 based multiphased ceramics," *Journal of the European Ceramic Society,* vol. 26, pp. 1245-1257, 2006.

[45] J. Schmidt and M. Moldover, "Dielectric permittivity of eight gases measured with cross capacitors," *International Journal of Thermophysics,* vol. 24, pp. 375-403, 2003.

[46] G. H. Haertling, "Ferroelectric ceramics: history and technology," *J. Am. Ceram. Soc.,* vol. 82, pp. 797-818, 1999.

[47] J. Herbert, "Ceramic Dielectrics and Capacitors, Electrocomponent Science Monographs, Vol. 6," *New York: Gordon and Breach Science Publishers,* 1985.

[48] E. R. Myers and A. I. Kingon, "Ferroelectric Thin Films. Materials Research Society Symposium Proceedings Held in San Francisco, California on April 16-20, 1990. Volume 200," DTIC Document1990.

[49] R. R. Tummala, E. J. Rymaszewski, and Y. Lee, "Microelectronics packaging handbook," ed: American Society of Mechanical Engineers, 1989.

[50] E. Wainer and A. N. Salomon, "Titanium Alloy Manufacturing Co," *Electr. Rep,* vol. 8, p. 1943, 1942.

[51] B. Wul and I. Goldman, "Dielectric constants of titanates of metals of the second group," *Compt. rend. Acad. sci. URSS,* vol. 46, pp. 139-42, 1945.

[52] "Transducer and method of making the same," ed: Google Patents, 1949.

[53] J. Curie and P. Curie, "Développement, par pression, de l'électricité polaire dans les cristaux hémièdres à faces inclinées," *Comptes Rendus,* vol. 91, pp. 294-295, 1880.

[54] W. P. Mason, "Piezoelectricity, its history and applications," *The Journal of the Acoustical Society of America,* vol. 70, pp. 1561-1566, 1981.

[55] G. Lippman, "Principe de la conservation de l'électricité," in *Annales de chimie et de physique*, 1881, pp. 381-394.

[56] P. Langevin, "Piezoelectric signaling apparatus," ed: Google Patents, 1941.

[57] B. Jaffe, R. Roth, and S. Marzullo, "J," Piezoelectric properties of modified PbTiO3 ceramics"," *Appl. Phys,* vol. 25, pp. 809-810, 1954.

[58] A. Safari and E. K. Akdogan, *Piezoelectric and acoustic materials for transducer applications*: Springer Science & Business Media, 2008.

[59] B. Jaffe, *Piezoelectric ceramics* vol. 3: Elsevier, 2012.

[60] R. Whatmore, "Ferroelectric Materials," in *Springer Handbook of Electronic and Photonic Materials*, ed: Springer, 2007, pp. 597-623.

[61] S. B. Lang, "Guide to the literature of piezoelectricity and pyroelectricity. 10," *Ferroelectrics,* vol. 182, pp. 91-312, 1996.

[62] W. Da-Wei, J. Hai-Bo, Y. Jie, W. Bao-Li, Z. Quan-Liang, Z. De-Qing*, et al.*, "Mechanical reinforcement and piezoelectric properties of PZT ceramics embedded with nano-crystalline," *Chinese Physics Letters,* vol. 27, p. 047701, 2010.

[63] Y. Takahiro, K. Masako, and S. Norikazu, "Influence of poling conditions on the piezoelectric properties of PZT ceramics," *Journal of Materials Science: Materials in Electronics,* vol. 11, pp. 425-428, 2000.

[64] G. Shirane, K. Suzuki, and A. Takeda, "Phase transitions in solid solutions of PbZrO3 and PbTiO3 (II) X-ray study," *Journal of the Physical Society of Japan,* vol. 7, pp. 12-18, 1952.

[65] M. Dietze and M. Es-Souni, "Structural and functional properties of screen-printed PZT–PVDF-TrFE composites," *Sensors and Actuators A: Physical,* vol. 143, pp. 329-334, 2008.

[66] E. M. McKenna, A. S. Lin, A. R. Mickelson, R. Dinu, and D. Jin, "Comparison of r 33 values for AJ404 films prepared with parallel plate and corona poling," *JOSA B,* vol. 24, pp. 2888-2892, 2007.

[67] S. Huang, J. Luo, H. L. Yip, A. Ayazi, X. H. Zhou, M. Gould*, et al.*, "Efficient Poling of Electro-Optic Polymers in Thin Films and Silicon Slot Waveguides by Detachable Pyroelectric Crystals," *Advanced Materials,* vol. 24, pp. OP42-OP47, 2012.

[68] A. Safari, V. F. Janas, and A. Bandyopadhyay, "Development of fine-scale piezoelectric composites for transducers," *American Institute of Chemical Engineers. AIChE Journal,* vol. 43, p. 2849, 1997.

[69] R. Newnham, D. Skinner, and L. Cross, "Connectivity and piezoelectric-pyroelectric composites," *Materials Research Bulletin,* vol. 13, pp. 525-536, 1978.

[70] J. Xu, K.-S. Moon, C. Tison, and C. Wong, "A novel aluminum-filled composite dielectric for embedded passive applications," *Advanced Packaging, IEEE Transactions on,* vol. 29, pp. 295-306, 2006.

[71] K. Arlt and M. Wegener, "Piezoelectric PZT/PVDF-copolymer 0-3 composites: aspects on film preparation and electrical poling," *Dielectrics and Electrical Insulation, IEEE Transactions on,* vol. 17, pp. 1178-1184, 2010.

[72] H. Banno and K. Ogura, "Piezoelectric properties of 0-3 composite of polymer and ceramic powder mixture of PZT and PbTiO3," *Japanese journal of applied physics,* vol. 30, p. 2247, 1991.

[73] F. Levassort, M. Lethiecq, R. Desmare, and L. P. Tran-Huu-Hue, "Effective electroelastic moduli of 3-3(0-3) piezocomposites," *Ieee Transactions on Ultrasonics Ferroelectrics and Frequency Control,* vol. 46, pp. 1028-1034, Jul 1999.

[74] G. Rujijanagul, S. Boonyakul, and T. Tunkasiri, "Effect of the particle size of PZT on the microstructure and the piezoelectric properties of 0-3 PZT/polymer composites," *Journal of materials science letters,* vol. 20, pp. 1943-1945, 2001.

[75] S. Banerjee and K. A. Cook-Chennault, "An Analytical Model for the Effective Dielectric Constant of a 0-3-0 Composite," *Journal of Engineering Materials and Technology-Transactions of the Asme,* vol. 133, Oct 2011.

[76] V. Y. Topolov, C. R. Bowen, and P. Bisegna, "Electromechanical Coupling Factors of Novel 0-3-0 Composites Based on PMN-xPT Single Crystals," *Ferroelectrics,* vol. 422, pp. 40-43, 2011 2011.

[77] M. Lach, M. Platte, and A. Ries, "Piezoelectric materials for ultrasonic probes," *Artikel im INTERNET: www. NDT. net,* vol. 1, 1996.

[78] N. Sahu, B. Parija, and S. Panigrahi, "Fundamental understanding and modeling of spin coating process: A review," *Indian Journal of Physics,* vol. 83, pp. 493-502, 2009.

[79] A. G. Emslie, F. T. Bonner, and L. G. Peck, "Flow of a viscous liquid on a rotating disk," *Journal of Applied Physics,* vol. 29, pp. 858-862, 1958.

[80] D. Bornside, C. Macosko, and L.-E. Scriven, "On the modeling of spin coating," *Journal of imaging technology,* vol. 13, pp. 122-130, 1987.

[81] R. Yonkoski and D. Soane, "Model for spin coating in microelectronic applications," *Journal of applied physics,* vol. 72, pp. 725-740, 1992.

[82] C. Lawrence and W. Zhou, "Spin coating of non-Newtonian fluids," *Journal of non-newtonian fluid mechanics,* vol. 39, pp. 137-187, 1991.

[83] M. Zou, L. Cai, and H. Wang, "Adhesion and friction studies of a nano-textured surface produced by spin coating of colloidal silica nanoparticle solution," *Tribology Letters,* vol. 21, pp. 25-30, 2006.

[84] M. A. Rahman, B.-C. Lee, D.-T. Phan, and G.-S. Chung, "Fabrication and characterization of highly efficient flexible energy harvesters using PVDF–graphene nanocomposites," *Smart Materials and Structures,* vol. 22, p. 085017, 2013.

[85] I. Babu and D. Van den Ende, "Processing and characterization of piezoelectric 0-3 PZT/LCT/PA composites," *Journal of Physics D: Applied Physics,* vol. 43, p. 425402, 2010.

[86] S. Banerjee, "An experimental investigation of lead zirconate titanate-epoxy-multi-walled carbon nanotube bulk and flexible thick film composites," Rutgers University-Graduate School-New Brunswick, 2014.

[87] G. H. Feng, "A piezoelectric dome-shaped-diaphragm transducer for microgenerator applications," *Smart Materials & Structures,* vol. 16, pp. 2636-2644, Dec 2007.

[88] M. G. Smith, L. C. Chow, and N. Molin, "Attenuation of slat trailing edge noise using slat gap acoustic liners," in *12th AIAA/CEAS Aeroacoustics Conference*, Cambridge, Massachusetts, 2006.

[89] R. Y. Ting, "A review on the development of piezoelectric composites for underwater acoustic transducer applications," *IEEE transactions on instrumentation and measurement,* vol. 41, pp. 64-67, 1992.

[90] R. Y. Ting, "Composite piezoelectric materials for transduction," *Applied Acoustics,* vol. 41, pp. 325-335, 1994.

[91] J. Hossack and R. Bedi, "Design of composite piezoelectric transducers," in *Key engineering materials*, 1994, p. 301.

[92] Y. M. Poon, C. H. Ho, Y. W. Wong, and F. G. Shin, "Theoretical predictions on the effective piezoelectric coefficients of 0–3 PZT/Polymer composites," *Journal of materials science,* vol. 42, pp. 6011-6017, 2007.

[93] A. Safari, "DEVELOPMENT OF PIEZOELECTRIC COMPOSITES FOR TRANSDUCERS," *Journal De Physique Iii,* vol. 4, pp. 1129-1149, Jul 1994.

[94] B. S. Prakash and K. Varma, "Dielectric behavior of CCTO/epoxy and Al-CCTO/epoxy composites," *Composites Science and Technology,* vol. 67, pp. 2363-2368, 2007.

[95] H. W. Choi, Y. W. Heo, J. H. Lee, J. J. Kim, H. Y. Lee, E. T. Park*, et al.*, "Effects of ni particle size on dielectric properties of PMMA-Ni-BaTiO3 composites," *Integrated Ferroelectrics,* vol. 87, pp. 85-+, 2007.

[96] J. M. Park, H. Y. Lee, J.-J. Kim, E. T. Park, and Y.-K. Chun, "Dielectric properties of Ni-coated BaTiO 3-PMMA composite," *Ultrasonics, Ferroelectrics, and Frequency Control, IEEE Transactions on,* vol. 55, pp. 1038-1042, 2008.

[97] C. Zhang, J. Sheng, C. Ma, and M. Sumita, "Electrical and damping behaviors of CPE/BaTiO 3/VGCF composites," *Materials letters,* vol. 59, pp. 3648-3651, 2005.

[98] X. B. Ding and X. Yan, "Study of piezo-damping properties of CPE/ZKF/VGCF composites," *Journal of Applied Polymer Science,* vol. 102, pp. 3181-3185, Nov 2006.

[99] W. Zheng and S. C. Wong, "Electrical conductivity and dielectric properties of PMMA/expanded graphite composites," *Composites Science and Technology,* vol. 63, pp. 225-235, 2003.

[100] L. Xiaofang, X. Chuanxi, S. Huajun, D. Lijie, L. Rui, and L. Yang, "Characterization of PZT/PVC composites added with carbon black," *Journal of Wuhan University of Technology-Mater. Sci. Ed.,* vol. 20, pp. 60-64, 2005.

[101] Q. M. Liu, J. C. Tu, X. Wang, W. X. Yu, W. T. Zheng, and Z. D. Zhao, "Electrical conductivity of carbon nanotube/poly(vinylidene fluoride) composites prepared by high-speed mechanical mixing," *Carbon,* vol. 50, pp. 339-341, Jan 2012.

[102] X.-f. Liu, C.-x. Xiong, H.-j. Sun, L.-j. Dong, and Y. Liu, "Piezoelectric and dielectric properties of PZT/PVC and graphite doped with PZT/PVC composites," *Materials Science and Engineering: B,* vol. 127, pp. 261-266, 2006.

[103] L. Wang and S. H. Zhao, "Study on the Structure-Mechanical Properties Relationship and Antistatic Characteristics of SSBR Composites Filled with SiO(2)/CB," *Journal of Applied Polymer Science,* vol. 118, pp. 338-345, Oct 2010.

[104] E. Venkatragavaraj, B. Satish, P. R. Vinod, and M. S. Vijaya, "Piezoelectric properties of ferroelectric PZT–polymer composites," *Journal of Applied Physics D: Applied Physics,* vol. 34, pp. 487-492, 2001.

[105] W. Nhuapeng and T. Tunkasiri, "Properties of 0–3 Lead Zirconate Titanate–Polymer Composites Prepared in a Centrifuge," *Journal of the American Ceramic Society,* vol. 85, pp. 700-702, 2002.

[106] W. Thamjaree, W. Nhuapeng, A. Chaipanich, and T. Tunkasiri, "Fabrication of combined 0–3 and 1–3 connectivities PZT/epoxy resin composites," *Applied Physics A,* vol. 81, pp. 1419-1422, 2005.

[107] S. K. Bhattacharya and R. R. Tummala, "Next generation integral passives: materials, processes, and integration of resistors and capacitors on PWB substrates," *Journal of Materials Science-Materials in Electronics,* vol. 11, pp. 253-268, Apr 2000.

[108] Y. Zhen and J.-F. Li, "Preparation and electrical properties of fine-scale 1-3 lead zirconic titanate/epoxy composite thick films for high-frequency ultrasonic transducers," *Journal of Applied Physics,* vol. 103, p. 4119, 2008.

[109] S. Krupanidhi, N. Maffei, M. Sayer, and K. El-Assal, "RF planar magnetron sputtering and characterization of ferroelectric Pb (Zr, Ti) O3 films," *Journal of Applied Physics,* vol. 54, pp. 6601-6609, 1983.

[110] M. Okuyama, T. Usuki, Y. Hamakawa, and T. Nakagawa, "Epitaxial growth of ferroelectric PLZT thin film and their optical properties," *Applied physics,* vol. 21, pp. 339-343, 1980.

[111] R. Castellano and L. Feinstein, "Ion-beam deposition of thin films of ferroelectric lead zirconate titanate (PZT)," *Journal of Applied Physics,* vol. 50, pp. 4406-4411, 1979.

[112] K. Sreenivas, M. Sayer, and P. Garrett, "Properties of DC magnetron-sputtered lead zirconate titanate thin films," *Thin Solid Films,* vol. 172, pp. 251-267, 1989.

[113] B. Kwak, E. Boyd, and A. Erbil, "Metalorganic chemical vapor deposition of PbTiO3 thin films," *Applied physics letters,* vol. 53, pp. 1702-1704, 1988.

[114] M. Kojima, M. Okuyama, T. Nakagawa, and Y. Hamakawa, "Chemical Vapor Deposition of PbTiO3 Thin Film," *Japanese Journal of Applied Physics,* vol. 22, p. 14, 1983.

[115] M. Okada, S. Takai, M. Amemiya, and K. Tominaga, "Preparation of c-axis-oriented PbTiO3 thin films by MOCVD under reduced pressure," *Japanese Journal of Applied Physics,* vol. 28, p. 1030, 1989.

[116] K. D. Budd, S. Key, and D. Payne, "Sol-gel processing of PbTiO 3, PbZrO 3, PZT and PLZT thin films," in *BR. CERAM. PROC. Br. Ceram. Proc.*, 1985, p. 107.

[117] S. Dey, K. D. Budd, and D. A. Payne, "Thin-film ferroelectrics of PZT of sol-gel processing," *IEEE transactions on ultrasonics, ferroelectrics, and frequency control,* vol. 35, pp. 80-81, 1987.

[118] G. Spierings, M. Ulenaers, G. Kampschöer, H. Van Hal, and P. Larsen, "Preparation and ferroelectric properties of PbZr0. 53Ti0. 47O3 thin films by spin coating and metalorganic decomposition," *Journal of applied physics,* vol. 70, pp. 2290-2298, 1991.

[119] B. Tuttle, T. Headley, B. Bunker, R. Schwartz, T. Zender, C. Hernandez*, et al.*, "Microstructural evolution of Pb (Zr, Ti) O 3 thin films prepared by hybrid metallo-organic decomposition," *Journal of materials research,* vol. 7, pp. 1876-1882, 1992.

[120] S. Otsubo, T. Maeda, T. Minamikawa, Y. Yonezawa, A. Morimoto, and T. Shimizu, "Preparation of Pb (Zn0. 52Ti0. 48) O3 films by laser ablation," *Japanese journal of applied physics,* vol. 29, p. L133, 1990.

[121] H. Buhay, S. Sinharoy, W. Kasner, M. Francombe, D. Lampe, and E. Stepke, "Pulsed laser deposition and ferroelectric characterization of bismuth titanate films," *Applied physics letters,* vol. 58, pp. 1470-1472, 1991.

[122] D. Roy, S. Krupanidhi, and J. Dougherty, "Excimer laser ablated lead zirconate titanate thin films," *Journal of applied physics,* vol. 69, pp. 7930-7932, 1991.

[123] S. Corkovic, R. Whatmore, and Q. Zhang, "Sol-gel fabrication of PZT thick films for MEMS," *Integrated Ferroelectrics,* vol. 88, pp. 93-102, 2007.

[124] K. Li, H. Chan, K. Lee, and C. Choy, "Preparation of thick PZT films on stainless steel substrates," *Integrated Ferroelectrics,* vol. 30, pp. 253-260, 2000.

[125] S. Banerjee and K. A. Cook-Chennault, "Influence of aluminium inclusions on dielectric properties of three-phase PZT-cement-aluminium composites," *Advances in Cement Research,* vol. 26, pp. 63-76, Aug 2014.

[126] S. Banerjee, J. Torres, and K. A. Cook-Chennault, "Piezoelectric and dielectric properties of PZT-cement-aluminum nano-composites," *Ceramics International,* vol. 41, pp. 819-833, Jan 2015.

[127] T. T. Nguyen, T. T. M. Phan, N. C. Chu, V. Luu, X. H. Nguyen, I. Martin*, et al.*, "Elaboration and dielectric property of modified PZT/epoxy nanocomposites," *Polymer Composites,* 2014.

[128] J. Malmonge, L. Malmonge, G. Fuzari, S. Malmonge, and W. Sakamoto, "Piezo and dielectric properties of PHB–PZT composite," *Polymer Composites,* vol. 30, pp. 1333-1337, 2009.

[129] K. Hanner, A. Safari, R. Newnham, and J. Runt, "Thin film 0–3 polymer/piezoelectric ceramic composites: Piezoelectric paints," *Ferroelectrics,* vol. 100, pp. 255-260, 1989.

[130] R. Newnham, A. Safari, J. Giniewicz, and B. Fox, "Composite piezoelectric sensors," *Ferroelectrics,* vol. 60, pp. 15-21, 1984.

[131] D. Corker, Q. Zhang, R. Whatmore, and C. Perrin, "PZT 'composite'ferroelectric thick films," *Journal of the European Ceramic Society,* vol. 22, pp. 383-390, 2002.

[132] A. Kholkin, V. Yarmarkin, A. Wu, M. Avdeev, P. Vilarinho, and J. Baptista, "PZT-based piezoelectric composites via a modified sol–gel route," *Journal of the European Ceramic Society,* vol. 21, pp. 1535-1538, 2001.

[133] Z. Wang, W. Zhu, C. Zhao, and O. K. Tan, "Dense PZT thick films derived from sol-gel based nanocomposite process," *Materials Science and Engineering: B,* vol. 99, pp. 56-62, 2003.

[134] P. Thongsanitgarn, A. Watcharapasorn, and S. Jiansirisomboon, "Electrical and mechanical properties of PZT/PVDF 0–3 composites," *Surface Review and Letters,* vol. 17, pp. 1-7, 2010.

[135] V. Pascariu, L. Padurariu, O. Avadanei, and L. Mitoseriu, "Dielectric properties of PZT–epoxy composite thick films," *Journal of Alloys and Compounds,* vol. 574, pp. 591-599, 2013.

[136] N. K. James, D. van den Ende, U. Lafont, S. van der Zwaag, and W. A. Groen, "Piezoelectric and mechanical properties of structured PZT–epoxy composites," *Journal of Materials Research,* vol. 28, pp. 635-641, 2013.

[137] E. M. Sciences. (2012). *EMS Catalog #1232 Epofix Cold-Setting Embedding Resin*.

[138] A. Organics. (2012). *Physical Properties of Aluminum 99% powder, 200 mesh*.

[139] READE. (2010). *Properties of Lead Zirconate Titanate*.

[140] J. O. MANASSEN, "The mechanism of dehydration of alcohols over alumina catalysts," *Advances in catalysis,* vol. 16, p. 49, 1966.

[141] H. Adkins and P. P. Perkins, "Dehydration of alcohols over alumina," *Journal of the American Chemical Society,* vol. 47, pp. 1163-1167, 1925.

[142] K. H. Han, A. Safari, and R. E. Riman, "COLLOIDAL PROCESSING FOR IMPROVED PIEZOELECTRIC PROPERTIES OF FLEXIBLE 0-3 CERAMIC POLYMER COMPOSITES," *Journal of the American Ceramic Society,* vol. 74, pp. 1699-1702, 1991.

[143] K. Lam and H. Chan, "Piezoelectric and pyroelectric properties of 65PMN-35PT/P (VDF-TrFE) 0–3 composites," *Composites science and technology,* vol. 65, pp. 1107-1111, 2005.

[144] L. Jie, T. Dongyan, and L. Ji, "Preparation and Electric Properties of 0-3 Modified PZT/IPN Piezoelectric Composites," *Rare Metal Materials and Engineering,* vol. 36, p. 411, 2007.

[145] Y. Son, S. Kweon, S. Kim, Y. Kim, T. Hong, and Y. Lee, "Fabrication and electrical properties of PZT-PVDF 0–3 type composite film," *Integrated Ferroelectrics,* vol. 88, pp. 44-50, 2007.

[146] V. Y. Topolov, P. Bisegna, and C. R. Bowen, "Analysis of the piezoelectric performance of modern 0-3 type composites based on relaxor-ferroelectric single crystals," *Ferroelectrics,* vol. 413, 2011.

[147] G. Rujijanagul, S. Jompruan, and A. Chaipanich, "Influence of graphite particle size on electrical properties of modified PZT–polymer composites," *Current Applied Physics,* vol. 8, pp. 359-362, 2008.

[148] H. Scher and R. Zallen, "Critical density in percolation processes," *The Journal of Chemical Physics,* vol. 53, p. 3759, 1970.

[149] X. Jing, W. Zhao, and L. Lan, "The effect of particle size on electric conducting percolation threshold in polymer/conducting particle composites," *Journal of materials science letters,* vol. 19, pp. 377-379, 2000.

[150] B. Satish, K. Sridevi, and M. Vijaya, "Study of piezoelectric and dielectric properties of ferroelectric PZT-polymer composites prepared by hot-press technique," *Journal of Physics D: Applied Physics,* vol. 35, p. 2048, 2002.

[151] P. Lunkenheimer, S. Krohns, S. Riegg, S. Ebbinghaus, A. Reller, and A. Loidl, "Colossal dielectric constants in transition-metal oxides," *The European Physical Journal Special Topics,* vol. 180, pp. 61-89, 2010.

[152] T. Lewis, "Interfaces: nanometric dielectrics," *Journal of Physics D: Applied Physics,* vol. 38, p. 202, 2005.

[153] C. Yang, H. S. Song, and D. B. Liu, "Dielectric Composites Containing Core@ shell Structure Particles," in *Advanced Materials Research*, 2011, pp. 3113-3118.

[154] J. Xu and C. Wong, "Low-loss percolative dielectric composite," *Applied Physics Letters,* vol. 87, p. 2907, 2005.

[155] D. J. Bergman and Y. Imry, "Critical behavior of the complex dielectric constant near the percolation threshold of a heterogeneous material," *Physical Review Letters,* vol. 39, p. 1222, 1977.

[156] C. Pecharromán and J. S. Moya, "Experimental evidence of a giant capacitance in insulator–conductor composites at the percolation threshold," *Advanced Materials,* vol. 12, pp. 294-297, 2000.

[157] T. Pedersen, C. C. Hindrichsen, E. Thomsen, K. Hansen, and R. Lou-Møller, "Investigation of top/bottom electrode and diffusion barrier layer for PZT thick film MEMS sensors," in *Sensors, 2007 IEEE*, 2007, pp. 756-759.

[158] R. A. Matula, "Electrical resistivity of copper, gold, palladium, and silver," *Journal of Physical and Chemical Reference Data,* vol. 8, pp. 1147-1298, 1979.

[159] Y. Saito, H. Takao, T. Tani, T. Nonoyama, K. Takatori, T. Homma*, et al.*, "Lead-free piezoceramics," *Nature,* vol. 432, pp. 84-87, 2004.

[160] H. T. Kim and Y. H. Han, "Sintering of nanocrystalline BaTiO 3," *Ceramics International,* vol. 30, pp. 1719-1723, 2004.

[161] S. Liang, S. R. Chong, and E. P. Giannelis, "Barium titanate/epoxy composite dielectric materials for integrated thin film capacitors," in *Electronic Components & Technology Conference, 1998. 48th IEEE*, 1998, pp. 171-175.

[162] L. Ramajo, M. M. Reboredo, and M. S. Castro, "BaTiO3–epoxy composites for electronic applications," *International Journal of Applied Ceramic Technology,* vol. 7, pp. 444-451, 2010.